Universidade Federal do Espírito Santo

Programa de Pós-Graduação em Astrofísica, Cosmologia e Gravitação

Testing clustering dark energy models with the skewness of matter distribution

Raquel Emy Fazolo

Thesis submitted as part of the requirements for the degree of
Doctor of Philosophy in Astronomy & Physics

Supervisor: Prof. Hermano Endlich Schneider Velten
UFOP, Universidade Federal de Ouro Preto (Brazil)

Co-supervisor: Prof. Luca Amendola
ITP, Heidelberg University (Germany)

2022

ATA DA SESSÃO DA NONA DEFESA DA TESE DE DOUTORADO DA ALUNA RAQUEL EMY FAZOLO

Às 09:00h do dia 10 do mês de outubro do ano de 2022, estava reunida remotamente a banca examinadora, composta pelos Professores Doutores Hermano Endlich Schneider Velten, Luca Amendola, Christian Marinoni, Cornelius Rampf, Oliver Piattella, para avaliar a defesa de tese de doutorado da aluna Raquel Emy Fazolo, com o tema: "Testing clustering dark energy models with the skewness of matter distribution". Presentes os membros da banca e o examinado, o presidente deu início à sessão, passando a palavra ao candidato. Após exposição de 50 minutos por parte do examinando, o senhor presidente retomou a palavra e a cedeu aos membros da banca, um a um, para procederem à arguição. Em seguida, o senhor presidente colocou em off-line todo o público externo para que a banca pudesse deliberar. Ao final das deliberações o presidente da sessão convocou o doutorando e os interessados via online; com a palavra, o presidente da banca leu a decisão que resultou na aprovação da examinada. O senhor presidente, então, deu por encerrada a sessão, e eu, Rubia Nascimento, secretária do Programa de Pós-Graduação em Astrofísica, Cosmologia e Gravitação, lavrei a presente ata, que é assinada pelos membros da banca examinadora. Vitória, 10 de outubro de 2022.

Prof. Dr. Hermano Endlich Schneider Velten (UFOP/PPGCOSMO, orientador, presidente da banca)

Documento assinado digitalmente
gov.br HERMANO ENDLICH SCHNEIDER VELTEN
Data: 21/10/2022 14:00:05-0300
Verifique em https://verificador.iti.br

Prof. Dr. Luca Amendola (Heidelberg/PPGCOSMO, co-orientador)

Prof. Dr. Oliver Fabio Piattella (Università degli Studi dell'Insubria/Italy)

Documento assinado digitalmente
gov.br OLIVER FABIO PIATTELLA
Data: 18/10/2022 18:44:33-0300
Verifique em https://verificador.iti.br

Prof. Dr. Christian Marinoni (CPT-Marseille)

Prof. Dr. Cornelius Rampf (Universidade de Viena/Áustria)

UNIVERSIDADE FEDERAL DO ESPÍRITO SANTO

PROTOCOLO DE ASSINATURA

O documento acima foi assinado digitalmente com senha eletrônica através do Protocolo Web, conforme Portaria UFES nº 1.269 de 30/08/2018, por
VALERIO MARRA - SIAPE 2179379
Departamento de Física - DF/CCE
Em 31/10/2022 às 13:18

Para verificar as assinaturas e visualizar o documento original acesse o link:
https://api.lepisma.ufes.br/arquivos-assinados/594314?tipoArquivo=O

Abstract

This work aims to test clustering dark energy with the cosmological skewness, the third statistical moment of the matter density distribution. Usually, dark energy is treated as a cosmological constant or a fluid with negative pressure that has the properties to accelerate the cosmic background expansion. We start our analysis by explaining the standard treatment about dark energy, then cosmological perturbations are introduced. In general relativity it is not trivial to work with higher order perturbations so we make a transition to the Neo Newtonian cosmology, using the fluid dynamics equations that are equivalent to the general relativity ones to a good approximation. We then studied the cosmological skewness in two approaches: the single-fluid and two-fluid analysis. In the first approach, we model the universe as an effective single fluid where the dark energy background contributions and perturbations are included via the total equation of state parameter. This is indeed a very simplified attempt, but this analysis was useful to provide preliminary hints about how dark energy affects the skewness of matter distribution. We then apply a more general approach, modeling the universe as two non-interacting components, pressureless matter and dark energy which is a more realistic scenario. The single fluid analysis shows a great increase in skewness when including the clustering dark energy terms. This can be explained by including the terms directly in the matter equation, not just as an additional source for the gravitational field. The two fluid model results show values around the standard cosmological ones. Tests are performed to probe the skewness dependence with the cosmological parameters. Until this work, only an expression for the skewness as a function of the matter density parameter Ω_{m0} was available in the literature. We go beyond introducing several fits for the cosmological skewness value as a function of the dark energy equation of state w_{de} and the dark energy speed of sound c^2_{de}. This result has been presented in the literature for the first time. In order to check the consistency of our results, we finish with an observational analysis using CFHTLS-Wide data. Whereas the current available data is not enough to promote the skewness to the status of a precise cosmological test, further analysis and observations are indeed needed to make skewness a better tool to study dark energy models in the future.

Keywords: cosmology, dark energy, structure formation, cosmological perturbations, clustering dark energy, skewness.

Resumo

Este trabalho tem como objetivo testar o aglomeramento da energia escura com o skewness (assimetria) cosmológico, o terceiro momento estatístico da distribuição da densidade da matéria. Normalmente a energia escura é tratada como uma constante cosmológica ou um fluido com pressão negativa que tem as propriedades de acelerar a expansão do fundo cósmico. Começamos nossa análise explicando o tratamento padrão sobre energia escura, então as perturbações cosmológicas são introduzidas. Na relatividade geral não é trivial trabalhar com perturbações de ordem superior então fazemos uma transição para a cosmologia Neo-Newtoniana, usando as equações da dinâmica dos fluidos que são equivalentes às da relatividade geral por uma boa aproximação. Estudamos então o skewness cosmológico em duas abordagens: a análise de fluido único e a análise de dois fluidos. Na primeira abordagem, modelamos o universo como um fluido único efetivo, onde as contribuições e perturbações de fundo de energia escura são incluídas através da equação total do parâmetro de estado. Esta é realmente uma tentativa muito simplificada, mas esta análise foi útil para fornecer dicas preliminares sobre como a energia escura afeta o skewness da distribuição da matéria. Em seguida, aplicamos uma abordagem mais geral, modelando o universo em duas componentes que não interagem, matéria sem pressão e energia escura, que é um cenário mais realista. A análise de fluido único mostra um grande aumento na assimetria ao incluir os termos de energia escura de aglomeração. Isso pode ser explicado incluindo os termos diretamente na equação da matéria, não apenas como uma fonte adicional para o campo gravitacional. Os resultados dos dois modelos de fluidos mostram valores em torno dos cosmológicos padrão. Testes são realizados para sondar a dependência da assimetria com os parâmetros cosmológicos. Até este trabalho apenas uma expressão para a assimetria em função do parâmetro de densidade de matéria Ω_{m0} estava disponível na literatura. Vamos além introduzindo vários ajustes para o valor do skewness cosmológico em função da equação da energia escura do estado w_{de} e da velocidade da energia escura do som c_{de}^2. Este resultado foi apresentado pela primeira vez na literatura. Para verificar a consistência de nossos resultados finalizamos com uma análise observacional usando dados do CFHTLS-Wide. Considerando que os dados atuais disponíveis não são suficientes para promover o skewness ao status de um teste cosmológico preciso, análises e observações adicionais são realmente necessárias para tornar a assimetria uma ferramenta melhor para estudar modelos de energia escura no futuro.

Palavras-chave: cosmologia, energia escura, formação de estruturas, perturbações cosmológicas, aglomeração de energia escura, assimetria.

Acknowledgments / Agradecimentos

First I would like to thank my supervisor, Hermano Velten. Since my undergraduate days, he has been my advisor in cosmology and in life. His passion for physics and work is inspirational, having always great ideas for research in several areas and his knowledge in many areas of cosmology has always amazed me. I will always be grateful for your patience and teaching during these many years. I will always be rooting for your success and that your team (Flamengo) always wins more and more!
To my co-advisor Luca Amendola, thank you for the opportunity to meet and work in the amazing city of Heidelberg. Your care, fun lunches, and meetings together will always be cherished, even the ones online after coming back to Brazil. Thank you for always having an open door, for the respect and to make me feel at home while I stayed very far from my family in Germany. Your knowledge and passion will always be an inspiration.
I would like to mention some special teachers that are part of the Cosmo-UFES group that saw me grow from my undergraduate days to today. Professors Davi Rodrigues, Valerio Marra, Wiliam Ricaldi, and Julio Fabris, thank you for your companionship and teaching during all these years. Thank you Julio Fabris for your strength and leadership in the PPGCosmo program that made possible this thesis. I would like also to mention professor Oliver Piattella that taught me during all these years and made me company while I was in Heidelberg. Thank you for your care, friendship and dedication.
To my dear friends from UFES/PPGCosmo specially Guilherme Brando, Rahima Mokeddem, Renan Oliveira, and Eunice Omwoyo. To David Camarena and Leonardo Giani, for the good times in Heidelberg. Thank you David for being my family there and for the amazing foods and travels enjoyed together in Heidelberg.
To the dear cosmology group during my time in Heidelberg, Ana Marta, Manuel Wittner, Prajwal Hassan, Adrià Gómez-Valent, Giorgio Laverda, Arvid Weyrauch, Maya Hager, thank you for the nice moments in the office, helping me with my silly questions, for teaching me Durak and many other games during the breaks.
To my boyfriend/husband Syrios, making 9 years together now since we got close by both working with Hermano in 2013. Thank you for being my happiness and my greatest physicist of all time. Your strength and fight to become a researcher, your love for science, and willing to pass this knowledge to other people just make me admire you more. Thank you for always being by my side.
To my dear sister Silvia Fazolo and my dear mother-in-law Terezinha de Jesus, thank you always for your love and support.
To my online friends from Vai Ser Fácil discord, Discord Secreto do M and The Horde.
To my cats Bellatrix, Bigode, and Kerr, for being the best cats in the universe.
And finally to FAPES for my Ph.D. scholarship in Brazil, and CAPES for the financial support during my time abroad in Heidelberg.

Dedicated to my dear mother Verginia Yoshie Fazolo, my guardian angel.

"Stand tall, my friend/May all of the dark deep inside you find light again/This time, tumbling, turning, we make amends/Eternal winds from the land ascend/Here to lift us that we won't end"
Song: Tomorrow and Tomorrow - Final Fantasy XIV: Shadowbringers

Scientific Contributions

In 2013 during my undergraduate period, I started my studies in the cosmology area. I published my first paper before graduating in the year 2015 named *"Large-scale structure and integrated Sachs-Wolfe effect in decaying vacuum cosmology"* [1], which would start my interest in alternative dark energy models. My monography for the conclusion of the physics course was named *"Uma introdução às perturbações cosmológicas"* (An introduction to cosmological perturbations) where I presented an introduction to cosmological perturbations using general relativity and focused on obtaining the Boltzmann equations for the relevant components of the universe. During my master's studies I have published two other papers *"Revealing the nonadiabatic nature of dark energy perturbations from galaxy clustering data"* [2] and *"Degeneracy between nonadiabatic dark energy models and - CDM : Integrated Sachs-Wolfe effect and the cross correlation of CMB with galaxy clustering data"* [3] where the focus was to investigate dark energy models with nonadiabatic perturbations, these two works were the main theme of my master dissertation. This thesis is based on the works produced during my Ph.D. Both works have been published in Physical Review D namely, *"Skewness of matter distribution in clustering dark energy cosmologies"* [4] and *"Skewness as a test of dark energy perturbations"* [5].

Contents

List of Figures

List of Tables

Introduction

1.1 Introduction

To fully describe our universe we firstly need a theory for gravitational interaction and our standard choice is general relativity. We then describe the cosmic expansion with a homogeneous, isotropic, and expanding metric, also called the FLRW (Friedmann-Lemaître-Robertson-Walker) metric. The next step is to include the universe's matter/energy components. Of course, it is mandatory the inclusion of the standard particle model building blocks. But in cosmology, the contribution of all known particles is summarized in terms of the baryonic matter and radiative components (photons and neutrinos). Due to vast compelling observational evidence, we also need to add a dark sector in the matter-energy content of the universe. The dark matter is fundamental to explain astrophysical configurations like galactic rotation curves and galaxy cluster virial dynamics. But, it is really important to assume its existence in order to correctly explain the structure formation of the universe in a large scale. This component interacts with ordinary matter only via gravitation and we would not be able to explain the observed large scale structure.

The picture described above became insufficient in the last couple of decades. The study of the late time background expansion of the universe became mainly focused on the possible existence of a new cosmic component, dark energy (DE), responsible for accelerating the current expansion rate. Firstly comproved with supernova type Ia studies in the projects *Supernova Cosmology Project* in 1997 by Perlmutter et al. [8] and *High-Z Supernova Search Team* [9] in 1998 by Riess et al., the accelerated expansion is one of the key focus of modern cosmology. The cosmological constant Λ became the main candidate to explain this accelerated expansion phase, but it is also important to mention that a dynamical dark energy field remains a possibility as well as modified gravity.

Among many observational projects/surveys designed and implemented in the last two decades, one of the currently most important astronomical projects, the DES (Dark Energy Survey) [10], published its first results at the beginning of the year of 2018, with its main focus on the cosmic acceleration through observations of the structures in the universe, its geometry, and its expansion rate. This is the era of precision in cosmology and with it, several cosmological models have been put to the test. Although the standard cosmological model shows much success there are some disagreements related to the dark sector, in particular the dark energy phenomena. For example the *cosmological constant problem* [11] and the *cosmic coincidence problem* [12] still bring discussion in the community. There are also measurements made by Planck [13] where i.e. grosso modo less structures than the expected by the standard model have been reported. This can also be related to the dark energy, since the accelerated expansion impact the structure formation process in an opposite way compared to the gravitational clustering of matter.

If we want to go beyond the analysis of dark energy through the background, it is fundamental

to extend our study and focus on the perturbative level and properly incorporate dark energy as both a fluid with negative pressure and eventually also being able to cluster. But the latter does not occur if dark energy happens in the form of a cosmological constant Λ. For this reason, in this work, we also studied a dynamical dark energy component assuming an approach in which it can agglomerate. This possible perturbation in the dark energy sector of course have not any signatures at early times. By early times we mean the history of the universe as usual, where the big bang was followed by inflation and as our universe gets colder it passed through radiation domination. Later on, matter dominates and today the universe experiences a transition to an accelerated phase where dark energy dominates with 70% of the current universe content. It is in this latter moment that dark energy signatures can manifest. Then, this study will focus on late time events where we can use large scale structures to see the influences of dark energy and its perturbations. Then, our analysis focus on the use of skewness of the matter density cosmic field. With this quantity, we can assess the asymmetry in the distribution (or departures from a Gaussian distribution), usually used in statistics, also known as the third moment S_3. Using the skewness for the distribution of the density contrast of matter δ_m we can study the influence of dark energy both via its background effects as well as by including its perturbations. The latter contribution is parameterized by the dark energy speed of sound parameter.

We will employ in this thesis two different settings: an effective single fluid universe and a two fluid universe. The single fluid analysis would bring the matter and dark energy together. This has some consequences on the interpretation of how the skewness can be calculated. For the two fluid analysis, the dark energy fluid is separated from the matter content and would have its own perturbative equation.

Besides using skewness and evaluating some dark energy models, we also expand our analysis by considering dark energy perturbations, where its content can be clustered. We compare cases with and without this clustering dark energy contribution and also provide some interesting fits, to connect the skewness with other cosmological parameters, not usually set in the literature.

This work will be organized as follows: Chapter 2 introduces some basics around the background cosmology of our universe and also introduces general relativity. Chapter 3 focuses on the perturbative analysis, where we provide a detailed deviation of the Newtonian gauge and do other perturbative analyses with the Einstein equations. We also justify the use of a Neo Newtonian cosmology instead of the general relativity approach and finalize with some introduction to clustering dark energy. Next in chapter 4, we show the analysis of the skewness generated by a single fluid universe with effective negative pressure. Chapter 5 introduces the analysis of the skewness in a two-fluid model. This is a more general method where we also provide new fits for the skewness of matter distribution as a function of the cosmological parameters. And finally, the conclusions are set in the next chapter. The results are based on the papers [4] and [5].

The cosmic expansion and dark energy

In this chapter, it is introduced some fundamentals about cosmology towards the focus of my work with dark energy, structure formation, and skewness of the matter density field.

From the basics of general relativity, we aim to show the entanglement between structure formation and the universe's accelerated expansion today. All of these tools will also contribute to the fundamental cosmological perturbation theory that will be shown in more detail in a future chapter.

2.1 General Relativity and the universe expansion

The astronomer Edwin P. Hubble (1929) [14], revealed through what became his diagram that distant galaxies are getting further away from us with velocities that are proportional to their distances:

$$v = H \times d, \tag{2.1}$$

where H as seen in the above expression is the local Hubble constant that is measured through observational data and today its value is given around $H_0 \approx 70 kms^{-1}Mpc^{-1}$.

The scalar expansion function defines how the scale factor varies with time:

$$H(t) = \frac{da/dt}{a}, \tag{2.2}$$

where $a(t)$ is the scale factor that was introduced in cosmology to parameterize the universe's expansion. This parameter helps us to work with distances that were smaller in the past and are continuously increasing with time, i.e. the physical distance will be proportional to the scale factor and we define its today's value as $a(t_{today}) = 1$.

Almost everything in the Universe appears to be moving away from us and the further away, the more rapid the recession observed in the object. We can also measure this with the redshift. The redshift is "basically" the Doppler effect applied to light waves. If a galaxy is moving away from us, a movement caused by the universe's expansion, its emitted wavelength gets extended, so we observe a wavelength bigger than the emitted one having a lower frequency. This effect is called cosmological redshift. Since for blue light we have a higher frequency, this means the wavelength is more compressed. Then, if an object is moving toward us we observe a blueshift. For example, M31 is blueshifted.

In cosmology, we associate this redshift with the scale factor in relation to the wavelength emitted and observed. The redshift z is defined as:

$$1 + z \equiv \frac{\lambda_{obs}}{\lambda_{emit}} = 1/a. \tag{2.3}$$

We use the scale factor and redshift as measurements of time since both are related to the proper time t. From the definitions, the redshift for today assumes $z_0 = 0$.

2.1.1 The Einstein Equation

In General Relativity, the metric is a function that defines the distance between two points in space. i.e. with it, we can transform distances between coordinates into physical distances. The metric that describes a homogeneous and isotropic universe in expansion is the Friedmann-Lemaître-Robertson-Walker (FLRW) metric:

$$g_{\mu\nu} = \begin{pmatrix} -1 & 0 & 0 & 0 \\ 0 & a^2(t) & 0 & 0 \\ 0 & 0 & a^2(t) & 0 \\ 0 & 0 & 0 & a^2(t) \end{pmatrix}, \tag{2.4}$$

where μ and ν represent the 4 coordinates (1 of time and 3 of space). For only spatial coordinates, we use the i, j, k indexes.

The line element with this metric in spherical coordinates is defined as:

$$ds^2 = -dt^2 + a^2(t)\left(\frac{dr^2}{1-kr^2} + r^2 d\theta^2 + r^2 sin^2\theta d\phi^2\right), \tag{2.5}$$

where we are using $c = 1$ for the speed of light in our calculations.

For the geometry of the universe we could consider hyperbolic $k = -1$, flat $k = 0$ or spherical $k = +1$ cases. The flat universe follows the rules of Euclidean geometry and the idea that parallel lines remain separated by the same distance. Strong observation evidences, such as the localization of the first peak in the angular power spectrum of the Cosmic Microwave Background (CMB) have indicated that a flat universe is preferred giving us a value for the curvature parameter very near zero [15], [13]. So in this work, we will consider a flat universe where k (the curvature parameter) is zero.

The famous equation that relates the curvature of spacetime and the matter-energy distribution in the universe is the Einstein equation:

$$G_{\mu\nu} \equiv R_{\mu\nu} - \frac{1}{2} g_{\mu\nu}\mathcal{R} = 8\pi G T_{\mu\nu}, \tag{2.6}$$

where $G_{\mu\nu}$ is the Einstein tensor (measures the "curvature of spacetime") and $T_{\mu\nu}$ is the energy-momentum tensor (measures the "quantity and properties of matter" in the universe). By inserting the FLRW metric into this equation one has a description of the dynamics of the universe.

The Einstein tensor is composed by the Ricci tensor $R_{\mu\nu}$ and its scalar $\mathcal{R}$, that by definition depend on the metric and its derivatives:

$$R_{\mu\nu} = \Gamma^{\alpha}{}_{\mu\nu,\alpha} - \Gamma^{\alpha}{}_{\mu\alpha,\nu} + \Gamma^{\alpha}{}_{\beta\alpha}\Gamma^{\beta}{}_{\mu\nu} - \Gamma^{\alpha}{}_{\beta\nu}\Gamma^{\beta}{}_{\mu\alpha} \tag{2.7}$$

where $\Gamma^{\alpha}{}_{\mu\nu}$ are the Christoffel symbols defined as

$$\Gamma^{\mu}{}_{\alpha\beta} = \frac{g^{\mu\nu}}{2}\left[\frac{\partial g_{\alpha\nu}}{\partial x^{\beta}} + \frac{\partial g_{\beta\nu}}{\partial x^{\alpha}} - \frac{\partial g_{\alpha\beta}}{\partial x^{\nu}}\right]. \tag{2.8}$$

For a universe in expansion, we can apply the FLRW metric and obtain the following values for the Ricci tensors and its scalar

$$\begin{aligned} R_{00} &= -3\frac{\ddot{a}}{a}, \\ R_{0i} &= 0, \\ R_{ij} &= \delta_{ij}[2\dot{a}^2 + a\ddot{a}] \\ \mathcal{R} &= g^{\mu\nu}R_{\mu\nu} = 6\left[\frac{\ddot{a}}{a} - \left(\frac{\dot{a}}{a}\right)^2\right]. \end{aligned} \tag{2.9}$$

For the right hand side of Einstein's equation, the energy-momentum tensor is defined through the flux of energy density and momentum in spacetime. Treating the universe as a fluid with energy density ρ and pressure p, the energy momentum tensor is described by the following components

$$T_{\mu\nu} = (\rho + p)u_\mu u_\nu + p g_{\mu\nu}, \tag{2.10}$$

where u_μ is a 4-vector.

When solving Einstein's equation for the time and space quantities, one can obtain the Friedmann's equations

$$H^2 = \frac{8\pi G\rho}{3}, \tag{2.11}$$

$$\frac{\ddot{a}}{a} = -\frac{4\pi G}{3}(\rho + 3p), \tag{2.12}$$

where $G = 6.6743 \times 10^{-11} m^3 kg^{-1} s^{-2}$ is the gravitational constant. By conserving the energy-momentum tensor $T^{\mu\nu}{}_{;\mu} = 0$, a consequence of the Bianchi identities, we obtain the continuity equation

$$\dot{\rho} + 3H(\rho + p) = 0. \tag{2.13}$$

The above set of equations describes the FLRW dynamics of a flat universe seen as composed by a single perfect fluid. These are considered to be the background equations. It is worth noting that one can expand the analysis of the cosmic dynamics to other levels such as the cosmological perturbations that are introduced later in this thesis. Until this point, we also did not mention how to implement the current accelerated expansion of the universe in the above equations. For this, we need to add a cosmological constant known as Λ or consider the inclusion of a fluid with negative pressure.

2.2 The Standard Model and Dark energy

Now that we have described the dynamics of the universe and using the tools of time and distances described by the redshift (or scale factor), it is possible to understand the history/timeline/evolution of the universe.

Before describing this timeline, we must define what our universe is made of. Let us consider then radiation, baryonic matter, cold dark matter, and dark energy as our elements. These include in general neutrinos, photons, protons, neutrons, electrons, and the dark sector. In the dark sector, the dark matter is used to explain the amount of structures observed today and can also be used to explain galaxy rotations and other astrophysical observations. Dark energy

is used to explain the current accelerated expansion of the universe. This of course also affects the current quantity of structures being formed since the accelerated expansion goes against the expected clustering gravitational forces of the matter content of the universe.

Treating our universe as a fluid allows us to associate an equation of state parameter for each component. This parameter is defined as follows

$$w = \frac{p}{\rho}. \tag{2.14}$$

Effectively, for each component the following values are assumed: for matter (baryonic and CDM) $w_m = 0$, radiation $w_r = 1/3$ and for standard dark energy (cosmological constant like behavior) $w_{de} = -1$ where a negative pressure brings the accelerated expansion. The latter is the value used for dark energy in the standard model of cosmology ΛCDM. In the case of Λ domination, its evolution behaves as a scenario with constant density. It is good to remind that the cosmological constant contribution $\Lambda g_{\mu\nu}$ can be added to the left hand side of the Einstein's equation if it is seen as a geometrical quantity. On the other hand, we can apply the fluid conception and add it as a fluid component on the right hand side of Einstein's equation entering into the energy-momentum tensor components. This thesis will mainly work with the fluid definition to study dark energy models in further chapters.

By solving the continuity equation Equation 2.13 for a non-interacting component with equation of state given by Equation 2.14 one finds

$$\rho_x = \rho_0 \left(\frac{a}{a_0}\right)^{-3(1+w_x)}. \tag{2.15}$$

Using the respective equation of state parameters for each case gives

$$\begin{aligned} \rho_m &\propto a^{-3} \\ \rho_r &\propto a^{-4} \\ \rho_{de} &\propto constant. \end{aligned} \tag{2.16}$$

These relations can be used to see how each component density scales (or remain constant) with time.

Figure 2.1: Evolution of each density over time. Starts with a radiation era, followed by the equivalence time between matter and radiation, the matter era, and finally the accelerated expansion where dark energy dominates.

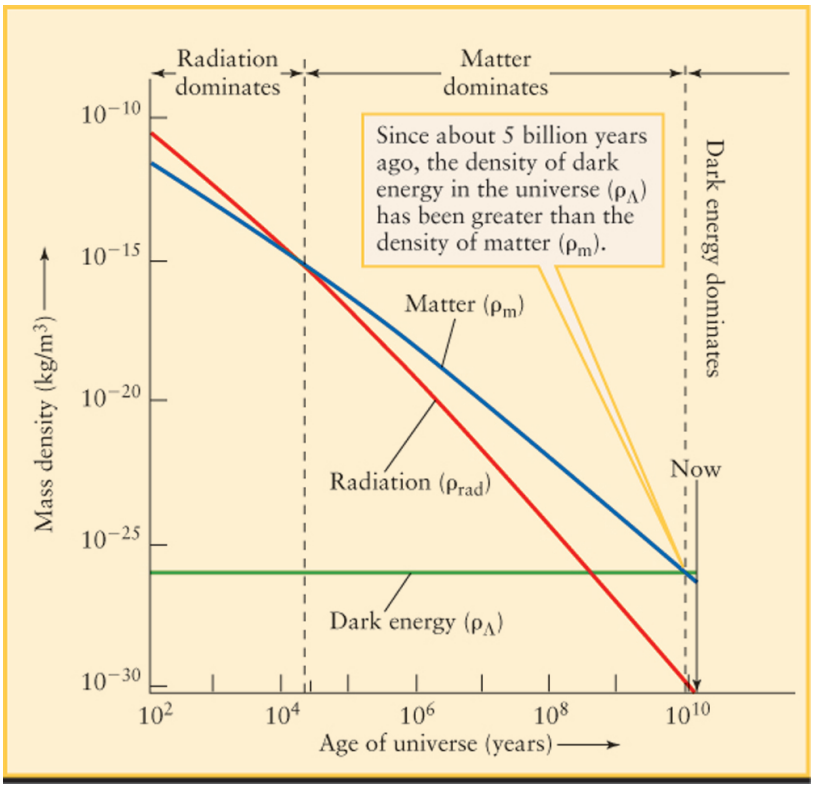

Source: https://sites.ualberta.ca/~pogosyan/teaching/ASTRO_122/lect30a/lecture30a.html

We can observe in Figure 2.1 the relations found in Equation 2.16 with appropriate values for their today's densities adopted following the standard cosmology. Radiation dominates the early universe but it scales faster with time. Next, it is followed by an equivalence era of radiation and matter that happened around a $z_{eq} \sim 3300$. Then one arrives at the matter dominated era scaling with $\sim a^{-3}$. This epoch is fundamental for structure formation. Recently, (around $z \sim 0.55$) the dark energy dominates the cosmic expansion and we observe the accelerated expansion of the universe.

The background dynamics of the standard cosmological model can be represented by the acronym ΛCDM. At late times it is effectively composed by the dark energy represented by Λ, cold dark matter (CDM), and ordinary matter. But radiation contributes to early times. This model is the most successful in explaining the history of our universe. Some of its fundamental ideas are the cosmic inflation, the cosmological principle (hypothesis that the universe is isotropic and homogeneous on large scales), and the inclusion of the dark sector.

Dominating around 70% of the total universe energy today, the idea of dark energy represents one of the main research areas currently. Figure 2.2 shows the values of each component for today. We can see that the current contribution of photons and neutrinos are negligible. The first observational evidence for this accelerated expansion came from measurements of supernovae type Ia [8], [9], showing that the universe was not expanding at a constant rate or decelerating.

Since then more and more measurements such as Cosmic Microwave Background, gravitational lensing, and late time large scale structure patterns corroborate to this model.

Figure 2.2: Current representation of the total energy of the universe. It is visible the domination of the dark energy component, followed by dark matter and the atoms that are a reference to elemental particles or as usually called baryonic matter.

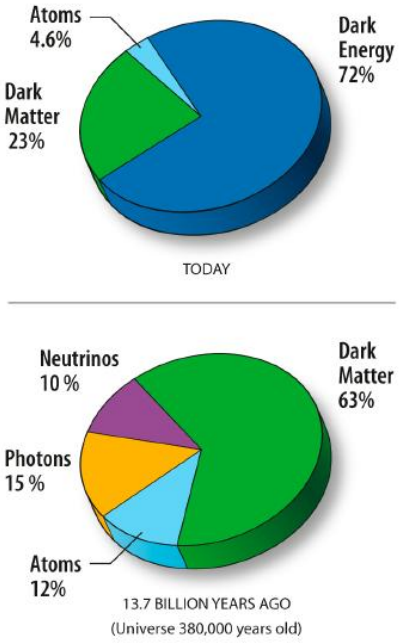

Source: https://wmap.gsfc.nasa.gov/universe/uni_matter.html

Although very promising, the dark energy does not escape from problems in its theory. In the cosmological constant problem [11], [16], the dynamical behavior of the vacuum energy theory in quantum field theory gets in disagreement with Λ values obtained from cosmology. This difference can be as large as 123 orders of magnitude.

The cosmic coincidence problem also is attributed to the dark energy [12], [17]. This problem regards about the current equivalence, in orders of magnitude, of the dark energy and dark matter densities. As mentioned before and looking into Figure 2.1, around $z \sim 0.55$ the matter (dark plus baryonic) and the dark energy densities were in a moment of equability. But why the dark energy had started its domination and why just recently these effects of accelerated expansion had begun is still a mystery.

With so many things yet to discover and wondering why we can not detect dark energy directly, the dark energy became a very strong field of research. This has opened in the last couple of decades many ways to investigate possible other models and also other modified gravity theories. Relying on the GR description for the gravitation interaction, in this thesis we will focus on dark energy models, testing different models with the help of higher order perturbation theory which will be more detailed in the next chapter.

For now, let us go back to the background equations found with the Einstein equations. To obtain the Friedmann equations for the ΛCDM model, one can describe the expansion rate of

the universe as a function of its components

$$\frac{H^2(a)}{H_0^2} = \frac{\Omega_{r0}}{a^4} + \frac{\Omega_{b0}}{a^3} + \frac{\Omega_{dm0}}{a^3} + \Omega_{de}. \tag{2.17}$$

The expression above uses the component's dynamical behavior as described in Equation 2.16 and the density parameters Ω that are defined by the density of each component divided by the today's critical density of the universe $\rho_{cr}(t_0) \approx 1.88h^2 \times 10^{-26} kgm^{-3}$, giving us ρ/ρ_{cr}. This parametrization allows us to have a total density of 1 when all the density parameters are summed $\Omega_{r0} + \Omega_{b0} + \Omega_{dm0} + \Omega_{de} = 1$.

Now that we have all this information about the components and how they evolve in time, we can start to understand in more detail Figure 2.3, that represents a timeline of the universe. According to the standard cosmological model, it starts with the Big Bang singularity where the universe was in a state of high temperature being very compact and with high energy. It follows the cosmic inflation where we have a rapid expansion. This increases extremely the scale factor and allows for the universe to get colder faster. After exiting from inflation, the universe keeps expanding and getting colder, but is still too hot to be observed, trapping the photons in this hot dense chaos where they are strongly coupled to the electrons due to the Thompson scattering. After the transition from the radiation domination era to the matter domination, the temperature keep decaying with the cosmic expansion at a rate of $T \sim a^{-1}$ and then around 380.000 years after the Big Bang, the photons are finally released as the first atoms were formed. These steps are called decoupling and recombination, respectively. This happens around $z = 1000$, where the Cosmic Microwave Background is released, traveling with almost no further interaction until its observation today. Such observations provide us with important information, including, the geometry of the universe, as discussed before, and also about its isotropic properties [15]. Even dark energy properties can be studied via the Integrated Sachs-Wolf effect.

Figure 2.3: Universe timeline showing each phase of the cosmic evolution, from Big Bang to today. The estimated age of the universe is 13,8 billion years.

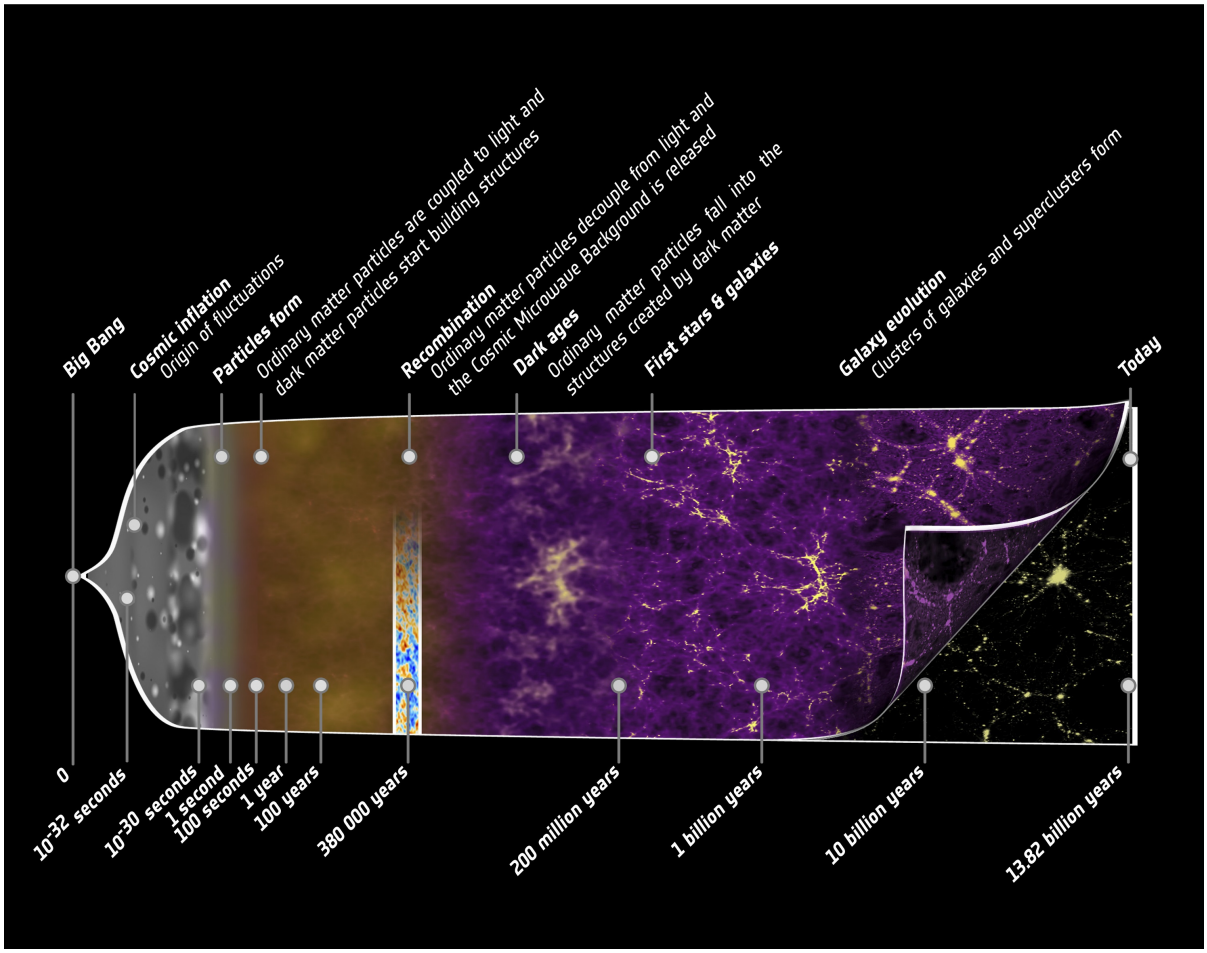

Source: https://www.nasa.gov/mission_pages/planck/multimedia

Inflation theory is necessary since it connects points that would be casually disconnected at CMB epoch. Inflation also provides a satisfactory solution for other problems. See a review in [18]. Inflation can also be connected to the CMB temperature fluctuation patterns. For structure formation, inflation is seen as the source for the primordial seeds for the large scale structure.

Following the universe's timeline, it is useful to see also in Figure 2.4 how perturbations have evolved. This figure helps us to understand how the universe has started in a very homogeneous and isotropic shape that has evolved until the large scale structure observed today where the structures are formed. One understands this picture using cosmological perturbation theory where it is inserted a small perturbation around physical quantities like densities, velocities, and potentials that are allowed to evolve over time. In this figure, radiation i.e., photons (*gamma*) and relativistic neutrinos (*ur*) have an oscillatory and decaying behavior. Cold Dark matter (*cdm*) starts to form its "wells" of gravitational potentials well before the decoupling. Baryonic matter (*b*) falls into the dark matter potential wells after decoupling from the radiation content. With this theory, we can explain how the structures observed today are formed from a previous homogeneous universe. Then, dark matter is a fundamental component to accelerated the clustering of baryonic structure. In this picture dark energy plays no role at all. Dark energy usually

is not treated as a component that could cluster. As a cosmological constant, it is inserted to explain the accelerated expansion at late times. As the cosmological constant is not the final answer for the dark energy phenomena, we will be interested in this thesis to treat dark energy as a fluid that can be perturbed and clustered, using late time large scale structures to test such approach.

Figure 2.4: Density contrast ($\delta = \delta\rho/\rho$)x conformal time. Each universe component is represented being gamma the photons, ur relativistic neutrinos, b baryonic matter, and cdm cold dark matter.

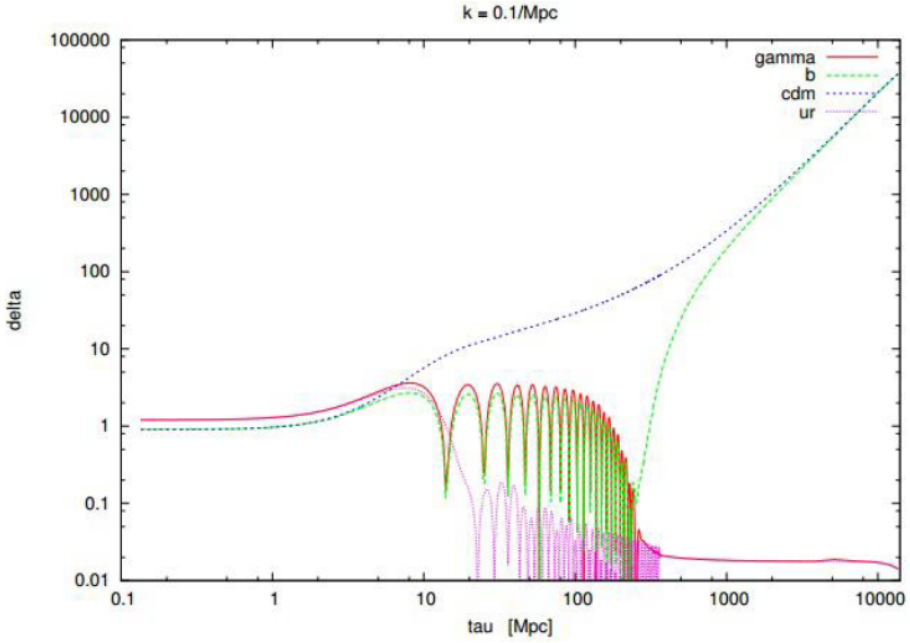

Source: CAMB code files [19].

Returning to Figure 2.3 we can finally understand what happens after CMB with help of Figure 2.4. Small structures begin to form and evolve to the point that larger structures and voids are formed. This process takes place continuously until more recent times when dark energy dominates the background expansion going against these process. This can leave observational imprints in the large scale structure. Next, we shall enter more deeply in the cosmological perturbations even going to higher orders to show how this is going to be used to test dark energy.

Cosmological perturbation theory

The goal of this chapter is to introduce some basics about cosmological perturbations that will be needed in this thesis. We start by presenting the formulation for the scalar perturbations in the general relativistic theory. However, since our final goal is to study higher order statistics of the cosmic density field via the skewness moment we have to go beyond the first order terms in perturbation theory. This is not so easy in the full relativistic theory. Therefore, we will introduce the Neo Newtonian cosmology and its perturbations. The latter is a reasonable approximation for the matter's scalar perturbations and will be used further in this thesis. Indeed, in the next chapters, we will calculate the skewness of the matter density field within a full non-relativistic theory i.e., the Neo-Newtonian approach.

3.1 Basics on the relativistic cosmological perturbation theory

Cosmological perturbation theory in general relativity is used to help us to understand how the universe evolved from a homogeneous and isotropic configuration until the point it has currently with inhomogeneities such as the large scale structures observed today. The idea is that by applying a small perturbation, let us say for example in the matter component, this allows to break the full homogeneity where overdense regions start to self attract gravitationally. This theory have extensive calculations, some will be provided here, but for a more deep insight is suggested the following books and papers [20], [21], [22], [23], [24], [25], [26].

In the previous chapter, we saw how we described our spacetime through the FLRW metric. The inhomogeneity in the distribution of matter in the relativistic fluid takes us to metric perturbations. Inserting these inhomogeneities is necessary to understand the structure formation and evolution. So let us use general relativity to describe this approach.

Considering small perturbations $\delta g_{\mu\nu}$ in the FLRW metric

$$\overline{g_{\mu\nu}} \to \overline{g_{\mu\nu}} + \delta g_{\mu\nu}, \tag{3.1}$$

and using conformal time $d\eta = dt/a$, the metric becomes

$$\overline{g_{\mu\nu}} dx^\mu dx^\nu = a^2(\eta)(-d\eta^2 + \delta_{ij} dx^i dx^j). \tag{3.2}$$

The metric perturbation can be characterized by three types: scalar, vector and tensor perturbations. In the δg_{00} the perturbation behaves like a scalar

$$\delta g_{00} = -2a^2\psi. \tag{3.3}$$

The components of the spacetime δg_{0i} part can be decomposed as a sum of the gradient of a scalar B and the vector S_i with null divergence. This will be better explained further

$$\delta g_{0i} = -a^2(B_{,i} + S_i). \tag{3.4}$$

Since δg_{ij} behaves like a tensor, we can decompose it with E as the scalar function, F_i a vector of null divergence, and the three-dimensional tensor h_{ij}

$$\delta g_{ij} = a^2(2\phi\delta_{ij}) - 2E_{,ij} + F_{i,j} + F_{j,i} + h_{ij}. \tag{3.5}$$

The terms ψ and ϕ introduced correspond to scalar functions for the metric perturbations.

To explain this structure of the perturbations it is used a tool that decomposes these perturbations in scalar-vector-tensor parts is called the Helmholtz theorem. In the same way as a three-dimensional vector can be decompose in a gradient of a scalar and a vector of null divergence

$$B_i = \underbrace{\partial_i B}_{scalar} + \underbrace{S_i}_{vector}, \tag{3.6}$$

with $\partial_i B_i = 0$.

Using the Helmholtz theorem for a symmetric tensor of rank-2, we can describe it as

$$H_{ij} = \underbrace{2\phi\delta_{ij} + 2E_{,ij}}_{scalar} + \underbrace{2F_{j,i}}_{vector} + \underbrace{2h_{ij}}_{tensor}, \tag{3.7}$$

where

$$\begin{aligned} E_{,ij} &\equiv \left(\partial_i\partial_j - \frac{1}{3}\delta_{ij}\nabla^2\right) E, \\ F_{j,i} &\equiv \frac{1}{2}\left(F_{j,i} + F_{i,j}\right). \end{aligned} \tag{3.8}$$

As previously described the vectors have null divergence $\partial^i F_i = 0$ and $\partial^i F_{ij} = 0$.

We also assume that the tensor perturbation has a null trace and is symmetric $h^i_i = 0$, $h^i_{j,i} = 0$. The decomposition of scalar-vector-tensor in the Einstein equations does not mix in linear order and can be treated separately.

Considering only scalar perturbations, the scalar perturbed metric becomes:

$$ds^2 = a^2[-(1+2\psi)d\eta^2 - 2B_{,i}\,dx^i d\eta + ((1+2\phi)\delta_{ij} - 2E_{,ij})dx^i dx^j]. \tag{3.9}$$

The metric perturbations are not defined uniquely but depend on the choice of coordinates or gauge choice. By choosing different gauges we can change the value of the perturbative variables. To obtain gauge invariant variables, we start by considering a change of coordinates $x^\mu \to \hat{x}^\mu$, $g_{\mu\nu} \to \hat{g}_{\mu\nu}$.

For this, we need to know how a four-vector transforms under coordinate changes

$$\begin{aligned} \hat{A}^\mu &= \frac{\partial x^\mu}{\partial \hat{x}^\rho} A^\rho, \\ \hat{A}_\mu &= \frac{\partial x^\rho}{\partial \hat{x}^\mu} A^\rho, \end{aligned} \tag{3.10}$$

where the partial derivatives form the transformation of coordinates matrices (Jacobian matrices). Notice that $\hat{}$ is going to be used for the transformed term.

The change of coordinates for the metric will then be

$$\hat{g}_{\mu\nu} = \frac{\partial x^\rho}{\partial \hat{x}^\mu}\frac{\partial x^\sigma}{\partial \hat{x}^\nu} g_{\rho\sigma} \to \hat{g}_{\mu\nu}\frac{\partial \hat{x}^\mu}{\partial x^\rho}\frac{\partial x^\mu}{\partial \hat{x}^\sigma} = g_{\rho\sigma}. \tag{3.11}$$

The change of coordinates given by $\hat{x}_\mu = x^\mu + \xi^\mu(x)$ for the metric becomes

$$\hat{g}_{\mu\nu}(x+\xi)\partial_\rho(x^\mu + \xi^\mu)\partial_\sigma(x^\nu + \xi^\nu) = g_{\rho\sigma}(x), \tag{3.12}$$

as $\hat{g}(x+\xi) = \hat{g}_{\mu\nu}(x) + \xi^\lambda \partial_\lambda g_{\mu\nu}(x)$ and $\xi^\lambda \partial_\lambda g_{\mu\nu} = \delta g_{\mu\nu}$. After some multiplication of terms and canceling second order terms (since the perturbations are considered very small), the transformed metric is given by

$$\hat{g}_{\rho\sigma}(x) = g_{\rho\sigma}(x) - g_{\rho\nu}\partial_\rho\xi^\nu - g_{\mu\sigma}\partial_\rho\xi^\nu - \xi^\lambda\partial_\lambda g_{\rho\sigma}. \tag{3.13}$$

For the $\hat{g}_{00}$ term, we have under the transformation of coordinates

$$\hat{\psi} = \psi - \dot{\xi}^0 - \frac{\dot{a}}{a}\xi^0. \tag{3.14}$$

In the same way for the other perturbative terms, we have for $g_{0i} \to \hat{g}_{0i}$

$$\phi \to \hat{\phi} = \phi + \frac{\dot{a}}{a}\xi^0. \tag{3.15}$$

Writing the space part of the infinitesimal vector $\xi^\rho \equiv (\xi^0, \xi^i)$ as $\xi^i = \xi^i_\perp + \zeta^{,i}$ where $\xi^i_\perp$ is a three-dimensional vector of null divergence $(\xi^i_{\perp},_i) = 0$) and ζ is a scalar function.

It is obtained the same way as for $\hat{\psi}$ and $\hat{\phi}$:

$$\begin{aligned} B \to \hat{B} &= B + \dot{\zeta} - \xi^0, \\ E \to \hat{E} &= E + \zeta. \end{aligned} \tag{3.16}$$

Since the terms ξ^0 and ζ contribute only to the transformation of scalar perturbations, choosing them properly we can set to zero two of the four functions ψ, ϕ, B, E. Manipulating the functions, for example by assuming $E \neq 0$ to eliminate $\hat{E} = 0$, we must simply choose $\zeta = -E$. Rewriting in a simpler way, the combination of these functions in a gauge invariant form is the expression known as Bardeen potentials [27]:

$$\Psi = \psi - \frac{1}{a}\frac{d}{d\eta}[a(\dot{E} + B)], \qquad \Phi = -\phi + \frac{\dot{a}}{a}(\dot{E} + B). \tag{3.17}$$

These equations can be used for the definition of different gauges, like the Newtonian gauge where B=0 and E=0:

$$ds^2 = a^2[-(1+2\Psi)d\eta^2 + (1+2\Phi)\delta_{ij}dx^i dx^j], \tag{3.18}$$

so that in this gauge $\Psi = \psi$ and $\Phi = -\phi$, here Ψ and Φ correspond to the Newtonian potential and Φ the perturbation to the spatial curvature, respectively.

Another famous gauge is the Synchronous gauge, making $\psi = 0$ and $B = 0$:

$$ds^2 = a^2[-d\eta^2 + ((1+2\Phi)\delta_{ij} - 2E_{ij})dx^i dx^j] \tag{3.19}$$

where $\Psi = \frac{1}{a}\frac{d}{d\eta}[a\dot{E}]$ and $\Phi = \phi - a\dot{a}\dot{E}$.

3.2 Perturbed Einstein Equation

For the following calculations, we are going to choose the Newtonian gauge. By the definition of the Christoffel symbol in Equation 2.8, the zero-th order properties for the FLRW metric are:

$$\begin{aligned}
\Gamma^0{}_{00} &= 0,\\
\Gamma^0{}_{0i} &= \Gamma^0{}_{i0} = 0,\\
\Gamma^0{}_{ij} &= \delta_{ij} a\dot{a},\\
\Gamma^i{}_{0j} &= \Gamma^i{}_{j0} = \delta_{ij}\frac{\dot{a}}{a}.
\end{aligned} \tag{3.20}$$

The perturbed Christoffel symbols are obtained by applying the perturbed metric Equation 3.18 resulting in

$$\begin{aligned}
\Gamma^0{}_{00} &= \frac{1}{a}\dot{\Psi},\\
\Gamma^0{}_{0i} = \partial_i\Psi &\xrightarrow{Fourier} ik_i\tilde{\Psi},\\
\Gamma^0{}_{ij} &= \delta_{ij}a^2(H + 2H(\Phi - \Psi) + \Phi_{,0}),\\
\Gamma^i{}_{00} = \frac{\Psi_{,i}}{a^2} &\xrightarrow{Fourier} \frac{ik^i\Psi}{a^2},\\
\Gamma^i{}_{j0} = \Gamma^i{}_{0j} &= \delta_{ij}(H + \Phi_{,0}),\\
\Gamma^i{}_{jk} = 2\delta_{ij}\partial_k\phi + 2\delta_{ik}\partial_j\Phi - \delta_{jk}\partial_i\Phi &\xrightarrow{Fourier} i\Phi[\delta_{ij}k_k + \delta_{ij}k_j - \delta_{ik}k_i].
\end{aligned} \tag{3.21}$$

In the results above, one must be careful since there are some approximations in the calculations, for example in terms like $g^{00} = 1/g_{00} = -\frac{1}{1+2\Psi} \sim -1 + 2\Psi$ and also we applied Fourier transformations.

The perturbed Ricci tensor and its scalar in similar calculations are:

$$\begin{aligned}
R_{00} &= -3\frac{d^2a}{dt^2}\frac{1}{a} - \frac{k^2}{a}\Psi - 3\Phi_{,00} + 3H(\Psi_{,0} - 2\Phi_{,0}),\\
R_{ij} &= \delta_{ij}\left[\left(2a^2H^2 + a\frac{d^2a}{dt^2}\right)(1 + 2\Phi - 2\Psi) + a^2H(6\Phi_{,0} - \Psi_{,0}) + a^2\Phi_{,00} + k^2\Phi\right] + k_ik_j(\Phi + \Psi),\\
\mathcal{R} &= 6\left(H^2 + \frac{d^2a}{dt^2}\frac{1}{a}\right) - 12\Psi\left(H^2 + \frac{d^2a}{dt^2}\frac{1}{a}\right) + \frac{2k^2}{a^2}\Psi + 6\Phi_{,00} - 6H(\Psi_{,0} - 4\Phi_{,0}) + \frac{4k^2}{a^2}\Phi.
\end{aligned} \tag{3.22}$$

Now we just need the perturbed energy-momentum tensor that is defined through the flux of energy and density in spacetime. Assuming the universe as a single fluid with density ρ and pressure p

$$T^0{}_0 = -(\rho + \delta\rho), \quad T^0{}_\alpha = (\rho + p)v_{,\alpha}, T^\alpha{}_\beta = (\rho + \delta p)\delta^\alpha_\beta + \Pi^\alpha_\beta,$$

where $\delta\rho$, δp, v are perturbations in the density, pressure, and scalar potential associated with the velocity respectively. The term Π^α_β is the anisotropic contribution (from shear viscosity for example) that we shall consider as zero.

Previously we saw the background solutions for the Einstein equations in the forms of Friedmann's equation, and the conservation of the energy-momentum tensor with the continuity equation. For scalar perturbations in the first order, the Einstein equations $(0-0, 0-i, i-j)$ results are

$$-\frac{\nabla^2}{a^2}\Phi + 3H^2\Phi + 3H\dot{\Phi} = -4\pi G\delta\rho, \tag{3.23}$$

$$H\Phi + \dot{\Phi} = 4\pi a(\rho + p)v, \tag{3.24}$$

$$3\ddot{\Phi} + 9H\dot{\Phi} + (6\dot{H} + 6H^2 + \frac{\nabla^2}{a^2})\Phi = 4\pi G(\delta\rho + 3\delta p) \tag{3.25}$$

In the equations above it is considered the $i-j$ traceless contribution, that lead us to $\Psi = \Phi$ due to $\Pi^{\alpha}_{\beta} = 0$. The conservation of the energy momentum tensor with perturbations is given in the form

$$\delta\dot{\rho} + 3H(\delta\rho + \delta p) = (\rho + p)\left(3\dot{\Phi} + \frac{\nabla^2}{a}v\right) \tag{3.26}$$

and for the conservation of momentum

$$\frac{[a^4(\rho + p)v]^{\cdot}}{a^4(\rho + p)} = \frac{1}{a}\left(\Psi + \frac{\delta p}{\rho + p}\right). \tag{3.27}$$

The perturbative cosmological theory can evaluate the evolution of structure formation with the definition of the density contrast $\delta = \delta\rho/\rho$. To reach its equation we need to make a combination of equations Equation 3.23-3.26. This is done to find an equation where the density contrast depends on the gravitational potential.

Transforming to Fourier space $\nabla^2 \to -k^2$ (where k is the wavenumber) and canceling second order terms, results in the following set of equations:

-Beginning with the relation of the total density contrast with the potential Φ

$$\delta = -\left(\frac{2k^2}{3a^2H^2}\right)\Phi - 2\Phi - 2\frac{\dot{\Phi}}{H}. \tag{3.28}$$

-Followed by the relation of the evolution of δ with the potential associated with the perturbed velocity v

$$\dot{\delta} = -3H\Theta + 3(1 + w)\dot{\Phi} - (1 + w)\frac{k^2}{a}v, \tag{3.29}$$

where we defined $\Theta = (c^2 - w)\delta$.

We can also find another equation through the (i-j) component from the Einstein equations

$$\Theta = \frac{2}{3H^2}[\ddot{\Phi} + H(4 + 3w)\dot{\Phi} + w\frac{k^2}{a^2}\Phi]. \tag{3.30}$$

And finally, the dynamics for the velocity term v is found through the Euler equation

$$\dot{v} = -vH(1 - 3w) - \frac{\dot{w}}{1 + w}v + \frac{1}{a}\left[\Phi + \frac{w}{1 + w}\delta + \frac{\Theta}{1 + w}\right]. \tag{3.31}$$

To obtain the equation for the total density contrast we can isolate v in Equation 3.28 and replace it in Equation 3.31 and ignoring second order terms the complete equation is

$$\ddot{\delta} + \dot{\delta}(2 - 3w)H + \frac{k^2}{a^2}w\delta + \frac{k^2}{a^2}(1 + w)\Phi = 3(1 + w)[\ddot{\Phi} + \dot{\Phi}(2 - 3w)H] + 3\dot{w}\dot{\Phi} - 3H\dot{\Theta} + \Theta\left[-\frac{k^2}{a^2} + \frac{3H^2}{2}(1 + 9w)\right]. \tag{3.32}$$

For the density contrast of matter, we have that $w = 0$ since the matter has zero pressure. Also taking the quasi-static limit, where the time derivatives of the potentials are neglected in relation to the spacial ones ($\ddot{\Phi} << \nabla^2\Phi$) we reach the final form

$$a^2\delta_m'' + \left(\frac{aH'}{H} + 3\right) a\delta_m' + \frac{k^2 H_0^2}{a^2 H^2(a)}\Phi = 0, \tag{3.33}$$

where ' represents the derivative in the scale factor a.

This same equation with time derivatives can be written as:

$$\ddot{\delta}_m + 2H\dot{\delta}_m - 4\pi G\rho_m\delta_m = 0. \tag{3.34}$$

Figure 3.1: Evolution of the matter density contrast ($\Delta = \delta_m = \delta\rho_m/\rho_m$) $\times$ a (scale factor) for Equation 3.33 adopting the ΛCDM background.

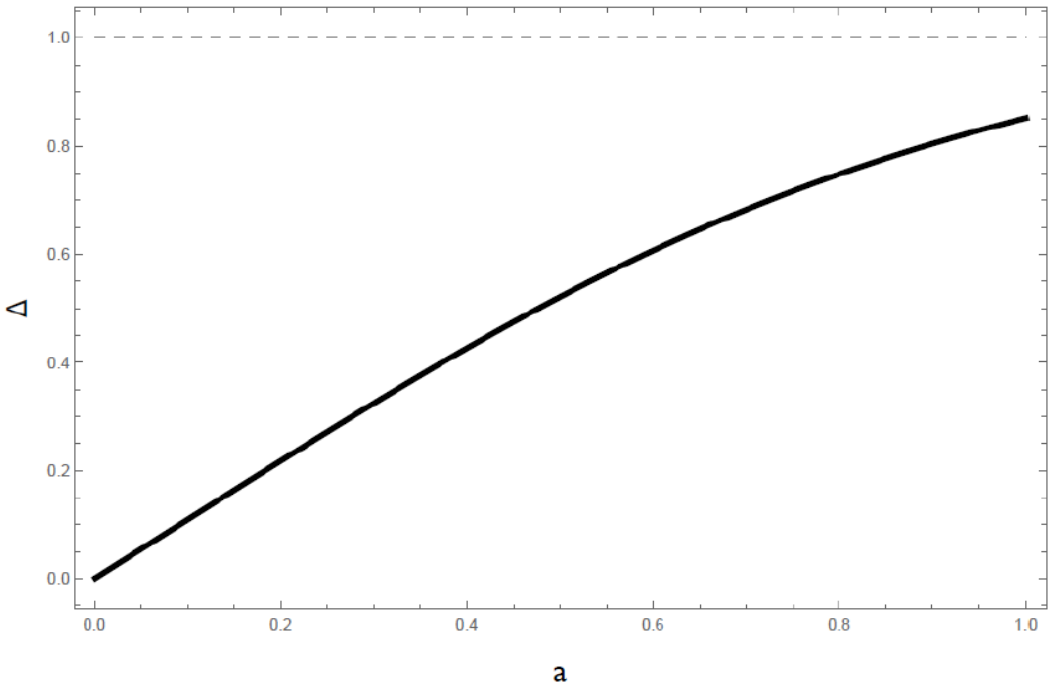

Source: produced by the author.

In Figure 3.1 we see that δ_m increases with time as structures are being formed, in the end, this growth is reduced due to the dark energy dominance at late times. If the quantity for dark energy is increased, the last term in the Equation 3.34 is smaller since this affects the matter density. This results in less matter to cluster into structures. From Equation 2.17 we see that to keep the density parameter balance, this decreases, even more, the evolution of δ_m. This can be seen in the example of Figure 3.2.

Figure 3.2: Example of the density contrast evolution in case of increase or decrease of the last term that contains the density of matter.

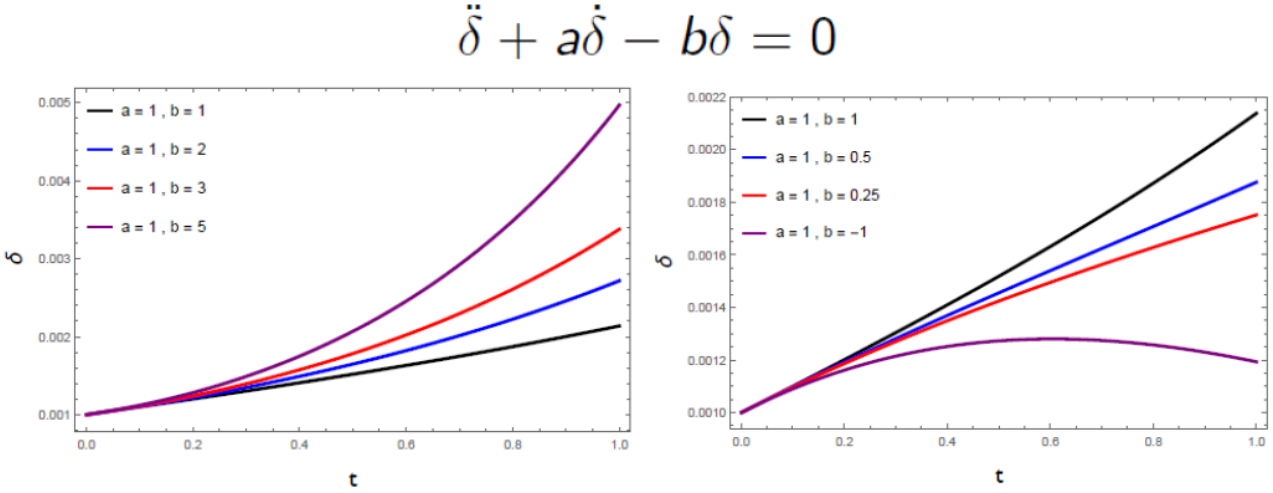

Source: produced by the author.

The distribution of matter is predominant during the late times. We can relate its potential to the primordial inflationary potential Φ_p by relating [20]

$$\Phi(\vec{k}, a) = \Phi_p(\vec{k}) \times \{\text{Transfer Function(k)}\} \times \{\text{Growth Function(a)}\}, \tag{3.35}$$

where the scale dependent transfer function is defined as

$$T(k) \equiv \frac{\Phi(k, a_{late})}{\Phi_{Large-Scale}(k, a_{late})}. \tag{3.36}$$

As its name suggests, this function corresponds to the evolution of perturbations in the epoch of the horizon crossing and radiation/matter transition, so we need its dependence on scale k. For large scales, the transfer function is equal to 1 since the growth factor will describe the late time growth independent of the wavelength k. So a_{late} corresponds to this late time epoch after the transfer function operation regime. A well-known transfer function is the Bardeen, Bond, Kaiser, and Szalay [28]

$$T(x \equiv k/k_{eq}) = \frac{ln[1 + 0.171x]}{0.171x} \left[1 + 0.284x + (1.18x)^2 + (0.399x)^3 + (0.490x)^4\right]^{-0.25}. \tag{3.37}$$

The growth function is evaluated right after the transfer function regime, where the ratio of the potential can be described as

$$\frac{\Phi(a)}{\Phi(a_{late})} \equiv \frac{D_1(a)}{a} \tag{3.38}$$

for $a > a_{late}$ and D_1 is called the growth function. We can observe that for a matter dominated universe where the potential is constant $D_1(a) = a$. Solving for large scales and neglecting anisotropic stress we can obtain that the relation with the primordial potential is given by a factor of (9/10). The potential for late times ($a > a_{late}$) can be described as

$$\Phi(\vec{k}, a) = \frac{9}{10}\Phi_p(\vec{k})T(k)\frac{D_1}{a}. \tag{3.39}$$

Assuming $a > a_{late}$ and using the Poisson equation we can relate the matter distribution to this potential (neglecting radiation for these late times)

$$\Phi = \frac{4\pi G \rho_m a^2 \delta}{k^2}. \tag{3.40}$$

It is possible to isolate the density contrast by using the definitions of the density parameter and the Hubble expansion rate

$$\delta(\vec{k}, a) = \frac{k^2 \Phi(\vec{k}, a) a}{(3/2)\Omega_m H_0^2}, \tag{3.41}$$

replacing the potential for late times

$$\delta(\vec{k}, a) = \frac{3}{5} \frac{k^2}{\Omega_m H_0^2} \Phi_p(\vec{k}) T(k) D_1(a). \tag{3.42}$$

As previously stated, by observing the temperature distribution of the CMB we need to connect how the scales uncorrelated today had such identical temperatures. The theory of inflation predicts that at a very early universe when relevant scales are causally connected, quantum-mechanical perturbations are produced, then these scales are transferred rapidly to outside the horizon by the inflationary mechanism. These scales enter the horizon much later linking the initial conditions for anisotropy with structure growth. By describing these perturbations in Fourier modes, the mean of a given Fourier mode for the gravitational potential is zero $< \Phi(\vec{k}) >= 0$, being then all modes uncorrelated. But we have a nonzero variance

$$< \Phi(\vec{k}) \Phi^*(\vec{k}') >= (2\pi)^3 P_\Phi(k) \delta_D(\vec{k} - \vec{k}'), \tag{3.43}$$

the δ_D is the Dirac delta function since, for the same wavelengths the equation above is zero, this forces the independence of different modes.

In this work we do not focus on inflation theory, more details can be seen in [29], [20], [24]. We just need to know that using the primordial power spectra

$$P_\Phi(k) = \frac{50\pi^2}{9k^3} \left(\frac{k}{H_0} \right)^{n-1} \delta_H^2 \left(\frac{\Omega_m}{D_1(a=1)} \right)^2, \tag{3.44}$$

where δ_H corresponds to the horizon-sized scale ($k = H_0$ in $c = 1$ units), the power spectrum of matter at late times is

$$P(k, a) = 2\pi^2 \delta_H^2 \frac{k^n}{H_0^{n+3}} T^2(k) \left(\frac{D_1(a)}{D_1(a=1)} \right)^2. \tag{3.45}$$

Figure 3.3: Matter power spectrum depending of the scale for different redshifts (red $z = 0$ and green $z = 2$). The solid curve is the theory and the traced line represents simulations for the nonlinear regime.

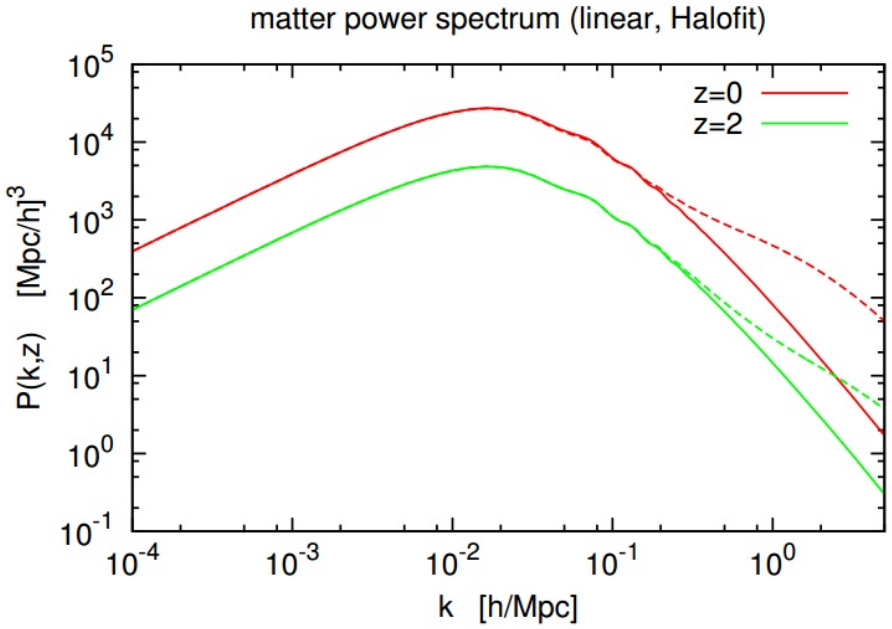

Source: CAMB code files [19].

In Figure 3.3 it is possible to observe how the power spectrum depends on scale and time. The nonlinear effects on large scales needed to be simulated as it is needed a nonlinear study of perturbations for this scale. For large scales, the transfer function is unity, $P \propto k$. As for the small scales, the power spectrum turns over since such modes enter the horizon before the radiation/matter equality epoch.

But perturbations in general relativity can have peculiar details. With a change of coordinates, one may give origin to terms not related to the perturbation of the energy content in the Einstein equation (only related to the curvature of spacetime). We can simplify and use Newtonian equations for the calculations, while also being free to change coordinates, without having to worry about transformation terms being introduced. This is valid when the length of the perturbation wave is smaller than the Hubble radius, avoiding relativistic effects in the spacetime curvature [30], [24].

3.3 The Neo Newtonian cosmology

Throughout the history of cosmology, Newtonian equations were studied to see the limits that would still be applied when compared to the equations of the dynamics of our universe in general relativity. In 1934 Milne [31] and McCrea [32] have shown that relativistic equations could be obtained using Newtonian equations for the case of zero pressure. Some years later in 1951 [33], there was an application with a nonzero pressure. This was the start of Neo Newtonian cosmology [34]. Together with the results also of Harrison (1965) [35] that also coincide with the results of McCrea, would be created the hydrodynamical equations for Neo Newtonian cosmology. This approach is based on three main equations:

The continuity equation, representing the conservation of energy, where the term $p\vec{\nabla}_r \cdot \vec{u}$ is inserted as a way to be equivalent to the general relativity predictions for scalar matter perturbations [34]

$$\left(\frac{\partial \rho}{\partial t}\right)_r + \vec{\nabla}_r \cdot (\rho \vec{u}) + p\vec{\nabla}_r \cdot \vec{u} = 0, \tag{3.46}$$

the Euler equation, providing the momentum conservation for a fluid with a source given by the gravitational potential ϕ

$$\left(\frac{\partial \vec{u}}{\partial t}\right)_r + (\vec{u} \cdot \vec{\nabla}_r)\vec{u} = -\vec{\nabla}_r \phi - (\rho + p)^{-1}\vec{\nabla}_r p, \tag{3.47}$$

and finally, the Poisson equation, that relates the gravitational potential with the mass density content

$$\nabla_r^2 \phi = 4\pi G(\rho + 3p). \tag{3.48}$$

These equations describe a fluid with density ρ, pressure p, moving with velocity $\vec{u}$ affected by the Newtonian gravitational potential ϕ.

If one replaces ρ by $\rho + p$ in the usual continuity and Euler equations and ρ by $\rho + 3p$ in the Poisson equation one finds

$$\left(\frac{\partial \rho}{\partial t}\right)_r + \vec{\nabla}_r \cdot (\rho + p)\vec{u} = 0, \tag{3.49}$$

$$\left(\frac{\partial \vec{u}}{\partial t}\right)_r + (\vec{u} \cdot \vec{\nabla}_r)\vec{u} = -\vec{\nabla}_r \phi - (\rho + p)^{-1}\vec{\nabla}_r p, \tag{3.50}$$

$$\nabla_r^2 \phi = 4\pi G(\rho + 3p). \tag{3.51}$$

By comparison, the correction appears in the pressure term of the continuity equation (that also carries a velocity of light c^{-2} term) with the objective to coincide with general relativity results, more details in [35].

The continuity equation Equation 3.49 assuming the fluid velocity $\vec{u} = \frac{\dot{a}}{a}\vec{r}$ is the same obtained from the Einstein equations as shown in the previous chapter Equation 2.13 assuming a perfect fluid in a homogeneous and isotropic spacetime. This equation in perturbation theory does agree with the general relativity results and this is mainly because of the pressure term in the continuity equation that generates an extra term.

The next chapter will introduce the perturbative equations for the Neo Newtonian cosmology keeping even second order terms. To avoid repetitions let us compare for now the first order perturbed continuity equations, starting by perturbing the standard one Equation 2.13

$$\ddot{\delta} + 2\frac{\dot{a}}{a}\dot{\delta} - 4\pi G(1 + w)(1 + 3w)\delta + \frac{\dot{a}}{a}w\vec{v} \cdot \vec{\nabla}\dot{\delta} + \frac{\ddot{a}}{a}w\vec{v} \cdot \vec{\nabla}\delta = \frac{c_s^2}{a^2}\nabla^2\delta, \tag{3.52}$$

followed by the perturbed Neo Newtonian Equation 3.46

$$\ddot{\delta} + 2\frac{\dot{a}}{a}\dot{\delta} - 4\pi G(1 + w)(1 + 3w)\delta = \frac{c_s^2}{a^2}\nabla^2\delta, \tag{3.53}$$

it is visible the two extra terms on the left side of the equation of Equation 3.52 that disagrees with the relativistic theory of cosmological perturbations. The equations above are in comoving coordinates and this transformation will also be shown in the next chapter. This does not mean that the standard continuity equation is not valid in the homogeneous case, it is only not valid when small perturbations are inserted.

The correction can be explained by doing a conservation of energy $dE + PdV = 0$, in a volume V of radius $r \sim a(t)$ the energy contained is $E \sim \rho a^3$, for a volume changing system

$$\frac{d\rho}{dt} + (\rho + p)\frac{1}{a^3}\frac{d}{dt}a^3 = 0, \tag{3.54}$$

that using the definition of $\vec{u}$ gives

$$\frac{d\rho}{dt} + (\rho + p)\vec{\nabla}_r \cdot \vec{u} = 0. \tag{3.55}$$

Expanding the total derivative $d/dt = \partial/\partial t + \vec{u} \cdot \vec{\nabla}_r$, its obtained the correct Newtonian approach including pressure effects Equation 3.46. The last term in Equation 3.46 can be related to the work needed to expand the fluid in its volume $V + dV$

$$\frac{1}{V}\frac{dW}{dt} = p\frac{4\pi a^2 da}{\frac{4}{3}\pi a^3} = 3\frac{\dot{a}}{a}p = p\vec{\nabla}_r \cdot \vec{u}, \tag{3.56}$$

where this term added accounts for the work related to the local fluid expansion.

Now with a valid Newtonian cosmology that works with a nonzero pressure term even at the perturbative level, it is possible to expand our study using these equations. This will also be used for a dark energy fluid that when perturbed is treated as a clustering dark energy.

3.4 Clustering Dark Energy

The clustering of the matter content has been observed in may surveys, and it represents an important tool for the study of the late time universe. This tool is also used to study cosmic expansion, as dark energy accelerates the universe expansion and impacts structure formations going against such matter clustering. Previously in section 2.2 was explained some problems in the dark energy theory, such as the cosmological constant [11] and cosmic coincidence problems [12], there is also the Planck satellite that detected via the Sunyaev-Zel'dovich effect [36] fewer clusters than the predicted in the standard model ΛCDM by CMB anisotropies [13]. Clustering dark energy could bring possible effects to explain such tensions. The next two chapters will show two different ways to study clustering dark energy, both using Neo Newtonian cosmology at the perturbative level.

Using our perturbed metric in the Newtonian gauge Equation 3.18 and assuming a universe composed of matter and dark energy contents, we can analyze how dark energy perturbations behave. Discarding radiation effects since we are interested in the effects of dark energy that has a dominated era at late times, considering no anisotropic stress and solving for the Einstein equation at the (0-0) its obtained Equation 3.23 in Fourier space and conformal time as

$$k^2\Phi + 3\mathcal{H}(\Phi' + \mathcal{H}\Phi) = 4\pi G a^2(\rho_m\delta_m + \rho_{de}\delta_{de}). \tag{3.57}$$

For each fluid (matter and dark energy) the conservation equation of the energy-momentum tensor $\nabla^\nu \delta T^\mu_\nu = 0$ is written as

$$\delta' + 3\mathcal{H}(c_s^2 - w)\delta + (1 + w)(\theta - 3\Phi') = 0 \tag{3.58}$$

$$\theta' + \mathcal{H}(1 - 3c_s^2)\theta = k^2\Phi + \frac{c_s^2 k^2 \delta}{1 + w} \tag{3.59}$$

where $\theta = ik^j v_j$ is the divergence for the fluid peculiar velocity and c_s^2 the sound speed of the fluid, define as:

$$c_s^2 = \frac{\delta P}{\delta \rho}. \tag{3.60}$$

In general, if the fluid pressure can depend on entropy (dissipative effects, like heat exchange) and the total c_s^2 has an adiabatic and non-adiabatic part

$$c_s^2 = \frac{\delta P(\rho, s)}{\delta \rho} = \frac{\partial P}{\partial \rho} + \frac{\partial P}{\partial s}\frac{\partial s}{\partial \rho} = c_{ad}^2 + c_{nad}^2, \tag{3.61}$$

these non-adiabatic effects where studied in perturbative levels for dark energy in previous work by the author [2], [3]. In this work, we are considering only an adiabatic fluid so $c_s^2 = c_{ad}^2$ in our case.

Using Equation 3.58 and Equation 3.59, for an adiabatic dark energy fluid, its density contrast equation is

$$\begin{aligned} \delta_{de}'' + \mathcal{H}(1-3w)\delta_{de}' + &= [3\mathcal{H}'(c_s^2 - w) + 3\mathcal{H}^2(c_s^2 - w)(1 - 3c_s^2) + c_s^2 k^2]\delta_{de} \\ &= -(1+w)\left[k^2\Phi - 3\mathcal{H}(1-c_s^2)\Phi' - 3\Phi''\right] \end{aligned} \tag{3.62}$$

Now it is possible to analyze the magnitude of this dark energy perturbation [37]. On small scales $k^2 >> \mathcal{H}^2, \mathcal{H}'$ and $k^2\Phi >> \mathcal{H}\Phi', \Phi''$, during the matter dominated era $\delta_m \propto a$ and $\Phi = constant$, its evolution is

$$\delta_{de}'' + \mathcal{H}(1-3w)\delta_{de}' + c_s^2 k^2 \delta_{de} = (1+w)k^2\Phi. \tag{3.63}$$

This makes it easier to visualize that Equation 3.62 has the constant solution

$$\delta_{de} = -\frac{(1+w)}{c_s^2}\Phi. \tag{3.64}$$

But for $c_s^2 = 0$ the solution becomes [37],[38], [39], [40]

$$\delta_{de} = -\frac{(1+w)}{(1-3w)}\delta_m. \tag{3.65}$$

Going back to Equation 3.57, we can see that $\delta_m \sim k^2\Phi$, so on small scales dark energy perturbations are negligible compared to the matter one.

These results show us the dependence of the dark energy perturbations on its equation of state parameter and the fluid sound velocity. Then if $w \neq -1$ its perturbation can have a magnitude comparable to the matter perturbations. But if its EoS parameter is close to the standard value $w \simeq -1$ its influence is suppressed.

In the next chapters, there will be tests around these values of w and c_s^2 for clustering dark energy. This study will use Neo Newtonian equations, but there several other approaches and models for dark energy perturbations [41], [24], [42], [43], [44], some of these models are: quintessence and k-essence [45], [46], tachyon field [47], [48], [49], [50] and spherical collapse [51], [52], [53]. For more about clustering dark energy we recommend the following reading [54], [37], [55].

3.5 Skewness in cosmology

The studies of cosmological perturbations can have different layers. We can have linear and nonlinear perturbations and also first to higher orders. For this study, we are going to use linear perturbations but we need higher orders for the calculation of skewness.

3.5.1 Statistical introduction

The word skewness is known in statistics to represent the third statistical moment. Moments can provide us with characteristics of the shape of a function if the function is a probability distribution. The moments are named as

- The first moment: Mean;
- Second moment: Variance;
- Third moment: Skewness;
- Fourth moment: Kurtosis.

There are higher moments, but to understand our objective there is no need to go further. Skewness describes how the format of the function is according to its asymmetry. Kurtosis can be associated with the tail of the function, or its peak. Both are equivalent because a longer tail would mean a lower peak, and a higher peak for example would mean a shorter tail in a PDF [56].

In Figure 3.4 we provide a better way to visualize this asymmetry associated with skewness.

Figure 3.4: Example of the asymmetry measured by the skewness.

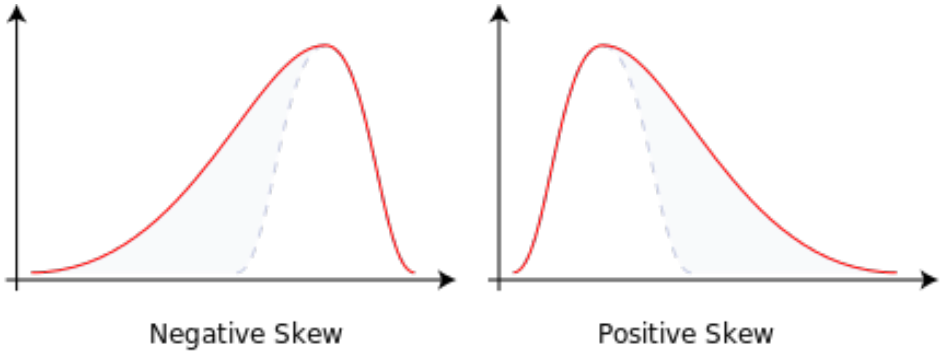

Source: https://www.freecodecamp.org/news/skewness-and-kurtosis-in-statistics-explained/

To understand how skewness can be seen in cosmology, let us start assuming a density distribution function $f(\delta)$ defined by

$$f(\delta) \equiv \frac{\Delta N}{N \Delta \delta} \tag{3.66}$$

representing the normalized number of elements (N is the number of independent elements, let us suppose they are matter elements since we are associating with the density contrast) within the range of the density contrast $\delta, \delta + d\delta$. This quantity can represent the first moment, as it makes a mean of the number of elements with respect to the total range of the density contrast.

The second moment is the variance

$$\sigma^2 = \frac{1}{N}\sum_{j=1}^{N}\delta_j^2 = \langle\delta^2\rangle \tag{3.67}$$

providing the dispersion of this density field.

And finally, for the skewness of this PDF, the third moment is

$$S = \frac{1}{N}\sum_{j=1}^{N}\left(\frac{\delta_j}{\sigma}\right)^3 = \frac{\langle\delta^3\rangle}{\sigma^3}. \tag{3.68}$$

Comparing to the cosmological moments seen in the literature [56], [57], [58]

$$S_p = \langle\delta^p\rangle/\sigma^{2(p-1)}, \tag{3.69}$$

where

$$\langle\delta^p\rangle = \int_0^\infty d\delta f(\delta)\delta^p. \tag{3.70}$$

For skewness $p = 3$, as being the third moment this results in

$$S_3 = \frac{\langle\delta^3\rangle}{\langle\delta^2\rangle^2}. \tag{3.71}$$

that when compared to Equation 3.68, $S = S_3 \times \sigma$, showing that the cosmological skewness S_3 is an amplitude parameters of the mathematical S, as the mathematical one can be viewed as a power-law function of σ [59]. This analogy helps us see and differentiate a normal PDF skewness from a cosmological one.

Skewness in clustering dark energy cosmology: preliminary approach

Since the computation of the skewness demands access to higher perturbative orders, it is more convenient to work with the Neo Newtonian cosmology. We are going to use the Neo Newtonian fluid dynamical approach for cosmology to evaluate models with dark energy perturbations. We will be looking for the matter density contrast up to second order as a tool for these tests. This chapter begins with looking into the universe being composed of a single fluid which is an effective description for a mixture of matter and dark energy content.

4.1 Evolution of perturbations in the Neo Newtonian cosmology

Returning to the definition of Einstein's equation Equation 2.6. Assuming a universe composed of two fluids, one being the matter content including baryonic matter and cold dark matter, and the other fluid for dark energy. Einstein's equation can be rewritten as:

$$R_{\mu\nu} - \frac{1}{2}g_{\mu\nu}\mathcal{R} = 8\pi G T^{m}_{\mu\nu} + 8\pi G T^{de}_{\mu\nu}, \tag{4.1}$$

where the first term on the right hand side contains the energy momentum tensor of the total matter fluid and the second for the dark energy fluid.

The expansion rate can also be rewritten and becomes

$$\frac{H^2(a)}{H_0^2} = \frac{\Omega_{m0}}{a^3} + \Omega_{de}(a), \tag{4.2}$$

here we are neglecting radiation effects since our interest is on how structure formation is affected by late time effects. The sum of the density parameters then must be $\Omega_{m0} + \Omega_{de0} = 1$.

Using Equation 2.14 for a dark energy fluid with pressure p_{de} and density ρ_{de}, its equation of state parameter can be written as $w_{de} = p_{de}/\rho_{de}$. The relation of dark energy with the scale factor can be written in the following function

$$\frac{H^2(a)}{H_0^2} = \frac{\Omega_{m0}}{a^3} + (1 - \Omega_{m0})e^{-3\int da \frac{1+w_{de}}{a}}. \tag{4.3}$$

The dynamics of this system can also be described as shown in the Neo Newtonian set of equations given by the continuity Equation 3.46, Euler Equation 3.47 and Poisson Equation 3.48.

The following calculations are demonstrated for a single fluid, but it is valid for both fluids if they are non-interacting and connected by the Poisson equation since it contains the total mass density of the two fluids (more details in the next chapter).

Assuming the small perturbations on the density $\delta\rho$, pressure δp, potential φ and velocity field $\vec{v}$:

$$\rho = \rho_0 + \delta\rho, \tag{4.4}$$
$$p = p_0 + \delta p, \tag{4.5}$$
$$\vec{u} = \vec{u}_0 + \vec{v}. \tag{4.6}$$

Applying perturbations in the fluid equations Equation 3.46 and Equation 3.47 we will find the following set of equations

$$\left(\frac{\partial\rho_0}{\partial t}\right)_r + \left(\frac{\partial\delta\rho}{\partial t}\right)_r + \vec{\nabla}_r[(\rho_0+\delta\rho)(\vec{u}_0+\vec{v})] + (p_0+\delta p)\vec{\nabla}_r\cdot(\vec{u}_0+\vec{v}) = 0, \tag{4.7}$$

$$\left(\frac{\partial\vec{v}}{\partial t}\right)_r + [(\vec{u}_0+\vec{v})\cdot\vec{\nabla}_r](\vec{u}_0+\vec{v}) = -\vec{\nabla}_r(\phi_N) - (\rho_0+\delta\rho+p_0+\delta p)^{-1}\vec{\nabla}_r(p_0+\delta p), \tag{4.8}$$

where ϕ_N is the gravitational potential in the Neo Newtonian gravity that satisfies the Poisson equation

$$\vec{\nabla}_r\phi_N = 4\pi G(\rho+3p). \tag{4.9}$$

It is important to notice that the Newtonian potential would not have the pressure term.

To simplify the calculations, we are going to change to comoving coordinates $\vec{x}$. We apply the following transformations

$$\begin{aligned} \vec{r} = a\vec{x}, \qquad & \vec{\nabla}_x = a\vec{\nabla}_r, \\ \left(\frac{\partial f(\vec{x},t)}{\partial t}\right)_r = \left(\frac{\partial f}{\partial t}\right)_x & - \frac{\dot{a}}{a}(\vec{x}\cdot\vec{\nabla}_x)f, \\ \vec{u} = \dot{a}\vec{x} & + \vec{v}(\vec{x},t), \end{aligned} \tag{4.10}$$

and we are also going to use the definitions for the equation of state parameter Equation 2.14 and the sound velocity Equation 3.60.

4.1.1 The continuity equation

Let us focus now on the perturbed continuity equation. With these definitions, changing the coordinates and perturbations, the continuity equation becomes

$$\left(\frac{\partial\delta\rho}{\partial t}\right)_x - \frac{\dot{a}}{a}(\vec{x}\cdot\vec{\nabla}_x)\delta\rho + \frac{\vec{\nabla}_x}{a}[\rho_0\vec{u}_0 + \rho_0\vec{v} + \delta\rho\vec{u}_0 + \delta\rho\vec{v}] + (p_0+\delta p)\frac{\vec{\nabla}_x}{a}\cdot(\vec{u}_0+\vec{v}) = 0. \tag{4.11}$$

We are interested in leaving only first and second order terms for the calculation of the skewness of the matter density. The way that these terms are going to be useful will be shown further. We then get the following equation

$$\left(\frac{\partial\delta\rho}{\partial t}\right)_x + (\rho_0+p_0)\frac{\vec{\nabla}_x}{a}\vec{v} + (\delta\rho+\delta p)\frac{\vec{\nabla}_x}{a}\vec{v} + \vec{v}\frac{\vec{\nabla}_x}{a}(\rho_0+\delta\rho) + (\delta\rho+\delta p)\frac{\vec{\nabla}_x}{a}\vec{u}_0 = 0. \tag{4.12}$$

Dividing by ρ_0, adopting $\delta\rho = c_s^2\delta p$ and using the background continuity equation

$$\dot{\rho}_0 + 3H(\rho_0+p_0) = 0, \tag{4.13}$$

to replace some terms such that

$$\frac{\delta\dot{\rho}}{\rho} = \dot{\delta} - \frac{\dot{\rho}}{\rho}\delta = \dot{\delta} - 3H(\rho_0 + p_0)\frac{\delta}{\rho_0}, \tag{4.14}$$

this results in

$$\dot{\delta} - 3H(\rho_0 + p_0)\frac{\delta}{\rho_0} + (1 + \frac{p_0}{\rho_0})\frac{\vec{\nabla}_x}{a}\vec{v} + (\delta + c_s^2\delta)\frac{\vec{\nabla}_x}{a}\vec{v} + \vec{v}\frac{\vec{\nabla}_x}{a}(1+\delta) + (\delta + c_s^2\delta)\frac{\vec{\nabla}_x}{a}\vec{u}_0 = 0. \tag{4.15}$$

The equation of state parameter can finally be introduced using its definition Equation 2.14. Then,

$$\dot{\delta} - 3H(1+w)\delta + (1+w)\frac{\vec{\nabla}_x}{a}\vec{v} + (\delta + c_s^2\delta)\frac{\vec{\nabla}_x}{a}\vec{v} + \vec{v}\frac{\vec{\nabla}_x}{a}\delta + 3H(1+c_s^2)\delta = 0. \tag{4.16}$$

Some terms can be canceled and reorganized to result

$$\dot{\delta} + 3H(c_s^2 - w)\delta + (1+w)\frac{\vec{\nabla}_x}{a}\vec{v} + (\delta + c_s^2\delta)\frac{\vec{\nabla}_x}{a}\vec{v} + \vec{v}\frac{\vec{\nabla}_x}{a}\delta = 0. \tag{4.17}$$

We perform a transformation of the time derivative with $\partial/\partial t \to \partial/\partial lna$, leading to

$$\frac{\mathcal{H}}{a}\delta' + \frac{3\mathcal{H}}{a}(c_s^2 - w)\frac{\nabla_x}{a}\vec{v} + (1+w)\delta\frac{\vec{\nabla}_x}{a}\vec{v} + \vec{v}\frac{\vec{\nabla}_x}{a}\delta = 0. \tag{4.18}$$

With this time transformation, we can use two terms from the equation above to write the total derivative of δ with respect to $N = ln(a)$ as

$$\frac{d\delta(\vec{x},t)}{dN} = \delta' + \frac{\vec{v}}{\mathcal{H}}\vec{\nabla}\delta. \tag{4.19}$$

Multiplying the previous equation by $\frac{a}{\mathcal{H}}$:

$$\frac{d\delta}{dN} + 3(c_s^2 - w)\delta + (1+w)\frac{\nabla\vec{v}}{\mathcal{H}} + (1+c_s^2)\delta\frac{\nabla\vec{v}}{\mathcal{H}} = 0 \tag{4.20}$$

Since we are looking for the evolution of the density contrast, the term $\frac{\nabla\vec{v}}{\mathcal{H}}$ is isolated, resulting in:

$$\frac{\nabla\vec{v}}{\mathcal{H}} = \frac{-d\delta/dN - 3(c_s^2 - w)\delta}{1 + w + (1+c_s^2)\delta}, \tag{4.21}$$

this is done since this velocity derivative will be replaced in the Euler equation after.

4.1.2 The Euler equation

Starting by changing to comoving coordinates the perturbed Euler equation writes

$$\left(\frac{\partial\vec{v}}{\partial t}\right)_x - \ddot{a}\vec{x} - H\dot{a}\vec{x} - H(\vec{x}\cdot\vec{\nabla}_x)\vec{v} + H\dot{a}\vec{x} + H\vec{v} + H(\vec{x}\cdot\vec{\nabla}_x)\vec{v} + \frac{1}{a}(\vec{v}\cdot\nabla_x)\vec{v} = -\frac{\vec{\nabla}_x}{a}\phi_N - \frac{\vec{\nabla}_x(p_0 + \delta p)}{a(\rho_0 + \delta\rho + p_0 + \delta p)}. \tag{4.22}$$

Using the second term $\ddot{a}\vec{x}$ and replacing with $\ddot{a}\vec{\nabla}\vec{x}^2/2$ we can use it to define the effective gravitational potential

$$\Phi \equiv -\left(\phi_N + \frac{1}{2}a\ddot{a}\vec{x}^2\right). \tag{4.23}$$

Leaving again only first and second order terms it results in

$$\frac{\partial\vec{v}}{\partial t} + H\vec{v} + (\vec{v}\cdot\frac{\vec{\nabla}_x}{a})\vec{v} = \frac{\vec{\nabla}_x}{a}\Phi - \frac{\vec{\nabla}_x\delta p}{a(\rho_0+p_0)}. \tag{4.24}$$

Doing the time derivative transformation $\partial/\partial t \to \partial/\partial lna$

$$\frac{\partial\vec{v}}{\partial lna}\frac{\mathcal{H}}{a} + \frac{\mathcal{H}}{a}\vec{v} + \frac{(\vec{v}\cdot\vec{\nabla}_x)\vec{v}}{a} = \frac{\vec{\nabla}_x}{a}\Phi - \frac{\vec{\nabla}_x\delta p}{a(\rho_0+p_0)}. \tag{4.25}$$

Since we isolated the divergence of $\vec{v}$ before, it is also interesting to do the divergence of the Euler equation, this way we can obtain by future substitution an equation of evolution for the density contrast

$$\mathcal{H}v_i' + \mathcal{H}v_i + v_j\nabla^j v_i = \nabla_i\Phi - \frac{\nabla_i\delta p}{(\rho_0+p_0)}, \tag{4.26}$$

reorganizing and using the definition of the EoS parameter and sound velocity leads to

$$\mathcal{H}\nabla^i v_i' + \mathcal{H}\nabla_i v_i + \nabla^i(v_j\nabla^j v_i) = \nabla^2\Phi - \nabla^i\left[\frac{\nabla_j c_s^2\delta}{1+w+(1+c^2)\delta}\right]. \tag{4.27}$$

The following velocity term can be separated in

$$\nabla^i(v_j\nabla^j v_i) = (\nabla^i v_j)(\nabla^j v_i) + v_j\nabla^j\nabla^i v_i, \tag{4.28}$$

on the right side, the last term can be used to make a total derivative and the first term can be simplified by neglecting shear and vorticity.

Assuming that the velocity field remains purely radial we can write:

$$\vec{v} = \frac{v}{\sqrt{3}}\{1,1,1\}, \tag{4.29}$$

so that

$$(\nabla^i v_j)(\nabla^j v_i) = \frac{1}{3}\mathcal{H}^2\left(\frac{\nabla^i v_i}{\mathcal{H}}\right)^2. \tag{4.30}$$

Dividing 4.27 by $\mathcal{H}^2$ and making the product derivative to replace the first term on 4.27:

$$\left(\frac{\nabla^i v_i}{\mathcal{H}}\right)' + \left(1+\frac{\mathcal{H}'}{\mathcal{H}}\right)\frac{\nabla^i v_i}{\mathcal{H}} + \frac{1}{\mathcal{H}^2}\nabla^i(v_j\nabla^j v_i) = \frac{1}{\mathcal{H}^2}\nabla^2\Phi - \frac{1}{\mathcal{H}}\nabla^i\left[\frac{\nabla_j c_s^2\delta}{1+w+(1+c_s^2)\delta}\right], \tag{4.31}$$

reorganizing doing the total derivative with we get finally to

$$\frac{d(\nabla^i v_i/\mathcal{H})}{dN} + \left(1+\frac{\mathcal{H}'}{\mathcal{H}}\right)\frac{\nabla^i v_i}{\mathcal{H}} + \frac{1}{3}\left(\frac{\nabla^i v_i}{\mathcal{H}}\right)^2 = \frac{1}{\mathcal{H}^2}\nabla^2\Phi - \frac{1}{\mathcal{H}}\nabla^i\left[\frac{\nabla_j c_s^2\delta}{1+w+(1+c_s^2)\delta}\right]. \tag{4.32}$$

Using 4.21 and defining $A = 1+w+(1+c_s^2)\delta$ to simplify, its possible to replace the velocity divergence parts in terms of the density contrast (here $'$ is total derivative d/dN):

$$\left(\frac{\nabla^i v_i}{\mathcal{H}}\right)' = \frac{-\delta'' - 3\delta'(c_s^2 - w) - 3\delta(c_s'^2 - w')}{A} + \frac{w'\delta' + 3w'(c_s^2 - w)\delta + \delta'^2 + 3(c_s^2 - w)\delta\delta'}{A^2} + \frac{c_s'^2\delta\delta' + 3(c_s^2 - w)c'^2\delta^2 + c_s^2\delta'^2 + 3(c_s^2 - w)c_s^2\delta'\delta}{A^2}, \tag{4.33}$$

$$\left(\frac{\nabla^i v_i}{\mathcal{H}}\right)^2 = \frac{\delta'^2 + 3(c_s^2 - w)\delta\delta' + 9(c_s^2 - w)^2\delta^2}{A^2}. \tag{4.34}$$

Replacing the last two equations in 4.32 and also multiplying by A. The evolution of the density contrast can finally be obtained in the form of

$$\begin{aligned}
&\delta'' + \delta'\left[3(c_s^2 - w) + \left(1 + \frac{\mathcal{H}'}{\mathcal{H}}\right) - \frac{w'}{A}\right] - \delta'^2\left[\frac{4/3 + c_s^2}{A}\right] \\
&+ \delta\delta'\left[\frac{(w - c_s^2)(5 + 3c_s^2) - c_s'^2}{A}\right] + \delta^2\left[\frac{3(w - c_s^2)c'^2 + 3(w - c_s^2)^2}{A}\right] \\
&+ 3\delta\left[(c_s'^2 - w') + \left(1 + \frac{\mathcal{H}'}{\mathcal{H}}\right)(c_s^2 - w) + \frac{w'(w - c_s^2)}{A}\right] + \frac{A}{\mathcal{H}^2}\nabla^2\Phi = \frac{A}{\mathcal{H}^2}\nabla\left[\frac{\nabla(c_s^2\delta)}{A}\right].
\end{aligned} \tag{4.35}$$

In these calculations we do not specify any fluid (matter or dark energy for our study), this is a equation of the evolution of the density contrast that can be used for any fluid provided that the due properties are taken into account. This equation also contains second order terms, if one needs only a first order equation, the second order terms just need to be canceled.

4.1.3 The Poisson equation

For the Poisson equation, using the effective potential defined in Equation 4.23 we can replace the second Friedmann equation

$$\frac{\ddot{a}}{a} = -\left(\frac{4\pi G}{3}(\rho_{0T} + 3p_{0T})\right), \tag{4.36}$$

to write

$$\nabla^2\left(\phi_N - \frac{2}{3}\pi G a^2(\rho_{0T} + 3p_{0T})\vec{x}^2\right) = 4\pi G a^2\delta(\rho_T + 3\delta p_T). \tag{4.37}$$

And using the definition of the Newtonian potential Equation 4.9, the Poisson equation in terms of the effective gravitational potential is

$$\frac{\nabla^2}{a^2}\Phi = -4\pi G(\delta\rho_T + 3\delta p_T). \tag{4.38}$$

In the next chapter, this expression will be worked further for a two separated fluid scenario, for the analysis in this chapter we only need to treat the single fluid universe.

4.2 The Universe as one Fluid

In a previous work [4], Equation 4.35 was modified to be in terms of the total equation of state parameter and in its effective speed of sound $c_{\text{eff}}^2 = \delta p/\delta\rho$ to treat a single fluid universe.

It is possible to rewrite the Poisson equation and the expansion rate in terms of these parameters

$$\begin{aligned}\nabla^2\Phi &= 4\pi G a^2\rho_0(1+c^2_{eff}),\\ \mathcal{H}^2 &= \frac{8\pi G}{3}a^2\rho,\\ \mathcal{H}' &= -\frac{\mathcal{H}^2}{2}(1+3w).\end{aligned} \tag{4.39}$$

This method was inspired by the paper [60].

For the sake of the results, since they were obtained using the equation in terms of the scale factor, the derivatives d/da in this section are indicated by $'$. The density contrast equation for a single fluid universe in terms of w and c^2_{eff} is then

$$\begin{aligned}a^2\delta''+a\delta'&\left[\frac{aH'}{H}+3-3w+3c^2_{\text{eff}}-\frac{w'a}{1+w+\delta\left(1+c^2_{\text{eff}}\right)}\right]\\ &-\delta'^2a^2\left[\frac{4/3+c^2_{\text{eff}}}{1+w+\delta\left(1+c^2_{\text{eff}}\right)}\right]+\delta\delta'a\left[\frac{\left(w-c^2_{\text{eff}}\right)\left(5+3c^2_{\text{eff}}\right)-c^{2\prime}_{\text{eff}}a}{1+w+\delta\left(1+c^2_{\text{eff}}\right)}\right]\\ &+\delta^2\left[\frac{3\left(w-c^2_{\text{eff}}\right)c^{2\prime}_{\text{eff}}a-3\left(w-c^2_{\text{eff}}\right)^2}{1+w+\delta(1+c^2_{\text{eff}})}-\frac{3}{2}\left(1+3c^2_{\text{eff}}\right)\left(1+c^2_{\text{eff}}\right)\right]\\ &+\frac{3}{2}\delta\left[\left(3w^2-2w-1\right)-2c^2_{\text{eff}}(1+3w)-2\left(w'a-c^{2\prime}_{\text{eff}}a\right)+\frac{2\left(w-c^2_{\text{eff}}\right)w'a}{1+w+\delta\left(1+c^2_{\text{eff}}\right)}\right]\\ =&\frac{1+w+\delta\left(1+c^2_{\text{eff}}\right)}{a^2H^2}\nabla_x\left(\frac{\nabla_x\left(c^2_{\text{eff}}\delta\right)}{1+w+\delta\left(1+c^2_{\text{eff}}\right)}\right).\end{aligned} \tag{4.40}$$

The one term $\mathcal{H}'/\mathcal{H}$, was left so we could insert the background values to solve this system $(H_0, \Omega_{m0}, \Omega_{de})$. In the further sections, it is shown how these density contrast equations are going to be calculated and it is going to be understood why was needed to keep second order terms in the perturbed calculations.

4.3 The cosmological skewness for the matter density

There are several forms to calculate skewness related to the density contrast [56], [57], [24], [59]. From [56] and [24] we can start to define the cosmological skewness by analysing the dynamics [58], [24] of a flat ΛCDM universe

$$\begin{aligned}\frac{\partial}{\partial t}\delta(\vec{x},t)+\frac{1}{a}\nabla_x[(1+\delta(\vec{x},t))\vec{v}(\vec{x},t)],\\ \frac{\partial}{\partial t}\vec{v}(\vec{x},t)+\frac{\ddot{a}}{a}\vec{v}(\vec{x},t)+\frac{1}{a}[\vec{v}(\vec{x},t)\cdot\vec{\nabla}_x]\vec{v}(\vec{x},t)=-\frac{1}{a}\nabla_x\phi(\vec{x},t),\\ \nabla^2_x\phi(\vec{x},t)=4\pi G\rho a^2\delta(\vec{x},t),\end{aligned} \tag{4.41}$$

where we derive the equations above from Equation 3.46-3.48 using the comoving coordinates transformations define in Equation 4.10 and the definitions of the density contrast δ.

Following the same steps in section 4.1 we can write the evolution equations

$$\frac{1}{H}\dot{\delta}+(1+\delta)\theta+\frac{1}{aH}\nabla_x\cdot(\delta v)=0$$
$$\frac{1}{H}\dot{\theta}+\left(2+\frac{\dot{H}}{H^2}\right)\theta+\frac{3}{2}\Omega_m\delta+\frac{1}{aH}\nabla_x\cdot(v\cdot\nabla_x)v=0 \tag{4.42}$$

where $\theta=\nabla^i v_i/aH$ is the velocity divergence and we keep proper time derivatives represented by the dots $\dot{}$. We are omitting the time and space dependence sometimes for simplicity.

Also using the perturbative relation of the field velocity described in Equation 4.10 we can rewrite using the expansion rate relation with the density parameters definition the following equation [58]

$$u(\vec{x})=-f(\Omega_m,\Lambda)\frac{H_0}{4\pi}\int\frac{\vec{x}-\vec{x}'}{|\vec{x}-\vec{x}'|}\delta(x)d^3\vec{x}', \tag{4.43}$$

where $f(\Omega_m,\Lambda)$ represents, in a more general way, a function containing the universe content represented by the density parameters for matter and dark energy constant, this is used to simplify the calculations. This relation can be extended to the definition of θ [58], [61], resulting in

$$\theta(\vec{x})=-f(\Omega_m,\Lambda)\delta(\vec{x}). \tag{4.44}$$

In the spatial derivatives, is also useful to make the Fourier transformations for the fields δ and θ

$$\delta(\vec{x},t)=\int\frac{d^3\vec{k}}{(2\pi)^{3/2}}\delta(\vec{k},t)\exp(i\vec{x}\cdot\vec{k}),$$
$$\theta(\vec{x},t)=\int\frac{d^3\vec{k}}{(2\pi)^{3/2}}\theta(\vec{k},t)\exp(i\vec{x}\cdot\vec{k}). \tag{4.45}$$

In Equation 4.29 we discussed the pure radial form of v, this leads to its Fourier transformation in the form of

$$\vec{v}(\vec{x},t)=\int\frac{d^3\vec{k}}{(2\pi)^{3/2}}\frac{-i\vec{k}}{k^2}\theta(\vec{k},t)\exp(i\vec{x}\cdot\vec{k}). \tag{4.46}$$

Using the set of equations above Equation 4.45-4.46 we can rewrite the equations of dynamics Equation 4.42 in Fourier space as

$$\frac{1}{H}\dot{\delta}(\vec{k},t)+\theta(\vec{k},t)+\int\frac{d^3\vec{k}'}{(2\pi)^{3/2}}\mathcal{F}(\vec{k}',\vec{k}-\vec{k}')\delta(\vec{k}-\vec{k}',t)\theta(\vec{k},t)=0$$
$$\frac{1}{H}\dot{\theta}(\vec{k},t)+\left(2+\frac{\dot{H}}{H^2}\right)+\frac{3}{2}\Omega_m\delta(\vec{k},t)=-\int\frac{d^3\vec{k}'}{(2\pi)^{3/2}}[\mathcal{F}(\vec{k}',\vec{k}-\vec{k}')+\mathcal{F}(\vec{k}-\vec{k}',\vec{k}')$$
$$-2\mathcal{G}(\vec{k}',\vec{k}-\vec{k}')]\theta(\vec{k}-\vec{k}',t)\theta(\vec{k}',t) \tag{4.47}$$

where the functions $\mathcal{F}$ and $\mathcal{G}$ are defined as

$$\mathcal{F}(\vec{k},\vec{k}')=1+\frac{\vec{k}\cdot\vec{k}'}{k^2}, \tag{4.48}$$
$$\mathcal{G}(\vec{k},\vec{k}')=1-\frac{\vec{k}\cdot\vec{k}'}{k^2k'^2}. \tag{4.49}$$

Now with the perturbative dynamics defined we need to filter these fields since perturbations are valid for very large scales (small $k's$), and for small scales, these perturbations (bigger $k's$) didn't evolve enough and needed to be smoothed out. For this we make use of window functions, these types of mathematical functions are often used in statistics since it makes zero outside of a chosen interval and also are used often in cosmology [62], [63].

For our calculations, we are going to use the top-hat window function that for a scale R_0 is

$$\begin{aligned} W_{th}(x) &= 1 \text{ if } |x| \leq R_0, \\ W_{th}(x) &= 0 \text{ for all other cases.} \end{aligned} \tag{4.50}$$

The density and velocity fields can be rewritten as

$$\delta(R_0) = \int d^3x W_{th}(x)\delta(x), \tag{4.51}$$

$$\theta(R_0) = \int d^3x W_{th}(x)\theta(x). \tag{4.52}$$

That applying Fourier transformations becomes

$$\delta(R_0) = \int \frac{d^3k}{(2\pi)^{3/2}} W_{th}(x)\delta(x), \tag{4.53}$$

$$\theta(R_0) = \int \frac{d^3k}{(2\pi)^{3/2}} W_{th}(x)\theta(x), \tag{4.54}$$

transforming also the format of the top-hat window function to

$$W_{th} = \frac{3}{(kR_0)^3}[sin(kR_0) - kR_0 cos(kR_0)], \tag{4.55}$$

where k is the norm of $\vec{k}$.

This allows us to provide the second statistical moment, the variance Equation 3.68, for these fields:

$$\begin{aligned} \sigma^2(R_0) &= \int \frac{d^3k}{(2\pi)^{3/2}} \frac{d^3k'}{(2\pi)^{3/2}} W_{th}(kR_0)\langle\delta(\vec{k}\delta(\vec{k'}))\rangle W_{th}(k'R_0) \\ &= D_1^2(t) \int \frac{d^3k}{(2\pi)^3} W_{th}^2(kR_0)P(k), \end{aligned} \tag{4.56}$$

$$\sigma_\theta^2(R_0) = f^2(\Omega_m)D_1^2(t) \int \frac{d^3k}{(2\pi)^3} W_{th}(kR_0)P(k), \tag{4.57}$$

where P(k) is the power spectrum and $f(\Omega_m)$ a function in terms of the matter density parameter.

$D_1(t)$ is the growing factor from the expansion of the density fluctuation and divergence velocity, that assuming Gaussian initial conditions [56], [57] produces

$$\begin{aligned} \delta^{(1)}(\vec{x}, t) =& D_1\epsilon(\vec{x}), \\ =& D_1(t) \int \frac{d^3\vec{k}}{(2\pi)^{3/2}} \epsilon_{\vec{k}} e^{i\vec{k}\cdot\vec{x}}, \end{aligned} \tag{4.58}$$

$$\theta^{(1)}(\vec{x}, t) = -f(\Omega_m)D_1(t) \int \frac{d^3\vec{k}}{(2\pi)^{3/2}} \epsilon_{\vec{k}} e^{i\vec{k}\cdot\vec{x}}. \tag{4.59}$$

The equation for θ uses the relation Equation 4.44 and $\epsilon_{\vec{k}}$ are random variables that obey the following the properties

$$\begin{aligned}\langle \epsilon_{\vec{k}} \epsilon_{\vec{k'}} \rangle &= \delta_D(\vec{k} - \vec{k}')P(k), \\ \langle \epsilon_{\vec{k}_1} \cdots \epsilon_{\vec{k}_{2p+1}} \rangle &= 0, \\ \langle \epsilon_{\vec{k}_1 \cdots \epsilon_{\vec{k}_{2p}}} \rangle &= \frac{1}{2^p p!} \sum_{permutations - s} \langle \epsilon_{\vec{k}_{s1}} \epsilon_{\vec{k}_{s2}} \rangle \cdots \langle \epsilon_{\vec{k}_{s2p-1}} \epsilon_{\vec{k}_{s2p}} \rangle. \end{aligned} \tag{4.60}$$

Finally, for skewness, the third statistical moment needs to be found. This can be made by expanding the distributions of $\delta(R_0)$ and$\theta(R_0)$. The expansion is made around the same random variable $\epsilon_{\vec{k}}$ from above. Until the third order, this expansion for the delta and theta field distribution is written as

$$\delta(R_0) = \delta^{(1)}(R_0) + \delta^{(2)}(R_0) + \delta^{(3)}(R_0) + ..., \tag{4.61}$$

$$\theta(R_0) = \theta^{(1)}(R_0) + \theta^{(2)}(R_0) + \theta^{(3)}(R_0) + ..., \tag{4.62}$$

by looking into our initial conditions Equation 4.58-4.59 we can assume that each delta function $\delta^j(R_0)$ is proportional to an j degree of the random variable $\epsilon^j_{\vec{k}}$ (the same can be said for θ). As seen in Equation 3.71 we need to reproduce the leading terms of $\langle \delta(R_0)^3 \rangle$ and $\langle \delta(R_0)^2 \rangle^2$ (same for θ since δ evolution equation Equation 4.47 needs also to be solved with it), this can be done by the doing the ensemble averages of $\overline{\delta(R_0)}^3$ and $\overline{\theta(R_0)}^3$

$$\begin{aligned}\langle \delta(R_0)^3 \rangle =& \langle (\overline{\delta^{(1)}(R_0) + \delta^{(2)}(R_0) + \delta^{(3)}(R_0) + ...})^3 \rangle \\ =& \langle (\overline{\delta^{(1)}})^3 \rangle + 3 \langle (\overline{\delta^{(1)}(R_0)})^2 \delta^{(2)}(R_0) \rangle + ... \end{aligned} \tag{4.63}$$

$$\begin{aligned}\langle \theta(R_0)^3 \rangle =& \langle (\overline{\theta^{(1)}(R_0) + \theta^{(2)}(R_0) + \theta^{(3)}(R_0) + ...})^3 \rangle \\ =& \langle (\overline{\theta^{(1)}})^3 \rangle + 3 \langle (\overline{\theta^{(1)}(R_0)})^2 \theta^{(2)}(R_0) \rangle + ... \end{aligned} \tag{4.64}$$

The first term on the right side of the result above is zero due to the properties of the random variables Equation 4.60. This leaves us with the second term as the leading term for the third moment.

The ratio and definition of skewness like Equation 3.71 for this case reads

$$S_3 = \frac{\langle \delta(R_0)^3 \rangle}{\langle \delta(R_0)^2 \rangle^2}, \tag{4.65}$$

and for the divergence of the velocity field, this ratio has a similar composition

$$T_3 = \frac{\langle \theta(R_0)^3 \rangle}{\langle \theta(R_0)^2 \rangle^2}. \tag{4.66}$$

The denominator term of Equation 4.65 can be obtained by doing the variance of the field Equation 4.44

$$\langle \theta(\vec{x})^2 \rangle = f(\Omega_m)^2 \langle \delta(x)^2 \rangle. \tag{4.67}$$

To fully solve Equation 4.65 we use the dynamics of a spherical collapse model [56], [64], [24]. This model describes the perturbation evolution in a symmetric spherical region. This depends

on the background dynamics for a ΛCDM universe within a region R where the perturbation evolves (similar to Friedmann's Equation 2.11)

$$\ddot{R} = -\frac{GM(< R)}{R^2} + \frac{\Lambda}{3}R, \tag{4.68}$$

where $M(< R)$ contains only the mass inside the region R. Notice that this model has similar conditions where we restricted to a region R_0 with a window function previously.

The density contrast δ for this spherical region represents the following overdensity

$$\delta = \left(\frac{R}{R_0}\right)^{-3} - 1 \tag{4.69}$$

with R_0 as the initial comoving radius for this perturbation, this equation represents the overdensity where the first term represents the change in the volume ratio minus the total quantity. This definition makes this density contrast inside the spherical shell being Equation 4.69 and outside $\delta = 0$ [24], it behaves like a top-hat function that makes the spacial derivatives for the density field be canceled.

Using the equations of dynamics and steps made to get the evolution of the density contrast Equation 4.35 (only first order terms) and considering that for this model we are only considering time derivatives for a ΛCDM model and also using Equation 4.2 the equation for the overdensity is determined by

$$\frac{1}{3}\frac{\ddot{\delta}}{(1+\delta)^2} - \frac{4}{9}\frac{\dot{\delta}^2}{(1+\delta^3)} + \frac{2}{3}\frac{H\dot{\delta}}{(1+\delta)^2} + \frac{1}{2}H^2\Omega_m\frac{1}{1+\delta} = \frac{1}{2}H^2\Omega_m. \tag{4.70}$$

The density contrast can be expanded since this equation is linearized in δ

$$\delta = \sum_{i=1}^{\infty}\delta_i = \sum_{i=1}^{\infty}\frac{D_i(\eta)}{i!}\delta_0^i.$$

This results for the first, second, and third order terms

$$\delta^{(1)}(t) = D_1(t)\delta_i;$$
$$\delta^{(2)}(t) = D_2(t)\frac{\delta_i^2}{2};$$
$$\delta^{(2)}(t) = D_3(t)\frac{\delta_i^3}{6}.$$

Applying in Equation 4.70 it is possible to obtain the following equations for each order of perturbation

$$\ddot{D}_1 + 2H\dot{D}_1 - \frac{3}{2}H^2\Omega_m D_1 = 0, \tag{4.71}$$

$$\ddot{D}_2 + 2H\dot{D}_2 - \frac{3}{2}H^2\Omega_n D_2 = 3H^2\Omega_m D_1^2 + \frac{8}{3}\dot{D}_1^2, \tag{4.72}$$

$$\ddot{D}_3 + 2H\dot{D}_3 - \frac{3}{2}H^2\Omega_n D_3 = 9H^2\Omega_m D_2 D_1 + 8\dot{D}_2\dot{D}_1 - 8\dot{D}_1^2 D_1 \tag{4.73}$$

Observing these equations for the spherical collapse model, the D_1 function is proportional to the expansion factor for a small time t or for $\Omega_m = 1$ that represents an EdS universe.

For the D_2 equation the initial condition when $t \to 0$ following the previous analysis for D_1 is $D_2(t) \sim \frac{34}{21} D_1(t)$ and for $D_3(t) \sim \frac{682}{189} D_1^3$.

The divergence of the velocity field can also be expanded, in a similar way to Equation 4.69, we can assume for the spherical collapse model

$$\theta(t) = \frac{3\dot{R}}{HR} - 3 \tag{4.74}$$

similar to Equation 4.69 the first relates to the ratio of the change in velocity and the last term is 3 representing the full quantity due to the 3 spatial coordinates. From Equation 4.44, in a similar way for this case, we can expand this velocity in terms of the δ_i expansion [58], [56]

$$\theta(t) = -f(\Omega_m, \Lambda) \left(E_1(t)\delta_i + E_2(t)\frac{\delta_i^2}{2} + E_3(t)\frac{\delta_i^3}{6} + ... \right), \tag{4.75}$$

from the solution of Equation 4.71 we know that D_1 is proportional do the expansion factor H, the first term of $f(\Omega_m, \Lambda)$ for this spherical collapse solution assuming Equation 4.74 is defined them as

$$f(\Omega_m, \Lambda) = \frac{a}{D_1}\frac{D_1}{da}. \tag{4.76}$$

Now also solving the dynamics for the divergence velocity, the same way as for the density contrast evolution equation Equation 4.70, following the same steps as in section subsection 4.1.2 with the proper time derivatives for a ΛCDM universe, we get

$$E_1(t) = D_1(t), \tag{4.77}$$

$$E_2(t) = D_1 \frac{d}{dD_1}(D_2 - D_1^2), \tag{4.78}$$

$$E_3(t) = D_1 \frac{d}{dD_1}(D_3 - 3D_2D_1 + 2D_1^3). \tag{4.79}$$

For more details about the spherical collapse model solutions, the studies in [58], [24] provides some analytic forms of these functions, on [58] he considers a non zero Λ case, in [24] it already assumes an EdS universe. In [56] there is a comparison of the numerical results for an ΛCDM model and compare to analytical results for a $\Lambda = 0$ case. We move forward to obtain the first, and second orders of the density and divergence velocity fields to calculate Equation 4.63 necessary to obtain the cosmological skewness Equation 4.65.

Starting with the linear solutions Equation 4.58-4.59 and also using the filtered fields properties shown in Equation 4.53 [56], we can write the fields equations for the first order $\delta^{(1)}(R_0)$ and $\theta^{(1)}(R_0)$ as

$$\delta^{(1)}(R_0) = \int \frac{d^3\vec{k}}{(2\pi)^{3/2}} \epsilon_{\vec{k}} W_{th}(kR_0) D_1(t), \tag{4.80}$$

$$\theta^{(1)}(R_0) = -f(\Omega_m, \Lambda) \int \frac{d^3\vec{k}}{(2\pi)^{3/2}} \epsilon_{\vec{k}} W_{th}(kR_0) D_1(t). \tag{4.81}$$

For the second order equations of $\delta^{(2)}(R_0)$ and $\theta^{(2)}(R_0)$ we need the set of equations of the

dynamics in Fourier space Equation 4.47, for second order of the fields

$$\frac{1}{H}\delta^{(2)}(\vec{k},t)+\theta^{(2)}(\vec{k},t)=a\frac{D_1}{da}D_1\int\frac{d^3\vec{k}}{(2\pi)^{3/2}}\mathcal{F}(\vec{k}',\vec{k}-\vec{k}')\epsilon_{\vec{k}-\vec{k}'}\epsilon_{\vec{k}'}, \tag{4.82}$$

$$\frac{1}{H}\dot{\theta}^{(2)}(\vec{k},t)+\left(2+\frac{\dot{H}}{H}\right)\theta^{(2)}(\vec{k},t)+\frac{3}{2}\Omega_m\delta^{(2)}(\vec{k,t})=-\left(a\frac{dD_1}{da}\right)^2\int\frac{d^3\vec{k}'}{(2\pi)^{3/2}}(\mathcal{F}(\vec{k}',\vec{k}-\vec{k}') + \mathcal{F}(\vec{k}-\vec{k}',\vec{k}')-2\mathcal{G}(\vec{k}',\vec{k}-\vec{k}'))\epsilon_{\vec{k}-\vec{k}'}\epsilon_{\vec{k}'}. \tag{4.83}$$

To better use the definitions of $\mathcal{F}$, $\mathcal{G}$ Equation 4.48 and to apply the properties of the random variables $\epsilon_{\vec{k}}$ Equation 4.60, we can work with the index notation such that for example $\mathcal{F}_{i,j}=\mathcal{F}(\vec{k}_i,\vec{k}_j)$ and $\mathcal{G}==\mathcal{F}(\vec{k}_i,\vec{k}_j)$, where i and j runs from 1 to 3. Remember that some terms will be canceled due to the properties of the random variables Equation 4.60. This results for Equation 4.82 and Equation 4.83

$$\delta^{(2)}(R_0)=\int\frac{d^3\vec{k}_1}{(2\pi)^{3/2}}\frac{d^3\vec{k}_2}{(2\pi)^{3/2}}\epsilon_{\vec{k}_1}\epsilon_{\vec{k}_2}W_{th}(|\vec{k}_1+\vec{k}_2|R_0)\left[D_1^2\mathcal{F}_{1,2}-\frac{3}{2}\mathcal{G}_{1,2}+\frac{3}{4}D_2\mathcal{G}_{1,2}\right] \tag{4.84}$$

$$\theta^{(2)}(R_0)=-\int\frac{d^3\vec{k}_1}{(2\pi)^{3/2}}\frac{d^3\vec{k}_2}{(2\pi)^{3/2}}\epsilon_{\vec{k}_1}\epsilon_{\vec{k}_2}W_{\mathrm{TH}}\left(\left|\vec{k}_1+\vec{k}_2\right|R_0\right)f(\Omega_m,\Lambda)\left[D_1^2\left(\mathcal{F}_{1,2}-\frac{3}{2}\mathcal{F}_{1,2}\right)+\frac{3}{4}E_2\mathcal{G}_{1,2}\right] \tag{4.85}$$

Now we have all pieces to obtain the cosmological skewness Equation 4.65, by replacing the terms we arrive at the form

$$S_3(R_0)=\frac{3}{\sigma^4(R_0)}\int\frac{d^3k_1}{(2\pi)^3}\frac{d^3k_2}{(2\pi)^3}P(k_1)P(k_2)W_1W_2W_{12}\mathcal{P}_{1,2} \tag{4.86}$$

where

$$\mathcal{P}=D_1^2(\mathcal{F}_{i,j}-\frac{3}{2}\mathcal{G}_{i,j})+\frac{3}{4}D_2\mathcal{G}_{i,j},\qquad W_i=W_{th}(k_iR_0),\qquad W_{ij}=W_{th}. \tag{4.87}$$

The solution of these integrals is done in every detail in the appendix of [56], these are very extensive, but basically uses geometry properties doing the integrations over a solid angle, combined with the Gaussian properties of the random variables Equation 4.60 and using the relations showed in this section for the density and divergence velocity fields, many terms ended up canceled and we end up with

$$S_3=\left(\frac{3D_2}{D_1^2}-\gamma_1\right), \tag{4.88}$$

where

$$\gamma_1=-\frac{d\log[\sigma^2(R_0)]}{d\log(R_0)}. \tag{4.89}$$

For an EdS case ($\Omega_m=1,\Lambda=0$) this reduces to the well-known value of

$$S_3=\frac{34}{7}-\gamma_1. \tag{4.90}$$

Many studies on the literature produce these calculations, but one must careful because that some authors already imply from the beginning that the calculations and approximations are done for an EdS universe [59], [57], [24], [58], [6], [65].

The calculations and steps to obtain this skewness are very extensive but also very well demonstrated in [56], [57], let us give a resume of what is basically done to get to this result. The skewness can be obtained by first expanding the quantities of the filtered density $\delta(R_0)$ and the divergence of the velocity field $\Theta(R_0)$ (obtained through the integration of a window function for a given scale R_0). These distributions ($\delta(R_0)$ and $\Theta(R_0)$) are then expanded with respect to random variables that are used to describe the initial density and velocity fluctuations, this is made to look for the leading order of the third moment distributions (skewness). Finding these leading terms results in the similar expression saw in this section $S_3 = \langle\delta(R_0)^3\rangle/\langle\delta(R_0)^2\rangle^2$ and $T_3 = \langle\Theta(R_0)^3\rangle/\langle\Theta(R_0)^2\rangle^2$.

With an equation of evolution of the density contrast (similar to the ones obtained in this chapter), it expands this density contrast in terms of growth functions. Here we obtain the growth functions of D_1, D_2 and D_3. After many mathematical manipulations and approximations its defined that $S_3(R_0) = (3D_2/D_1^2 - \gamma_1)$ where γ_1 is basically the logarithmic slope of the dispersion $\sigma^2(R_0)$ with the filtering radius R_0. This last term for our study can be neglected as this approximation is expected to work only for small amplitudes of perturbations $\sigma \lesssim 0.1$, this results for the skewness in the form

$$S_3 = 3\frac{D_2}{D_1^2}. \tag{4.91}$$

For more details is recommended [56], [57].

4.3.1 The growth functions for the single effective fluid

Now we return to our single effective fluid study since we know we need the density contrast equation in terms of the growth functions to be able to calculate the cosmological skewness for the matter density field. Assuming that all components are part of a single fluid, whose total EoS parameter is $w = w_m + w_{de}$ and square sound velocity $c^2 = c^2_{s(m)} + c^2_{s(de)}$. And assuming a total pressure $p = p_m + p_{de}$ with $p_m = 0$, the total EoS parameter is

$$w(a) = \Sigma\Omega_i(a)w_i(a) = \frac{\Omega_{de0}H_0^2}{H^2(a)}e^{-3\int da\frac{1+w_{de}}{a}}w_{de}(a). \tag{4.92}$$

The adiabatic sound speed for the fluid with total density of $\rho = \rho_m + \rho_{de}$ can be written as

$$c_a^2 = \frac{\dot{p}}{\dot{\rho}} = \frac{w}{1+w}\left[(1+w_{de}) - \frac{a}{3}\frac{w'_{de}}{w_{de}}\right]. \tag{4.93}$$

We apply the following decomposition

$$\delta = \sum_{i=1}^{\infty}\delta_i = \sum_{i=1}^{\infty}\frac{D_i(\eta)}{i!}\delta_0^i, \tag{4.94}$$

but in order to study the evolution of the density contrast at a first and second perturbative level, we will keep up to the $i = 2$ term. As a result, we are allowed to split Equation 4.34 into two equations. The first order perturbative equation for D_1 reads,

$$\begin{aligned} &a^2D_1'' + aD_1'\left(\frac{aH'}{H} + 3 - 3w + 3c_a^2 - \frac{aw'}{1+w}\right) \\ &-\frac{3}{2}\left(1 + 2w - 3w^2 + 2c_a^2(1+3w) + 2(aw' - c_a^2) - \frac{2aw'(w-c_a^2)}{1+w}\right) = 0. \end{aligned} \tag{4.95}$$

The equation for the second order perturbative term reads,

$$a^2 D_2'' + aD_2'\left(\frac{aH'}{H} + 3 - 3w + 3c_a^2 - \frac{aw'}{1-w}\right) - \frac{3}{2}D_2\left(1 + 2w - 3w^2 + 2(w'a - c_a^2) - \frac{2aw'(w - c_a^2)}{1+w}\right)$$
$$= a^2 D_1'^2\left(\frac{8/3 + c_a^2}{1+w}\right) - aD_1'D_1\left(\frac{2(w-c_a^2)(5+3c_a^2) - a^2c_a^2}{1+w} + \frac{2aw'}{(1+w)^2} + \frac{(8/3)c_a^2}{(1+w)^2}\right)$$
$$+ 3D_1^2\left((1+3c_a^2)(1+c_a^2) + \frac{2(w-c_a^2)^2 - 2(w-c_a^2)a^2c_a'^2}{1+w} + \frac{2a(w-c_a^2)w'}{(1+w^2)}\right), \tag{4.96}$$

where one can notice that the solution for D_1 found previously is used as a source term in the above equation.

Using Equation 4.91 and setting fixed values for H, w and c_a^2, we can study dark energy models. Since for the matter content $p = 0 \rightarrow w_m = 0$ and $c_{a(m)}^2 = 0$, the contribution of the dynamic dark energy will be inside the total equation of state parameter w and adiabatic sound velocity as described in Equation 4.92 and Equation 4.93.

4.4 Results for the single fluid analysis

In this chapter, we started with a detailed demonstration of the Neo Newtonian treatment of a hydrodynamic system. This system includes a portion of the matter content (baryonic and dark matter) and dark energy applying to a single fluid universe, where these fluids do not interact but can influence each other's evolution. To analyze how dark energy perturbations could influence structure formation we make use of the definition of skewness defined by Equation 4.91 [56], [57]. Expanding the equation of the evolution of density contrast Equation 4.34 into first Equation 4.95 and second order Equation 4.96 we can solve this system to obtain numerically D_1 and D_2. These results produced the published work [4].

The main difference in evaluating a case with and without dark energy perturbations will be how this dark energy is included. The density contrast δ is evaluated for the matter content since we are interested in the skewness of its distribution and the dark energy content can be included only in the background through the expansion rate H for the case without dark energy perturbations or we can include dark energy perturbations through the total equation of state parameter w and sound velocity c_a^2 in Equation 4.95 and Equation 4.96, this way we can evaluate different models for both cases. For matter, these terms are zero, so they will carry only the dark energy component in these terms.

It is set $\delta(a_0) = 10^{-3}$ and $\delta' = 0$ with $a_0 = 10^{-3}$ the scale factor around the decoupling era [60] for the initial conditions. We can assume an Einstein-de Sitter universe $\Omega_m = 1$ description during the period of radiation and matter equality before arriving at the dark energy era $z_{eq} < z < z_{de}$, where $z_{eq} \sim 3300$ and $z_{de} \lesssim 1$. As seen in Figure 2.1 and Figure 2.4, structures are formed during this period and with S_3 it is possible to measure the asymmetry generated by the matter fluctuations due to the formation of larger structures. Solving D_1 we can use its solution to also solve D_2, since it is a source term in Equation 4.96.

Since we are interested in the dark energy influence and effects on structure formation we are going to evaluate the solutions for skewness S_3 for today $a = 1$ and also show its dependence related to the matter density parameter Ω_{m0}. In Figure 4.1 we show the results of this analysis, this study is also present in [4]. Both figures show today's skewness $S_3(a = 1)$ in the function of the density parameter Ω_{m0}, we also analyze the dark energy equation of state parameter in a range of $-1.15 < w_0 < -0.85$ for all cases.

The left plot in Figure 4.1 shows cases without dark energy perturbations, these results are ranged around the ΛCDM model as expected since the only variation is in the values of the equation of state parameter for dark energy that are only included on the background, represented as w_0. Its value only enters in the expansion rate H for this case and the other terms with w in the perturbative growth rates are considered zero for the pressureless matter fluid and the adiabatic sound velocity is also zero $c_a^2 = 0$ as defined in Equation 4.93. The ΛCDM model is represented by the red line in both plots. On the left the variation around the model is small and the skewness value around a standard matter density parameter $\Omega_{m0} \sim 0.3$ is $S_3 \sim 4.91$. The range of lighter (yellow) to darker colors (dark green) goes from the quintessence range $w_{de} > -1$ and phantom range $w_{de} < -1$ respectively. Our sets of equations when evaluated for an EDS universe ($\Omega_{m0} = 1$) gives the expected value of $S_3 = 34/7$ [56], [57] (black dot in the right plot). These results agree with the literature [66].

For the right side of Figure 4.1 we include dark energy perturbations through the total equation of state parameter Equation 4.92 and sound velocity Equation 4.93 in Equation 4.95 and Equation 4.96, not just in the expansion rate as the previous case. Assuming a single fluid its total density contrast would be affected by the matter δ_m and dark energy δ_{de} fluctuations. Since both are sourced by the gravitational potential Φ (this can also be seen in Equation 4.35), the measurements around the matter clustering by the surveys can't distinguish between them. Using dark energy fluctuations in the total fluid perturbations can also be justified if we look into the usual quantity measured for the total matter perturbations δ_m, that is associated with the baryonic fluctuations within a dark matter potential well, both correlated by the bias factor $\delta_b = b\delta_{dm}$. Other studies involving dark energy perturbations use similar methods related to the total fluid fluctuations [67], [2], [3], [68].

Now the total fluid can include different sound velocities associated with the dark energy component, for the cases of $c_a^2 \neq 0$, this would leave a scale dependence if we look into Equation 4.40. By the definition of c_a^2 in Equation 4.93 this last term would remain small due to our range of tests for this analysis, so this term is neglected.

The right panel of Figure 4.1 shows a great increase in the skewness value for today when adding dark energy perturbations. The blue and orange stripes contain dark energy perturbations, both analyses are for a constant equation of state parameter w_{de} included in the total fluid parameter as defined in Equation 4.92. The blue one presents a case with $c_a^2 \neq 0$ where we use the definition of Equation 4.93. The orange stripe its set $c_a^2 = 0$ as done in [69], [54]. Both cases goes from the darker color for values of $w_0 = -1.15$ to lighter colors for $w_0 = -0.85$. Some interposition is made between the colored stripes where the darker orange superposition is a little part of the lighter blue. It also shows where the S_3 values for the PLANCK 2018 matter density parameter $\Omega_{m0} \sim 0.315$ would reach, being around a value of $S_3 \sim 17$. Compared to the EdS, $S_3 \sim 4.857$, also shown in this panel represented by the black dot, the values of S_3 get to 3 times higher. The ΛCDM case is also shown represented by the red dotted line, this is the same line as the previous left side panel, used only for comparison.

These results show that including the dark energy perturbations as part of the single fluid can increase substantially the values of skewness S_3. The usual way to calculate skewness is by only doing the calculation of equations D_1 and D_2 for the matter content, but in our case when including the dark energy content as a clustering component through w and c_a^2, the whole content of the universe is taken into account increasing significantly the skewness values. For skewness, there is also only a small dependence of the equation of state parameter for dark energy w_0 observed in this analysis. With these results, the interest in doing more analysis of these effects for clustering dark energy would rise. This is not the only way to include dark energy perturbations in the study of the skewness of the matter content. In the next chapter, a

different approach is made and different results would be produced.

Figure 4.1: Skewness as a function of today's matter density parameter Ω_{m0}. Left: Case without dark energy perturbations. For $\Omega_{m0} = 0.315$, the skewness is approximate $S_3 \approx 4.91$ and the red-dashed curved represents the ΛCDM model. The panel shows the values for the dark energy equation of state parameter w_0 without DE perturbations. The color schemes shows an increase ($w_0 > -1$ light green) and a decrease ($w_0 < -1$ darker green). Right: The colored stripes here consider dark energy perturbations. The blue color scheme is for cases with $c_a^2 = 0$. The orange one is for a c_a^2 defined by Equation 4.93. The black dot is for the EDS case $\Omega_{m0} = 1$ where $S_3 = 34/7 \approx 4.857$. The blacks lines show the limits for the Planck best fit value of $\Omega_{m0} = 0.315 \pm 0.07$.

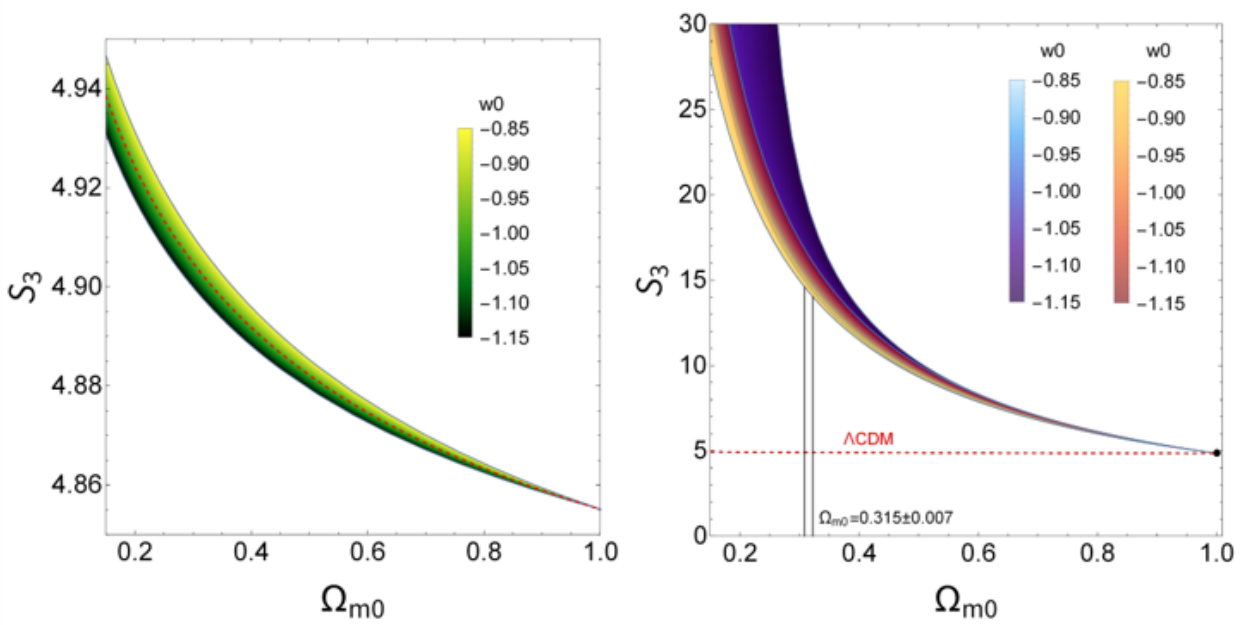

Source: Produced by the author [4].

Skewness in clustering dark energy cosmology: detailed approach

This study will show general equations that are also valid for a system of two non-interacting fluids, but in this case, instead of a set of 3 hydrodynamics equations (continuity, Euler, Poisson), we have 5 (2 continuities, 2 Euler, one Poisson).

5.1 Two Fluid Universe Dynamics

The search for the effects of dark energy clustering in structure formations continues in the following work [5]. The idea is to introduce a more general approach than the previous analysis, where the dark energy fluid would be a separated component with its own equation for the density contrast evolution δ_{de}. The system contains, for two fluids (one of matter and other of dark energy), the following 5 equations: 2 continuities Equation 3.46, 2 Euler Equation 3.47 and 1 Poisson Equation 3.48 equations. The fluids are connected to the gravitational potential in the Poisson equation that sources the gravitational clustering. Doing the same calculations in the previous chapter until Equation 4.35, we can separate two of these same equations for each fluid. In the following sections, the final system of equations will be reproduced for further analysis.

5.1.1 Dynamics of the matter and dark energy fluids

As previously suggested in this chapter, in a universe composed by two fluids, one of the total matter content and the other of dark energy, the Poisson equation can be written as:

$$\nabla^2\Phi = -4\pi G a^2(1+3c_{de}^2)\rho_{de}\delta_{de} - 4\pi G a^2\rho_m\delta_m. \tag{5.1}$$

Each density evolution is given by

$$\begin{aligned}\rho_m &= \rho_m^{(0)}\left(\frac{a_0}{a}\right)^3,\\ \rho_{de} &= \rho_{de}^{(0)} exp\left[-\int_1^0 \frac{3(1+w_{de})}{\tilde{a}}d\tilde{a}\right].\end{aligned} \tag{5.2}$$

Defined the density parameter, it is possible to isolate the density in terms of the density parameter as follows

$$\begin{aligned}\Omega_x &= \frac{8\pi G\rho_x}{3H^2} = \frac{8\pi G\rho_x a^2}{3\mathcal{H}^2},\\ \rho_x &= \frac{3\mathcal{H}\Omega_x}{8\pi G a^2}.\end{aligned} \tag{5.3}$$

That means that for our two fluids their respective density parameters can be used to replace the densities in the Poisson equation

$$\Omega_m^{(0)} + \Omega_{de}^{(0)} = 1,$$
$$\Omega_m^{(0)} = \frac{8\pi G\rho_m^{(0)}a^2}{3\mathcal{H}_0^2}, \qquad \Omega_{de}^{(0)} = \frac{8\pi G\rho_{de}^{(0)}a^2}{3\mathcal{H}_0^2}, \tag{5.4}$$

$$\nabla^2\Phi = -\frac{3}{2}\Omega_m\mathcal{H}^2\delta_m - \frac{3}{2}\Omega_{de}\mathcal{H}^2\delta_{de}(1+3c_{de}^2). \tag{5.5}$$

Finally, we have all terms to complete the evolution of the density contrast equation, but for simplicity, the two fluids Poisson equation will be replaced a bit further. For the dark energy fluid (with $A = 1 + w_{de} + (1+c_{de}^2)\delta_{de}$), its density contrast equation using Equation 4.35 is:

$$\begin{aligned}
&\delta_{de}'' + \delta_{de}'\left[3(c_{de}^2 - w_{de}) + \left(1+\frac{\mathcal{H}'}{\mathcal{H}}\right) - \frac{w_{de}'}{A}\right] - \delta_{de}'^2\left[\frac{4/3 + c_{de}^2}{A}\right] \\
&+ \delta_{de}\delta_{de}'\left[\frac{(w_{de}-c_{de}^2)(5+3c_{de}^2) - c_{de}'^2}{A}\right] + \delta_{de}^2\left[\frac{3(w_{de}-c_{de}^2)c_{de}'^2 - 3(w_{de}-c_{de}^2)^2}{A}\right] \\
&+ 3\delta_{de}\left[(c_{de}'^2 - w_{de}') + \left(1+\frac{\mathcal{H}'}{\mathcal{H}}\right)(c_{de}^2 - w_{de}) + \frac{w_{de}'(w_{de}-c_{de}^2)}{A}\right] \\
&+ \frac{A}{\mathcal{H}^2}\nabla^2\Phi = \frac{A}{\mathcal{H}^2}\nabla\left[\frac{\nabla(c_{de}^2\delta_{de})}{A}\right]
\end{aligned} \tag{5.6}$$

For the matter fluid, its pressure is zero, so Equation 4.35 simplifies greatly due to $w_m = 0$ and $c_m^2 = 0$:

$$\delta_m'' + \delta_m'\left(1+\frac{\mathcal{H}'}{\mathcal{H}}\right) - \delta_m^{2\prime}\left(\frac{4/3}{1+\delta_m}\right) + (1+\delta_m)\frac{\nabla^2\Phi}{\mathcal{H}^2} = 0. \tag{5.7}$$

These results were used in the work [5], and further in this chapter, it will be shown the analysis and results made with these equations.

5.1.2 The growth functions for the two fluid universe

Since our focus is on the skewness for the matter clustering, for the matter equation δ_m we are going to expand the density contrast like in the previous chapter

$$\delta = \sum_{i=1}^{\infty}\delta_i = \sum_{i=1}^{\infty}\frac{D_i(\eta)}{i!}\delta_0^i.$$

For the calculation of skewness, we need only until the second order term of the expansion such that,

$$\delta = D_1\delta_0 + \frac{D_2}{2}\delta_0^2. \tag{5.8}$$

Some terms have a fraction with the density contrast that is considered to be very small since it is a fluctuation. For these terms is possible to use the Taylor expansion as follows

$$\frac{1}{1+\delta_m} \to \frac{1}{1-(-\delta_m)} \to 1 + (-\delta_m). \tag{5.9}$$

Now replacing the expansions in the matter equation and considering only first and second order terms

$$D_1''\delta_0 + \frac{D_2''}{2}\delta_0^2 + \left(D_1\delta_0 + \frac{D_2}{2}\delta_0^2\right)'\left(1+\frac{\mathcal{H}'}{\mathcal{H}}\right) - \left(D_1'^2\delta_0^2\frac{4}{3}\right) + \left(1 + D_1\delta_0 + \frac{D_2}{2}\delta_0^2\right)\frac{\nabla^2\Phi}{\mathcal{H}^2} = 0. \tag{5.10}$$

The equation above provides us with two equations, one for first order that carries terms with only δ_0 terms that can be written as

$$D_1'' + D_1'\left(1+\frac{\mathcal{H}'}{\mathcal{H}}\right) - \frac{3}{2}D_1\Omega_m - \frac{3}{2}\Omega_{de}\delta_{de}(1+3c_{de}^2) = 0, \tag{5.11}$$

and other for second order equation that would carry δ_0^2 terms

$$D_2'' + D_2'\left(1+\frac{\mathcal{H}'}{\mathcal{H}}\right) - \frac{8}{3}D_1'^2 - \frac{3}{2}D_2\Omega_m - 3D_1^2\Omega_m - 3D_1\Omega_{de}\delta_{de}(1+3c_{de}^2) = 0. \tag{5.12}$$

As for the dark energy fluctuations equations, we can simplify Equation 5.6 only using the first order of perturbations, since for the calculation of skewness we only need high orders for the matter content where the calculations and measurements are made. The first order equation for the evolution of the dark energy fluctuations δ_{de} is defined as

$$\begin{aligned}&\delta_{de}'' + \delta_{de}'\left[3(c_{de}^2 - w_{de}) + \left(1+\frac{\mathcal{H}'}{\mathcal{H}}\right) - \frac{w_{de}'}{1+w_{de}}\right] \\ &+ 3\delta_{de}\left[(c_{de}^2 - w_{de}') + \left(1+\frac{\mathcal{H}'}{\mathcal{H}}\right)(c_{de}^2 - w_{de}) + \frac{w_{de}'(w_{de}-c_{de}^2)}{1+w_{de}}\right] \\ &- (1+w_{de})\frac{3}{2}\left[\Omega_m D_1 + \Omega_{de}\delta_{de}(1+3c_{de}^2)\right] = \frac{1+w_{de}}{\mathcal{H}^2}\nabla\left[\frac{\nabla(c_{de}^2\delta_{de})}{1+w_{de}}\right].\end{aligned} \tag{5.13}$$

This completes our set of equations that will be solved numerically obtaining the values of skewness using the definition in Equation 4.91. In terms of the scale factor these equations transformed as $d/dN \to d/da$, are rewritten in the following form (from here $'$ is d/da):

$$a^2D_1'' + aD_1'\left(\frac{aH'}{H}+3\right) - \frac{3}{2}D_1\Omega_m - \frac{3}{2}\Omega_{de}\delta_{de}(1+3c_{de}^2) = 0, \tag{5.14}$$

$$a^2D_2'' + aD_2'\left(\frac{aH'}{H}+3\right) - \frac{8}{3}a^2D_1'^2 - \frac{3}{2}D_2\Omega_m - 3D_1^2\Omega_m - 3D_1\Omega_{de}\delta_{de}(1+3c_{de}^2) = 0. \tag{5.15}$$

The dark energy perturbations equation can be transformed to Fourier space due to the last term with $\nabla_x \to ik^2$, this transformation gives

$$\begin{aligned}&\delta_{de}'' + \delta_{de}'\left[3(c_{de}^2 - w_{de}) + \left(1+\frac{\mathcal{H}'}{\mathcal{H}}\right) - \frac{w_{de}'}{1+w_{de}}\right] \\ &+ 3\delta_{de}\left[(c_{de}^{2\prime} - w_{de}') + \left(1+\frac{\mathcal{H}'}{\mathcal{H}}\right)(c_{de}^2 - w_{de}) - \frac{w_{de}'(c_{de}^2-w_{de})}{1+w_{de}}\right] \\ &- (1+w_{de})\frac{3}{2}\left[\Omega_m D_1 + \Omega_{de}(1+3c_{de}^2)\delta_{de}\right] + \frac{c_{de}^2k^2}{\mathcal{H}^2}\delta_{de} = 0.\end{aligned} \tag{5.16}$$

The set of equations above enables us to calculate the skewness for the clustering of matter through the solutions of D_1 and D_2. The equation for the dark energy density contrast is necessary since we treat this system for two separated fluids. The dark energy fluctuation term enters equations D_1 and D_2 through the Poisson component that connects the dynamics of the whole system. The results of this study are presented in the next section.

5.2 Results for the two fluid analysis

Using the main set of equations Equation 5.14-5.16 it is possible to obtain the skewness of the matter content through Equation 4.91. This chapter sets the initial conditions and values used to numerically evaluate these equations for this analysis of dark energy perturbations inserted this time by Equation 5.16. This study was also explored in [5].

For the dark energy equation, looking into the last term of Equation 5.16, there is a dependence on the wavenumber k. However, we have checked that S_3 is very weakly dependent on k-values on the range of scales of cosmological interest. These changes can get to as lower as 10^{-5} when compared to changes of values of the matter density parameter Ω_{m0}, and 10^{-3} for changes of the dark energy equation of state parameter w_{de}, these results can be seen in Figure 5.1 and are reproduced by numerically solving Equation 5.14-5.16 for the skewness values for today ($a = 1$). For the left panel, we have also tested for other values of fixed w_{de} and all results produce the same behavior, where for the same w_{de} the curves would remain indistinguishable for different values of Ω_{m0}. The k-dependence will be neglected by adopting k=0.01 h/Mpc for the next results, this is close to the range of scales effectively observed in large-scale surveys.

Figure 5.1: Impact of the wavenumber k values from a range of 0.01 to 0.1 on skewness S_3. On the left, there are 3 cases of Ω_{m0} of values 0.2, 0.3, and 0.4 but all cases are practically identical being only visible on one curve since all curves make superpositions, all cases are made for a same w_{de}, in this plot, we show for $w_{de} = -1$. For the right side, the colors are for different values of the equation of state parameter w_{de} being orange for a quintessence case $w_{de} = -0.85$, blue for $w_{de} = -1$ and magenta $w_{de} = -1.15$ and a fixed $\Omega_{m0} = 0.3$.

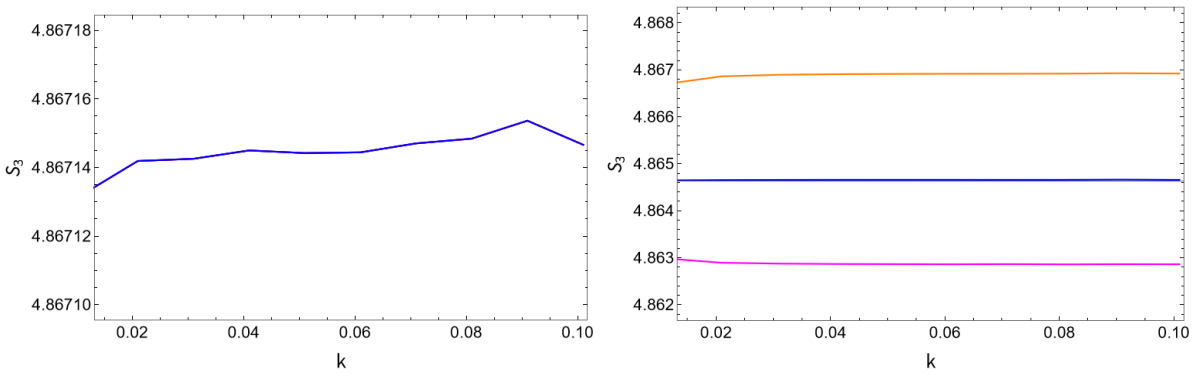

Source: Produced by the author.

We expand our analysis on skewness by not only evaluating its values with respect to cosmological parameters but also by providing a fit equation for some case studies. In the literature, the expansion of skewness is provided usually around the Einstein-De-Sitter universe ($\Omega_m = 1$ and $c_{de}^2 = 0$). In a work from Bernardeau (2002) [57] it is mentioned the importance of knowing the

dependence of skewness of cosmological parameters since it is induced by gravitational dynamics, it introduces by some explicit calculations from [70] and doing an expansion around and EdS universe the following result:

$$S_3 = \frac{34}{7} + \frac{6}{7}(\Omega_{m0}^{-0.03} - 1). \tag{5.17}$$

This equation demonstrates that skewness has a very weak dependence on the matter density parameter Ω_{m0}. In our work [5] we expand this to other cosmological parameters and for a universe where $\Omega_\Lambda \neq 0$, since usually for a flat $\Omega_m + \Omega_\Lambda = 1$ universe, a simple equation like Equation 5.17 is not provided. This last case ($\Lambda \neq 0$) is usually obtained by solving the set of equations Equation 5.14 and Equation 5.15 but considering $\delta_{de} = 0$ since it is not common to use dark energy perturbations. Without dark energy perturbations this set of equation is equal to the one usually solved for $\Omega_\Lambda \neq 0$ derived from Bernardeau (1994) [6], this case is also studied in [71, 65, 72].

With our set of equations Equation 5.14-5.16 we have a more general approach, where the simpler case without dark energy perturbations can be obtained by making $\delta_{de} = 0$ and an EdS case by solving D_1 and D_2 for $\Omega_{m0} = 1$. Since we have one more equation than usual, for δ_{de}, providing the cosmological variables for dark energy w_{de} and c_{de}^2, the goal is to make new equations for skewness S_3 with these extra variables.

Besides the fit equations we are going to provide, we solve numerically the set of equations to evaluate the skewness for different scenarios and since the dark energy sound speed c_{de}^2 is a free parameter we shall adopt the following values

- $c_{de}^2 = 0$;
- $c_{de}^2 = 1$;
- $c_{de}^2 = 1/3$.

From the constant values above one can notice we do a different approach from the previous work [4] mentioned in the previous chapter. Since there we use the definition for the sound velocity for dark energy given by Equation 4.93.

Looking into a scalar field model of dark energy, whose action is given by

$$S(\phi) = \int \sqrt{-g}\mathcal{L}(X, \phi)d^4x \tag{5.18}$$

where $\mathcal{L}(X, \phi)$ is the Lagrangian density of the scalar field [73], [74], [75], [76], [77]. The equation of state parameter and effective sound speed for such action can then be written as

$$w_{de} = \frac{\mathcal{L}(X, \phi)}{2\left(\frac{\partial \mathcal{L}}{\partial X}\right) X - \mathcal{L}(X, \phi)}, \tag{5.19}$$

$$c_s^2 = \frac{\left(\frac{\partial \mathcal{L}}{\partial X}\right)}{\left(\frac{\partial \mathcal{L}}{\partial X}\right) - 2X\left(\frac{\partial^2 \mathcal{L}}{\partial X^2}\right)}. \tag{5.20}$$

Assuming a constant c_s^2 the general form of the Lagrangian is obtained

$$\mathcal{L} = VX^{\frac{1+c_s^2}{2c_s^2}} - U, \tag{5.21}$$

where $U(\phi)$ and $V(\phi)$ are the potentials and $X = \phi_{;i}\phi^{;i}/2$ is the kinetic energy term for the field ϕ. So assuming an $c_{de}^2 = 1$ as mentioned above is considered the effective sound speed of a scalar field component, since for $c_s^2 = 1$ the Lagrangian is reduced to the canonical form $\mathcal{L} = X - U$.

For the limits of $c_{de}^2 = 0$ the work on [78] expand this analysis where essentially the dark energy perturbations follow the behavior of the pressureless-like clustering fluid. And last for $c_{de}^2 = 1/3$, is inspired by the analysis in [79] where it made and "model independent" reconstruction of dark energy suggesting this value for the sound speed of dark energy.

For initial conditions to solve Equation 5.14, Equation 5.15 and Equation 5.16 we set $a_i = 1/(1 + z_i)$, with $z_i \simeq 300000$. Such a greater (more in the past) initial condition for the redshift, when compared to the previous analysis where we utilize and $a_0 = 10^{-3}$, is adopted because when doing a more detailed analysis of the numerical solutions we noticed the need to make the time for the initial condition, to go to zero $t \to 0$, this is also mentioned in [6]. If the initial condition is not sufficient to make the time goes to a zero value this would carry a residual error that can be seen when solving the equations for an EdS universe $\Omega_m = 1$. The expected value of the skewness for this case $S_3^{EdS} = 34/7 \sim 4.85714$ would not be precisely obtained for a "lower" initial condition value, like the previously used $a_i = 10^{-3}$, making us obtain a value of $S_3 \sim 4.854$ for this analysis where the dark energy fluctuations have its own equation for its evolution being a two fluid system.

The results may vary the free parameters, sometimes fixing w_{de}, Ω_{m0} or c_{de}^2 and even time z will be fixed or varied. The value used for the majority of the results for H_0 is 70. Only one result will use a different value due to observational comparison, this will be mentioned when modified in Figure 5.8.

On Figure 5.2 we show the time evolution for the skewness. Here the ΛCDM model is represented by the blue line where it is set $w_{de} = -1$ and $\Omega_{m0} = 0.3$. The black line represents the EdS case with $\Omega_{m0} = 1$ hitting the value $S_3 \sim 4.857$ giving a constant behavior since we have a universe only composed of matter. Compared to the ΛCDM case one can notice already that the dark energy will produce more skewness with time, this makes sense since the expansion would spread the matter clusters creating more non-Gaussianity effects in the skewness of the matter content. This figure also provides other models where dark energy perturbations are included, setting $c_{de}^2 = 1$ for solid lines and $c_{de}^2 = 0$ for dot-dashed lines. The ΛCDM (blue line) appears with only one line. This is expected since for this model c_{de}^2 appears only for dark energy perturbations models (see equations Equation 5.14-5.16). So changing this value would not make a difference in its result. The results with dark energy perturbations have a fixed $\Omega_{m0} = 0.3$ value but different equations of state parameters being $w_{de} = -0.8$, $w_{de} = -0.9$ and $w_{de} = -1.2$. Cases without dark energy perturbations are represented by the dashed line. In these cases only w_{de} vary. The non-Gaussianity increases from $z \sim 1$ where we have the dark energy manifestation, reaching asymptotically constant values today.

The next figure shows the value of S_3 for today $z = 0$ as a function of the matter density parameter Ω_{m0} for several cases of w_{de} and c_{de}^2 in Figure 5.3. The left panel we notice the similar behavior as seen in Figure 5.2, where for $c_{de}^2 = 0$ the skewness depends more on the cosmological parameters, such that the quintessence [66] case of $w_{de} = -0.9$ (dot-dashed orange line) decreases and the phantom [80] $w_{de} = -1.2$ (dot-dashed magenta line) increases by an greater amount. The other cases $c_{de}^2 = 1$ and no DE perturbations, have a small change in S_3 (around 1%).

For the right panel of Figure 5.3 we already provide a fit equation represented by the red crosses. The fits numerically calculated in this analysis provide S_3 as a function of the cosmological parameters. The quality of the fits will be evaluated by two measurements: the maximum relative deviation (MRD) and the average standard relative deviation (ASRD). These are defined respectively as the following percentages

Figure 5.2: Skewness time evolution in function of redshift. Solid lines represents $c^2_{de} = 1$ cases, dot-dashed $c^2_{de} = 0$ and dashed no DE perturbations. The colors represents the following cases: blue for a ΛCDM case i.e., $\Omega_{m0} = 0.3$, $w_{de} = -1$; black for EdS case i.e., $\Omega_{m0} = 1$. Then, always putting $\Omega_{m0} = 0.3$, we employ orange for $w_{de} = -0.8$; red for $w_{de} = -0.9$ and magenta for $w_{de} = -1.2$.

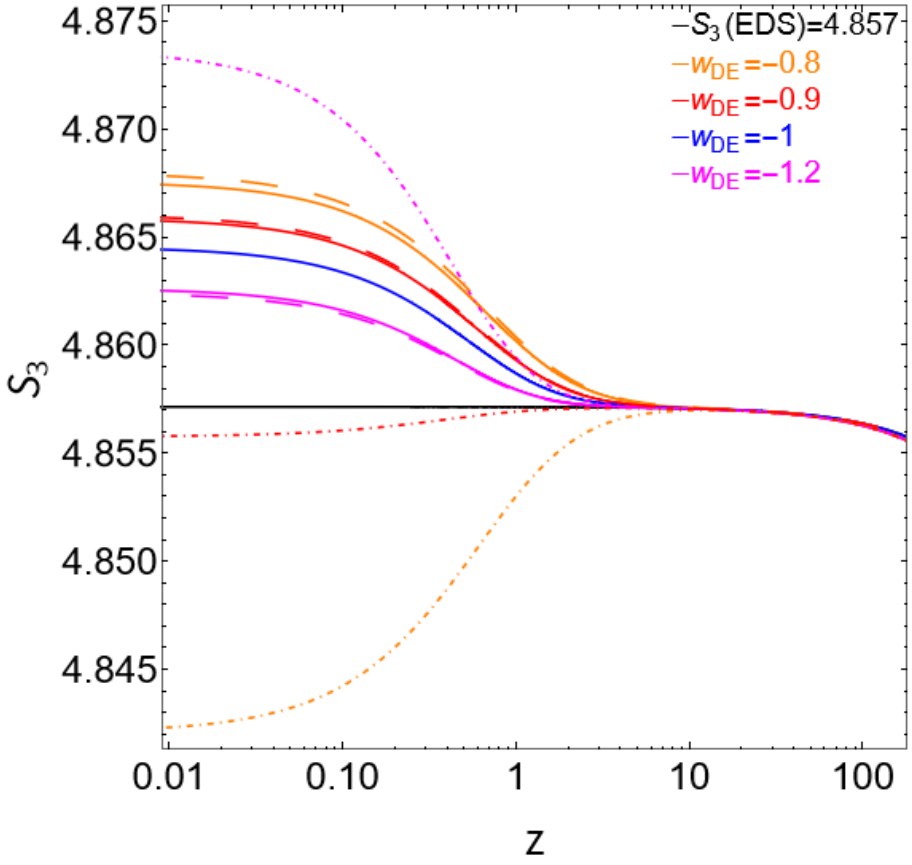

Source: Produced by the author [5].

$$MRD = 100\, Max\Big|\frac{Fit(i) - Data(i)}{Fit(i)}\Big|,$$
$$ASRD = 100\sqrt{\frac{1}{N}\sum\Big(\frac{Fit(i) - Data(i)}{Fit(i)}\Big)^2}, \tag{5.22}$$

where $Data(i)$ represents the numerical outcomes from solving our system of equations for a number i of parameter values and $Fit(i)$ is the numerical value for the fitted function. The goal is a precision greater than 1% for ASRD and maximum MRD across all the parametric ranges.

On the right panel of Figure 5.3 the ΛCDM case ($w_{de} = -1$ and $\delta_{de} = 0$) represented by the dashed black line is given a fitted equation represented by the red crosses. The fit provides the following equation

$$S_3(\Omega_{m0}) = 4.857 - 0.053(\Omega_{m0}^{0.129} - 1). \tag{5.23}$$

This fit has the quality measures of $MRD = 0.01\%$ and $ASRD = 0.02\%$. This case is almost

identical to Bernardeau's result in [6]. This is expected since Bernadeau's equations are the same as our set equations when $\delta_{de} = 0$. This panel also shows dark energy perturbations models for phantom and quintessence cases with $c^2_{de} = 1$ provided by the solid lines. These are the same lines as the ones in the left panel.

Figure 5.3: Dependence of the skewness on the density parameter Ω_{m0}. In the left panel the dot-dashed lines represent $c^2_{de} = 0$, solid lines $c^2_{de} = 1$ and dashed lines is the case without dark energy perturbations ($\delta_{de} = 0$). The colors refer to different w_{de} values: blue for $w_{de} = -1$, magenta for $w_{de} = -1.2$ and orange for $w_{de} = -0.9$. The dashed and solid blue lines are indistinguishable. On the right side we show the skewness for $\Lambda \neq 0$ by Bernardeau (1994) [6] (dashed blue) compared to our result (dashed black) for the ΛCDM case ($w_{de} = -1$, $\Omega_{m0} = 0.3$ (black dot) and no dark energy perturbations $\delta_{de} = 0$). The black line is for the EdS skewness value of $34/7 = 4.857$. The fit Eq.(5.23) is represented by the red cross symbols.

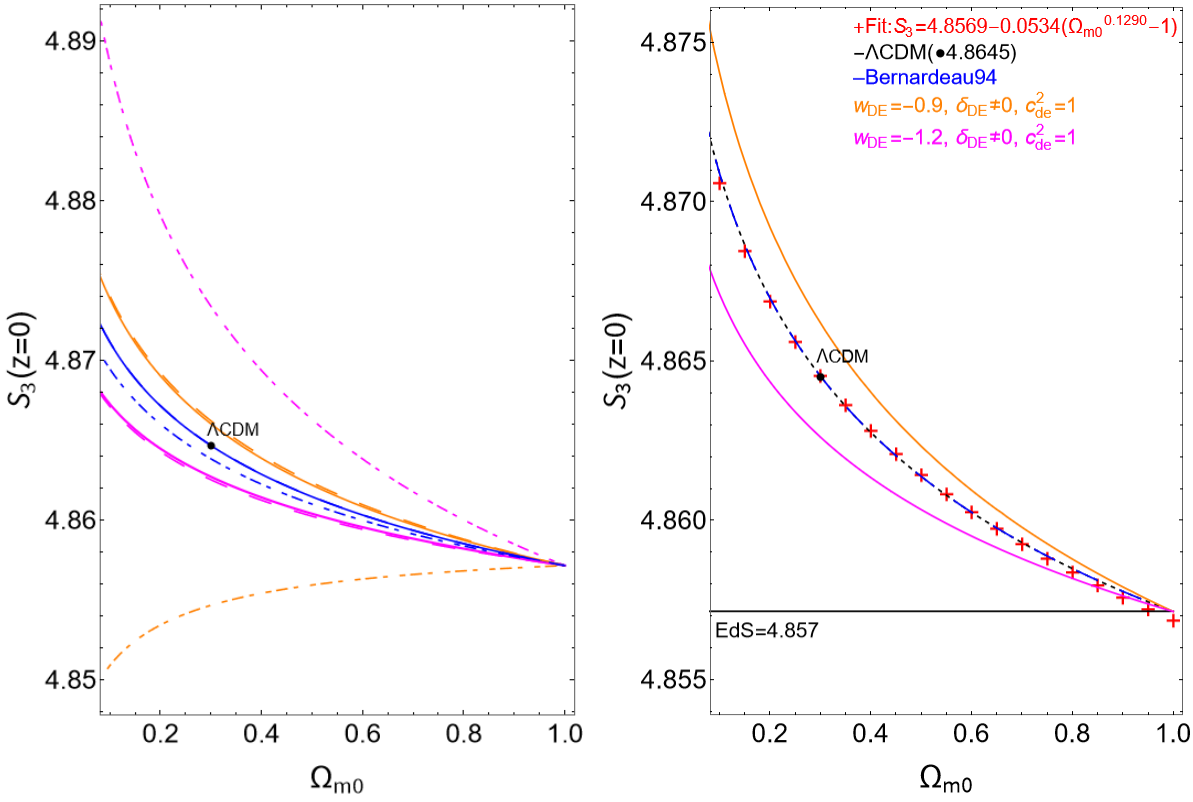

Source: Produced by the author [5].

The plot on Figure 5.4 shows a different point of view from the previous figure, where it shows the dependence of S_3 on the dark energy equation of state parameter w_{de}. The dot-dashed and solid lines still represents the cases of $c^2_{de} = 0$ and $c^2_{de} = 1$ respectively. Changing the point of view provides us with the same results where the difference between the cases without dark energy perturbations and $c^2_{de} = 1$ are very small. It is interesting to notice that around $w_{de} \sim -0.92$, for the $c^2_{de} = 0$ cases there is a change in the dependence of the skewness at the same time it crosses the usual S_3 EdS value, such that the cases with more matter $\Omega_{m0} = 0.4$ passes to have greater skewness for $w_{de} \geq -0.92$ cases than the $\Omega_{m0} = 0.2$ cases that have less matter quantity.

We also have the behavior of the growth functions D_1 and D_2 as a function of time in Figure 5.5.

Figure 5.4: Dependence of S_3 on the dark energy equation of state w_{de}. The colored curves refers to different values of the matter density parameter, namely $\Omega_{m0} = 0.2$ (red), $\Omega_{m0} = 0.3$ (blue) and $\Omega_{m0} = 0.4$ (purple). The black line sets the Einstein-de Sitter value 34/7. We assumed $c^2_{de} = 1$ for solid lines, $c^2_{de} = 0$ for dot-dashed lines and no DE perturbations ($\delta_{de} = 0$) for dashed lines (hardly visible next to the solid curves).

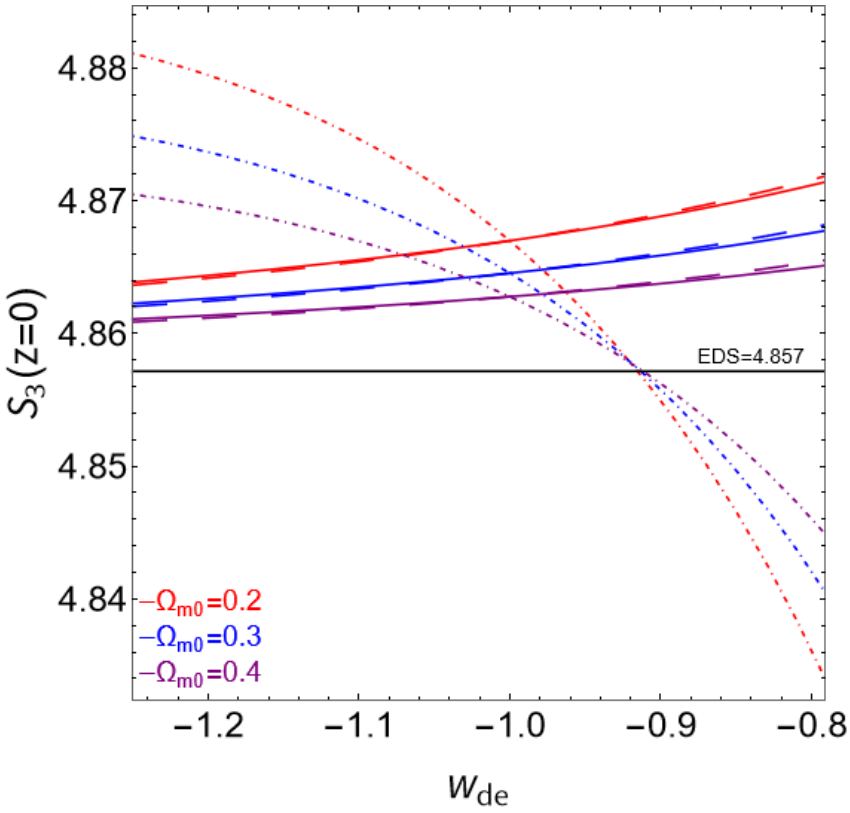

Source: Produced by the author [5].

This plot is made for several values of w_{de} as used in previous plots but fixed $\Omega_{m0} = 0.3$.

With our set equations we can provide more general fitting formulas of S_3 with the w_{de}, Ω_{m0} and c^2_{de} variables. First we set a simple parametrization using only Ω_{m0} and w_{de} as variables:

$$S_3(\Omega_{m0}, w_{de}) = a + b(\Omega^c_{m0} - 1) + d|(1 + w_{de})|^e + f(1 + \Omega_{m0} w_{de}). \tag{5.24}$$

The expression above for S_3 has six constants represented by the letters a, b, c, d, e and f. We provided tables for two scenarios, one for phantom Table 5.1 and the other for quintessence Table 5.2 cases. Each table shows which value of the dark energy sound velocity c^2_{de} is fixed and the respective MRD and ASRD measurements.

We have chosen the values of Table 5.2 for the fit of Equation 5.24 to show an example of the accuracy of our fit in Figure 5.6, since its the case with the largest MRD and ASRD. For the other parametrizations, since MRD and ASRD are smaller, it produces even better fits.

In tables Table 5.1 and Table 5.2 the results for $c^2_{de} = 1$ and $c^2_{de} = 1/3$ are very similar and $c^2_{de} = 0$ provides the more distinct result, this behavior was also observed in previous results Figure 5.2, Figure 5.3, Figure 5.4. This can be explained since $c^2_{de} = 0$ vanishes with the oscillations provided by the $(k/\mathcal{H}) \approx 10^3$ term from the DE perturbative equation Equation 5.16.

Figure 5.5: D1 and D2 evolutions with the scale factor a. All cases are made for a fixed $\Omega_{m0} = 0.3$ and different values of w_{de}, $w_{de} = -1.2$ magenta, $w_{de} = -1$ blue, $w_{de} = -0.8$ orange. The solid lines represent D1 functions and D2 by the dashed lines.

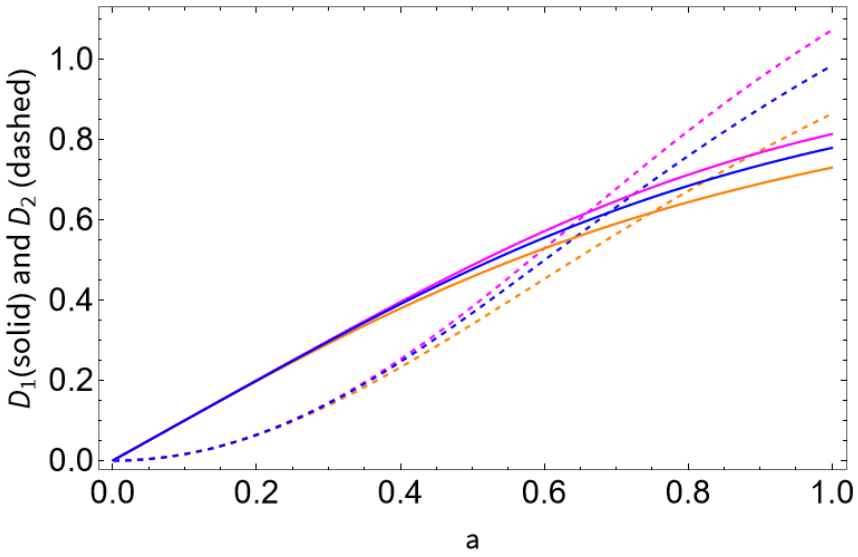

Source: Produced by the author [5].

Table 5.1: Fit values for Eq. (5.24) for the phantom regime $-1.25 \leq w_{de} \leq -1$.

Phantom ($-1.25 \leq w_{de} \leq -1$)	a	b	c	d	e	f	MRD%	ASRD%
$c^2_{de} = 0$	4.858	0.049	1.492	0.052	0.841	0.069	0.04	0.01
$c^2_{de} = 1$	4.857	-0.034	0.625	-0.012	0.926	-0.015	0.01	0.002
$c^2_{de} = 1/3$	4.857	-0.034	0.621	-0.012	0.930	-0.015	0.01	0.002

Source: Produced by the author [5].

A general fit with c^2_{de} as a variable is also provided, with seven constants (a, b,...g) defined as

$$S_3(\Omega_{m0}, w_{de}, c^2_{de}) = a + b(\Omega^c_{m0} - 1) + d|(1 + w_{de})|^e + f(1 + \Omega_{m0} w_{de}) + g(c^2_{de} + w_{de}). \quad (5.25)$$

When $c^2_{de} > \mathcal{H}/k$ the skewness becomes almost independent of c^2_{de}. This can also be observed in Figure 5.7 which shows an example for a fit using Figure 5.7. This fit will have greater MRD and ASRD values since we are adding one more variable. The results are provided by Table 5.3 and Figure 5.7.

To finish our analysis an observational approach is made. In Figure 5.8 our result represented by the red solid line is compared to observational data from the CFHTLS-Wide (Canada-France-Hawaii Telescope Legacy Survey) survey [81] studied in [7]. As in [57], [7], [56] and [82] we used the expression for skewness Equation 4.88.

In the work of Wolk et all[7], they use the data from CFHTLS-Wide to construct several samples, limited by a volume, of galaxies. These would contain more than one million galaxies around the redshift of $0.2 < z < 1$. They provide the skewness by using a count-in-cells technique.

The measured skewness used for Figure 5.8 is showed in Table 5.5, Table 5.6, Table 5.7 and Table 5.8. For the first column, we have the angular size of the square cell that was used to

Figure 5.6: Variation of skewness with Ω_{m0} and w_{de}. On the left panels we fix $\Omega_{m0} = 0.3$; on the right panels we fix $w_{de} = -0.9$. The red line represents the fit from Eq. (5.24) and Table 5.2, and the black dots the data. Here we have the case for $c^2_{de} = 0$ (top row) and $c^2_{de} = 1$ (lower row).

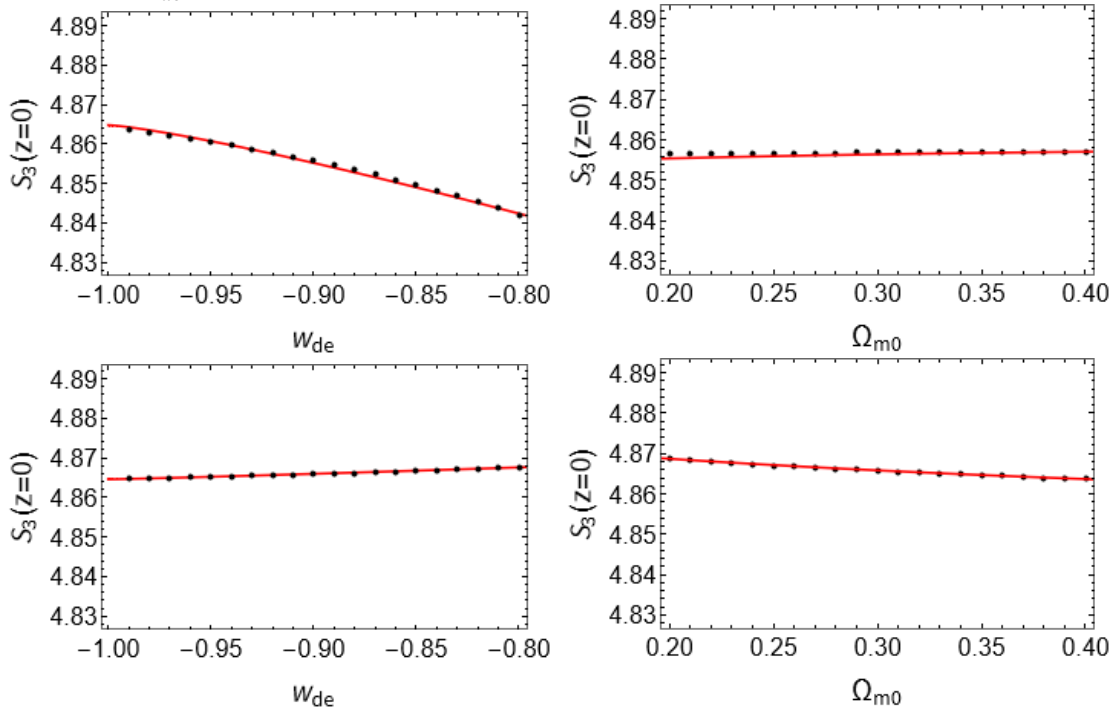

Source: Produced by the author [5].

Figure 5.7: Variation of skewness with c^2_{de}. The red line represents the fit Eq.(5.25) and Table 5.3 for $\Omega_{m0} = 0.3$ and $w_{de} = -0.9$; the black dots are the data.

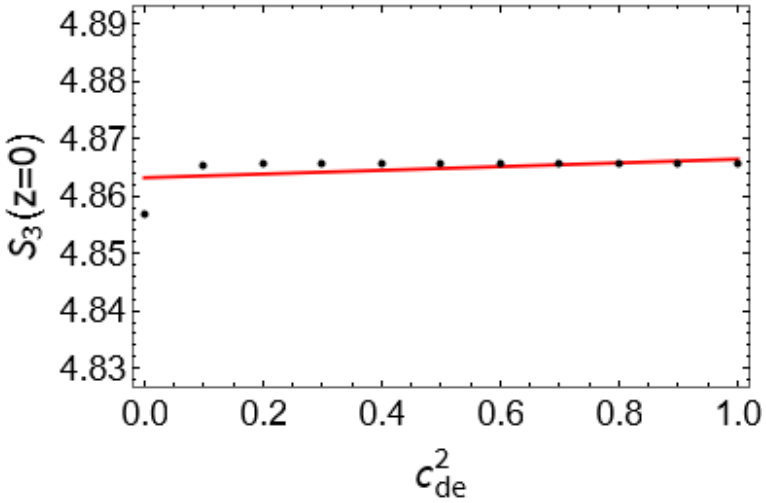

Source: Produced by the author [5].

Table 5.2: Fit values for Eq. (5.24) for the quintessence regime $-1 \leq w_{de} \leq -0.8$.

Quintessence ($-1 \leq w_{de} \leq -0.8$)	a	b	c	d	e	f	MRD%	ASRD%
$c_{de}^2 = 0$	4.853	0.186	0.946	-0.216	1.143	0.198	0.1	0.01
$c_{de}^2 = 1$	4.858	-0.050	0.574	0.026	1.075	-0.026	0.02	0.002
$c_{de}^2 = 1/3$	4.858	-0.050	0.556	0.024	1.070	-0.025	0.02	0.002

Source: Produced by the author [5].

Table 5.3: Fit values for Eq. (5.25) for the phantom and quintessence regimes.

	a	b	c	d	e	f	g	MRD%	ASRD%
Phantom ($-1.25 \leq w_{de} \leq -1$)	4.856	-0.032	0.413	-0.008	1.012	-0.007	-0.002	0.3	0.03
Quintessence ($-1 \leq w_{de} \leq -0.8$)	4.859	-0.053	0.172	-158780	14.258	0.003	0.003	0.8	0.06

Source: Produced by the author [5].

perform the measurement. The second column provides the skewness and the third one is its error bar. The measurement for skewness in this work [7] is done by a count-in-cells method. To convert the angular size θ to the physical scale of R, we used

$$R = x* \cdot \theta \tag{5.26}$$

where $x*$ is the characteristic scale of x that in [7] represents the comoving distance.

The $x*$ values for each set of bins used are in Table 5.4, more details about the method in [7]. With these measurements, we can associate each skewness measured to the physical scale of R resulting in the observational points in Figure 5.8.

The γ_1 term from Equation 4.88 provides the count-in-cells correction [6], [7]. To obtain our theoretical line we solve our set of equations Equation 5.14-5.16 and add this correction to the skewness value.

The $\sigma^2(R)$ equation in the definition of Equation 4.88 represents the variance of the density field in real space Equation 4.56.

We used the values of the power spectrum provided by CAMB [83], [84]. As for the window function, we selected a function that was less oscillating than the top-hat one given by

$$W(kR) = \frac{\sqrt{2}e^{-\frac{kR}{\sqrt{2}}}}{kR} \sin\left(\frac{kR}{\sqrt{2}}\right), \tag{5.27}$$

where W(kR) is the Fourier transform of the smoothed window function for a spherically symmetric region with characteristic radius R defined as $W(r) = 1/(1 + r/R^4)$ normalized to unity.

Table 5.4: Characteristic scale $x*$ values.

	x*
$(0.2 < z < 0.4)$	1280
$(0.4 < z < 0.6)$	1910
$(0.6 < z < 0.8)$	2530
$(0.8 < z < 1)$	3010

Characteristc scale value used in Wolk et all [7].

Table 5.5: Skewness data used for the reproduction of Figure 5.8. This table is for the set of the bin $(0.2 < z < 0.4)$.

θ $(0.2 < z < 0.4)$	S_3	σS_3
0.0011	9.34	4.84
0.0016	4.45	1.33
0.0027	4.72	1.21
0.0043	4.90	0.91
0.0070	4.39	0.55
0.0118	3.73	0.38
0.0193	3.62	0.21
0.0317	3.67	0.14
0.0516	3.71	0.22
0.0849	3.59	0.31
0.1392	3.30	0.40
0.2273	3.06	0.46
0.3729	2.99	0.65
0.6105	3.02	0.81
1.0001	2.81	0.63

Measurements from Wolk et all [7].

Table 5.6: Skewness data used for the reproduction of Figure 5.8. This table is for the set of the bin $(0.4 < z < 0.6)$.

θ $(0.4 < z < 0.6)$	S_3	σS_3
0.0011	8.18	4.10
0.0016	6.27	2.45
0.0027	4.46	1.03
0.0043	4.12	0.54
0.0070	4.01	0.27
0.0118	4.03	0.15
0.0193	4.10	0.09
0.0317	4.17	0.14
0.0516	4.09	0.13
0.0849	3.72	0.12
0.1392	3.30	0.10
0.2273	3.15	0.17
0.3729	3.07	0.35
0.6105	3.12	0.60
1.0001	4.01	0.87

Measurements from Wolk et all [7].

Table 5.7: Skewness data used for the reproduction of Figure 5.8. This table is for the set of the bin $(0.6 < z < 0.8)$.

θ $(0.6 < z < 0.8)$	S_3	σS_3
0.0011	7.32	3.43
0.0016	7.64	2.53
0.0027	5.30	1.08
0.0043	4.86	0.70
0.0070	4.64	0.54
0.0118	4.62	0.45
0.0193	4.60	0.44
0.0317	4.40	0.44
0.0516	4.05	0.49
0.0849	3.58	0.48
0.1392	3.13	0.45
0.2273	2.67	0.36
0.3729	2.13	0.41
0.6105	1.06	0.43
1.0001	-0.69	0.33

Measurements from Wolk et all [7].

Table 5.8: Skewness data used for the reproduction of Figure 5.8. This table is for the set of the bin $(0.8 < z < 1)$.

θ $(0.8 < z < 1)$	S_3	σS_3
0.0011	11.0	3.75
0.0016	11.5	3.18
0.0027	6.96	2.01
0.0043	5.54	1.55
0.0070	5.20	1.41
0.0118	5.01	1.19
0.0193	4.77	1.02
0.0317	4.54	0.93
0.0516	4.23	0.85
0.0849	3.60	0.62
0.1392	2.99	0.44
0.2273	2.45	0.34
0.3729	1.81	0.39
0.6105	0.99	0.47
1.0001	-0.36	0.95

Measurements from Wolk et all [7].

Figure 5.8: Skewness compared to observational data from [7]. The red line represents the theoretical plot using our set of equations with $\Omega_{m0} = 0.27$ and $H_0 = 71$ km/s/Mpc that was also used in [7]. The cases for different values of w_{de} and c^2_{de} are indistinguishable in this scale. Also, the theoretical curve is almost independent of z; we plot here the $z = 0.9$ case.

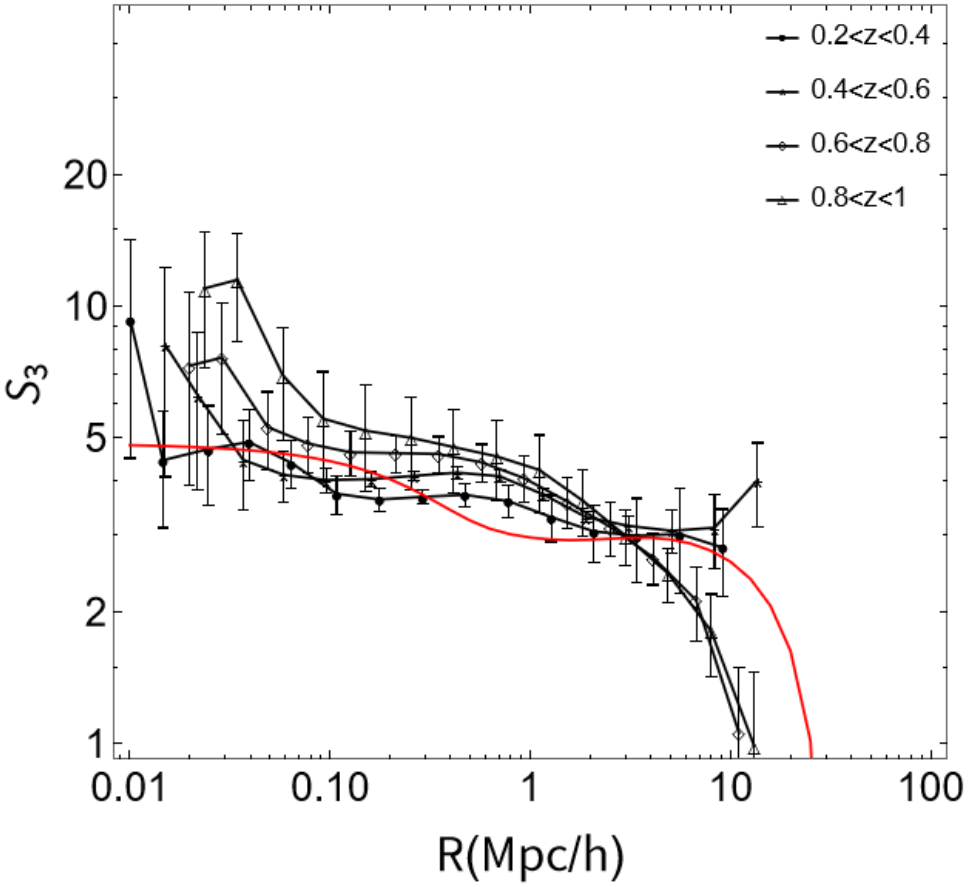

Source: Produced by the author [5].

The window function expresses the way the particles will be selected within a given region, being constant inside the survey and zero outside, in our case, we have just chosen a different expression to obtain a greater range and smoothed results in Figure 5.8.

When the theoretical line was calculated it was noticed that, at least on this plot scale, the skewness is almost independent of the redshift z, being indistinguishable from the intervals of z tested for this analysis. The intervals were like the ones from the observational data $z = \{0.3, \quad 0.4, \quad 0.7 \text{ and } 0.9\}$.

From this plot, we can only assume that very high precision is needed to evaluate such models with this kind of observational data since different models of w_{de} and c^2_{de} were indistinguishable on this scale. The analysis on [7] did not manage to provide a theoretical function through all the data like in our plot Figure 5.8, we assumed that this could be due to the window function used, but this information was not provided by the authors in their analysis.

Conclusions

6.1 Conclusion

The idea of clustering dark energy seems unnatural due to the usual denomination of a dark energy fluid that is responsible to accelerate the background expansion of the universe and, in principle, has no contribution to the mass quantity of galaxies and galaxy clusters. In fact, the main candidate to account for this effect, the cosmological constant Λ, behaves as its name i.e., it is constant in space and time admitting no clustering. This comes with the consequence that most alternative dark energy models do not consider any fluctuations in this component or have their fluctuations being negligible, such as in quintessence models, for scales below the horizon. Nevertheless, there is room for investigating clustering dark energy models. For example, studies about the abundance of galaxies clusters and the Planck satellite have shown fewer clusters than expected by the standard model through the Sunyaev-Zel'dovich effect [13], [85], [86], [54]. This analysis focus on the correlation between the CMB anisotropies and the structure formation patterns seen today. One can conclude that something could be interfering in these structure formation processes in a way that the ΛCDM model could not predict. This opens room to models that can present dark energy fluctuations and also for different values of w_{de} since the recent observations could not constrain how much this parameter can deviate in some intermediate redshifts. Also, the cosmological constant and coincidence problems mentioned previously also contribute to motivating such investigations in possible new dark energy scenarios.

Using higher order terms of the matter perturbation expansion we can put to test such time evolving model for dark energy. In this case, we used the skewness of the matter density field as a cosmological probe. Skewness in the case of the matter density is usually calculated for models where Λ can be zero (for EdS models) or for nonzero cases where it would be able to test some constant values for w_{de} [56], [57]. But we can go beyond and add dark energy perturbations. This has to be done carefully as seen in our different results from section 4.4 and section 5.2.

This work tested several clustering dark energy models that range from the quintessence to phantom cases. Four our first set of results in section 4.4 we have used the values for the sound speed for dark energy c_{de}^2 as dependent on the equation of state and also included these dark energy perturbations directly as a part of the matter contained in the total equation of state parameter. This would show a great impact and increase on skewness where this single fluid would have more "matter" and its sound velocity would have unusual values due to being directly connected to the w_{de} parameter.

This first result would make us wonder if this result would remain for a more general analysis where the dark energy fluctuations would have their own evolution equation acting as a source for the gravitational potential sided by the matter content and not directly included in the matter density contrast as before. These results in section 5.2 would give us another view, where the

skewness would have a closer value to the ΛCDM model. The greater differences would rise from models with $c_{de}^2 = 0$ both for phantom and quintessence cases. Depending on the regime this speed would increase or lower the skewness to greater values than for $c_{de}^2 > 0$ cases. As for values of $w_{de} = -1$ the skewness was shown to be not a useful tool to test different clustering dark energy models with different sound speeds.

This second set of results would also be used to provide fit equations for skewness. These fits aim to provide expressions with other parameters not usually provided in the literature, as in the literature is usually done an approximation around EdS and ΛCDM models. Such models would show that skewness has very low dependence on the matter density parameter Ω_m, but we had our interest to see and show how an equation would look like for extra parameters such as w_{de} and c_{de}. These fits can be useful to compare cosmological models to scale structures at high orders.

6.2 Future

During this research was very difficult to find observable data testing this matter density skewness for cosmological models. We have provided one observational result but this would only show that on that scale skewness was not useful to test models with observational data. Maybe future experiments such as Euclid can provide data to differentiate at least cases with and without dark energy fluctuations. The model itself with clustering dark energy is also not very explored in the literature and can be expanded much further. This analysis with skewness can be extended also for modified gravity since its an alternative tool to explain the accelerated cosmic expansion [87], [88]. This work shows that much can be explored both with skewness analysis and with clustering dark energy and that maybe future data with more precision to evaluate even small perturbations could bring more attention to this area.

Appendix

In the following pages, there are some of the codes used in this work starting with the code used to calculate skewness for the $c_{de}^2 = 0$ and $c_{de}^2 = 1$ cases from Figure 5.3.

Solving D1, D2, δde

In[1]:=
```
Clear[Ωm0, w0, ca, cde, D1q, D2q, wde, w1, FDE, δde]
```

In[2]:=
```
Ωm0 = 0.3;
w0 = -0.99999;
cde[x_] := 1;
wde[x_] = w0;
H0 = 1 / 3000;
FDE[x_] = Exp[-3 * Integrate[(1 + wde[x]) / x, x]];
Ωm[x_] := (Ωm0 * x^-3) / (Ωm0 * x^-3 + (1 - Ωm0) * FDE[x]);
Ωde[x_] := ((1 - Ωm0) * FDE[x]) / (Ωm0 * x^-3 + (1 - Ωm0) * FDE[x]);
H[x_] := H0 * (Ωm0 / x^3 + (1 - Ωm0) * FDE[x])^(1/2);
k = 0.01; (*h/Mpc*) (*oscillation less strong in 0.01 than 0.1*)
aeq = 1 / (1 + 300000);
```

In[13]:=
```
EQde[x_] := x^2 * δde''[x] + x * δde'[x] * (3 * (cde[x] - wde[x]) + (3 + x * H'[x] / H[x]) - (x * wde'[x] / (1 + wde[x]))) +
  3 * δde[x] (x * (cde'[x] - wde'[x]) +
    (2 + x * H'[x] / H[x]) * (cde[x] - wde[x]) + x * wde'[x] * (wde[x] - cde[x]) / (1 + wde[x])) -
  (1 + wde[x]) * (3 / 2) * (Ωm[x] * D1q[x] + Ωde[x] * δde[x] * (1 + 3 * cde[x])) +
  ((1 + wde[x]) / (x^2 * (H[x])^2)) * k^2 * (cde[x] * δde[x] / (1 + wde[x])) == 0;
EQ1[x_] := x^2 * D1q''[x] + x * D1q'[x] * (3 + x * H'[x] / H[x]) -
  (3 / 2) * D1q[x] * Ωm[x] - (3 / 2) * Ωde[x] * δde[x] * (1 + 3 cde[x]) == 0;
EQ2[x_] :=
  x^2 * D2q''[x] + x * D2q'[x] * (3 + x * H'[x] / H[x]) - (8 / 3) * x^2 * (D1q'[x])^2 - (3 / 2) * (D2q[x]) * Ωm[x] -
  3 * (D1q[x])^2 * Ωm[x] - 3 * (D1q[x]) * Ωde[x] * (δde[x]) * (1 + 3 * cde[x]) == 0;
solAll = NDSolve[{EQ1[x], EQde[x], EQ2[x],
  D1q[aeq] == aeq, D1q'[aeq] == D1q[aeq] / aeq, δde[aeq] == 10^-5, δde'[aeq] == 10^-5,
  D2q[aeq] == (aeq)^2, D2q'[aeq] == 2 * D2q[aeq] / aeq}, {D1q, δde, D2q}, {x, aeq, 1}];
```

In[17]:=
```
D1res[x_] = D1q[x] /. solAll;
D1r = D1res[1]; (*it will be evaluated today in a=1*)
D2res[x_] = D2q[x] /. solAll;
D2r = D2res[1];
S3 = 3 * (D2r) / (D1r)^2
```

Out[21]=
```
{4.86453}
```

cde=0 with Ωm0 and wde variation:

In[22]:=
```
Clear[Ωm0, w0, ca, cde, D1q, D2q, wde, w1, FDE, δde]
```

In[23]:=
```
wde[x_] = w0;
H0 = 1 / 3000;
FDE[x_] = Exp[-3 * Integrate[(1 + wde[x]) / x, x]];
Ωm[x_] := (Ωm0 * x^-3) / (Ωm0 * x^-3 + (1 - Ωm0) * FDE[x]);
Ωde[x_] := ((1 - Ωm0) * FDE[x]) / (Ωm0 * x^-3 + (1 - Ωm0) * FDE[x]);
H[x_] := H0 * (Ωm0 / x^3 + (1 - Ωm0) * FDE[x])^(1/2);
k = 0.01; (*h/Mpc*) (*oscillation less strong in 0.01 than 0.1*)
aeq = 1 / (1 + 300000);
```

In[31]:=
```
Ωm0min = 1 / 100; Ωm0max = 1; frac1 = 1 / 100;
w0min = -125 / 100; w0max = -79 / 100; frac2 = 2 / 100;
cde[x_] := 0;

dataS31 =
  ParallelTable[counter++;
   EQde[x_] :=
    x^2 * δde''[x] + x * δde'[x] * (3 * (cde[x] - wde[x]) + (3 + x * H'[x] / H[x]) - (x * wde'[x] / (1 + wde[x]))) +
      3 * δde[x] (x * (cde'[x] - wde'[x]) +
        (2 + x * H'[x] / H[x]) * (cde[x] - wde[x]) + x * wde'[x] * (wde[x] - cde[x]) / (1 + wde[x])) -
      (1 + wde[x]) * (3 / 2) * (Ωm[x] * D1q[x] + Ωde[x] * δde[x] * (1 + 3 * cde[x])) +
      ((1 + wde[x]) / (x^2 * (H[x])^2)) * k^2 * (cde[x] * δde[x] / (1 + wde[x])) == 0;
   EQ1[x_] := x^2 * D1q''[x] + x * D1q'[x] * (3 + x * H'[x] / H[x]) -
      (3 / 2) * D1q[x] * Ωm[x] - (3 / 2) * Ωde[x] * δde[x] * (1 + 3 cde[x]) == 0;
   EQ2[x_] :=
    x^2 * D2q''[x] + x * D2q'[x] * (3 + x * H'[x] / H[x]) - (8 / 3) * x^2 * (D1q'[x])^2 - (3 / 2) * (D2q[x]) * Ωm[x] -
      3 * (D1q[x])^2 * Ωm[x] - 3 * (D1q[x]) * Ωde[x] * (δde[x]) * (1 + 3 * cde[x]) == 0;
  solAll1 = NDSolve[{EQ1[x], EQde[x], EQ2[x],
      D1q[aeq] == aeq, D1q'[aeq] == D1q[aeq] / aeq, δde[aeq] == 10^-5, δde'[aeq] == 10^-5,
      D2q[aeq] == (aeq)^2, D2q'[aeq] == 2 * D2q[aeq] / aeq}, {D1q, δde, D2q}, {x, aeq, 1}];
   D1res[x_] = D1q[x] /. solAll1;
   D1r = D1res[1]; (*it will be evaluated today in a=1*)
  D2res[x_] = D2q[x] /. solAll1;
   D2r = D2res[1];
   S31 = {Ωm0, w0, 3 * (D2r) / (D1r)^2 [[1]]}
   , {Ωm0, Ωm0min, Ωm0max, frac1}, {w0, w0min, w0max, frac2}];
```

In[42]:=
```
c0newdatas3 = Flatten[dataS31, 1];
```

In[43]:=
```
MatrixQ@c0newdatas3
```

Out[43]=
```
True
```

In[44]:=
```
c0dataw0m011 = c0newdatas3 /. {x_, y_ /; y ≠ -1.19, z_} → Nothing;
c0dataw0m10 = c0newdatas3 /. {x_, y_ /; y ≠ -0.99, z_} → Nothing;
c0dataw0m09 = c0newdatas3 /. {x_, y_ /; y ≠ -0.89, z_} → Nothing(*-0.89 or -0.91*);
c0data2Dw0m11 = Map[Drop[#, {2}] &, c0dataw0m011];
c0data2Dw0m10 = Map[Drop[#, {2}] &, c0dataw0m10];
c0data2Dw0m09 = Map[Drop[#, {2}] &, c0dataw0m09];
```

In[50]:=
```
MatrixQ@c0data2Dw0m10
```

Out[50]=
```
True
```

In[51]:=
```
c0plotw0m10 =
 ListLinePlot[c0data2Dw0m10, PlotStyle → {Blue, Dashing → {0.025, 0.025 / 2, 0.01}}, Frame → True,
  FrameLabel → {StyleForm["Ωm0", "Subsection", Black], StyleForm["S3", "Subsection", Black]},
  FrameTicksStyle → Directive[Black, 16], PlotRange → All]
```

Out[51]=

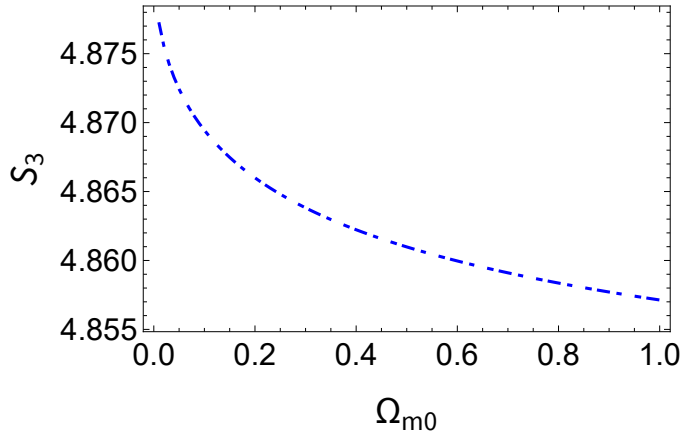

In[52]:=
```
c0plotw0m11 = ListLinePlot[c0data2Dw0m11,
   PlotStyle → {Magenta, Dashing → {0.025, 0.025 / 2, 0.01}}, Frame → True,
   FrameLabel → {StyleForm["Ωm0", "Subsection", Black], StyleForm["S3", "Subsection", Black]},
   FrameTicksStyle → Directive[Black, 16], PlotRange → All];
```

In[53]:=
```
c0plotw0m09 = ListLinePlot[c0data2Dw0m09,
   PlotStyle → {Orange, Dashing → {0.025, 0.025 / 2, 0.01}}, Frame → True,
   FrameLabel → {StyleForm["Ωm0", "Subsection", Black], StyleForm["S3", "Subsection", Black]},
   FrameTicksStyle → Directive[Black, 16], PlotRange → All];
```

cde=1;

In[54]:=
```
Clear[Ωm0, w0, ca, cde, D1q, D2q, wde, w1, FDE, δde]
```

In[55]:=
```
cde[x_] := 1;
wde[x_] = w0;
H0 = 1 / 3000;
FDE[x_] = Exp[-3 * Integrate[(1 + wde[x]) / x, x]];
Ωm[x_] := (Ωm0 * x^-3) / (Ωm0 * x^-3 + (1 - Ωm0) * FDE[x]);
Ωde[x_] := ((1 - Ωm0) * FDE[x]) / (Ωm0 * x^-3 + (1 - Ωm0) * FDE[x]);
H[x_] := H0 * (Ωm0 / x^3 + (1 - Ωm0) * FDE[x])^(1/2);
k = 0.01; (*h/Mpc*) (*oscillation less strong in 0.01 than 0.1*)
```

In[63]:=
```
Ωm0min = 1 / 100; Ωm0max = 1; frac1 = 1 / 100;
w0min = -125 / 100; w0max = -79 / 100; frac2 = 2 / 100;
(*w1min=-0.2;
w1max=0.2;*)
```

In[65]:=
```
dataS32 =
  ParallelTable[counter++;
   EQde[x_] :=
    x^2 * δde''[x] + x * δde'[x] * (3 * (cde[x] - wde[x]) + (3 + x * H'[x] / H[x]) - (x * wde'[x] / (1 + wde[x]))) +
     3 * δde[x] (x * (cde'[x] - wde'[x]) +
       (2 + x * H'[x] / H[x]) * (cde[x] - wde[x]) + x * wde'[x] * (wde[x] - cde[x]) / (1 + wde[x])) -
     (1 + wde[x]) * (3 / 2) * (Ωm[x] * D1q[x] + Ωde[x] * δde[x] * (1 + 3 * cde[x])) +
     ((1 + wde[x]) / (x^2 * (H[x])^2)) * k^2 * (cde[x] * δde[x] / (1 + wde[x])) == 0;
   EQ1[x_] := x^2 * D1q''[x] + x * D1q'[x] * (3 + x * H'[x] / H[x]) -
     (3 / 2) * D1q[x] * Ωm[x] - (3 / 2) * Ωde[x] * δde[x] * (1 + 3 cde[x]) == 0;
   EQ2[x_] :=
    x^2 * D2q''[x] + x * D2q'[x] * (3 + x * H'[x] / H[x]) - (8 / 3) * x^2 * (D1q'[x])^2 - (3 / 2) * (D2q[x]) * Ωm[x] -
     3 * (D1q[x])^2 * Ωm[x] - 3 * (D1q[x]) * Ωde[x] * (δde[x]) * (1 + 3 * cde[x]) == 0;
  solAll2 = NDSolve[{EQ1[x], EQde[x], EQ2[x],
     D1q[aeq] == aeq, D1q'[aeq] == D1q[aeq] / aeq, δde[aeq] == 10^-5, δde'[aeq] == 10^-5,
     D2q[aeq] == (aeq)^2, D2q'[aeq] == 2 * D2q[aeq] / aeq}, {D1q, δde, D2q}, {x, aeq, 1}];
  D1res[x_] = D1q[x] /. solAll2;
  D1r = D1res[1]; (*it will be evaluated today in a=1*)
  D2res[x_] = D2q[x] /. solAll2;
  D2r = D2res[1];
  S3 = {Ωm0, w0, 3 * (D2r) / (D1r)^2 [[1]]}
  , {Ωm0, Ωm0min, Ωm0max, frac1}, {w0, w0min, w0max, frac2}];
```

In[66]:=
```
newdatas32 = Flatten[dataS32, 1];
```

In[67]:=
```
MatrixQ@newdatas3
```

Out[67]=
```
False
```

In[68]:=
```
dataw0m0112 = newdatas32 /. {x_, y_ /; y ≠ -1.19, z_} → Nothing;
dataw0m102 = newdatas32 /. {x_, y_ /; y ≠ -0.99, z_} → Nothing;
dataw0m092 = newdatas32 /. {x_, y_ /; y ≠ -0.89, z_} → Nothing(*-0.89 or -0.91*);
data2Dw0m112 = Map[Drop[#, {2}] &, dataw0m0112];
data2Dw0m102 = Map[Drop[#, {2}] &, dataw0m102];
data2Dw0m092 = Map[Drop[#, {2}] &, dataw0m092];
```

In[74]:=
```
plotw0m102 = ListLinePlot[data2Dw0m102, PlotStyle → {Blue}, Frame → True,
  FrameLabel → {StyleForm["Ωm0", "Subsection", Black], StyleForm["S3", "Subsection", Black]},
  FrameTicksStyle → Directive[Black, 16], PlotRange → All]
```

Out[74]=

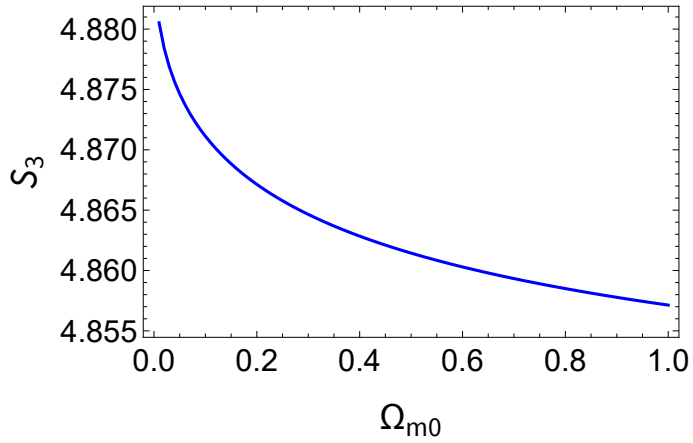

In[75]:=
```
plotw0m112 = ListLinePlot[data2Dw0m112, PlotStyle → {Magenta, Thickness[0.005]}, Frame → True,
   FrameLabel → {StyleForm["Ωm0", "Subsection", Black], StyleForm["S3", "Subsection", Black]},
   FrameTicksStyle → Directive[Black, 16], PlotRange → All];
```

In[76]:=
```
plotw0m092 = ListLinePlot[data2Dw0m092, PlotStyle → {Orange}, Frame → True,
   FrameLabel → {StyleForm["Ωm0", "Subsection", Black], StyleForm["S3", "Subsection", Black]},
   FrameTicksStyle → Directive[Black, 16], PlotRange → All];
```

No DE perturbations

In[77]:=
```
Clear[Ωm0, w0, ca, cde, D1q, D2q, wde, w1, FDE, δde]
```

In[78]:=
```
cde[x_] := 1;
wde[x_] = w0;
H0 = 1 / 3000;
FDE[x_] = Exp[-3 * Integrate[(1 + wde[x]) / x, x]];
Ωm[x_] := (Ωm0 * x^-3) / (Ωm0 * x^-3 + (1 - Ωm0) * FDE[x]);
Ωde[x_] := ((1 - Ωm0) * FDE[x]) / (Ωm0 * x^-3 + (1 - Ωm0) * FDE[x]);
H[x_] := H0 * (Ωm0 / x^3 + (1 - Ωm0) * FDE[x])^(1/2);
k = 0.01;
(*h/Mpc*)
```

In[86]:=
```
Ωm0min = 1 / 100; Ωm0max = 1; frac1 = 1 / 100;
w0min = -125 / 100; w0max = -79 / 100; frac2 = 2 / 100;
```

In[88]:=
```
dataS3n =
  ParallelTable[counter++;
   EQ1[x_] := x^2 * D1q''[x] + x * D1q'[x] * (3 + (x * H'[x]) / H[x]) - (3 / 2) * D1q[x] * Ωm[x] == 0;
   EQ2[x_] := x^2 * D2q''[x] + x * D2q'[x] * (3 + (x * H'[x]) / H[x]) -
     (8 / 3) * x^2 * (D1q'[x])^2 - (3 / 2) * (D2q[x]) * Ωm[x] - 3 * (D1q[x])^2 * Ωm[x] == 0;
  solAlln = NDSolve[{EQ1[x], EQ2[x], D1q[aeq] == aeq, D1q'[aeq] == D1q[aeq] / aeq,
     D2q[aeq] == (aeq)^2, D2q'[aeq] == 2 * D2q[aeq] / aeq}, {D1q, D2q}, {x, aeq, 1}];
   D1res[x_] = D1q[x] /. solAlln;
   D1r = D1res[1]; (*it will be evaluated today in a=1*)
  D2res[x_] = D2q[x] /. solAlln;
   D2r = D2res[1];
   S3 = {Ωm0, w0, (3 * (D2r)) / (D1r)^2 [[1]]}
   , {Ωm0, Ωm0min, Ωm0max, frac1}, {w0, w0min, w0max, frac2}];
```

In[89]:=
```
newdatas3n = Flatten[dataS3n, 1];
```

In[90]:=
```
MatrixQ@newdatas3
```

Out[90]=
```
False
```

In[91]:=
```
dataw0m011n = newdatas3n /. {x_, y_ /; y ≠ -1.19, z_} → Nothing;
dataw0m10n = newdatas3n /. {x_, y_ /; y ≠ -0.99, z_} → Nothing;
dataw0m09n = newdatas3n /. {x_, y_ /; y ≠ -0.89, z_} → Nothing(*-0.89 or -0.91*);
data2Dw0m11n = Map[Drop[#, {2}] &, dataw0m011n];
data2Dw0m10n = Map[Drop[#, {2}] &, dataw0m10n];
data2Dw0m09n = Map[Drop[#, {2}] &, dataw0m09n];
```

In[97]:=
```
nodeplotw0m10 = ListLinePlot[data2Dw0m10n, PlotStyle → {Dashing → {0.05}, Blue}, Frame → True,
  FrameLabel → {StyleForm["Ωm0", "Subsection", Black], StyleForm["S3", "Subsection", Black]},
  FrameTicksStyle → Directive[Black, 16], PlotRange → All]
```

Out[97]=

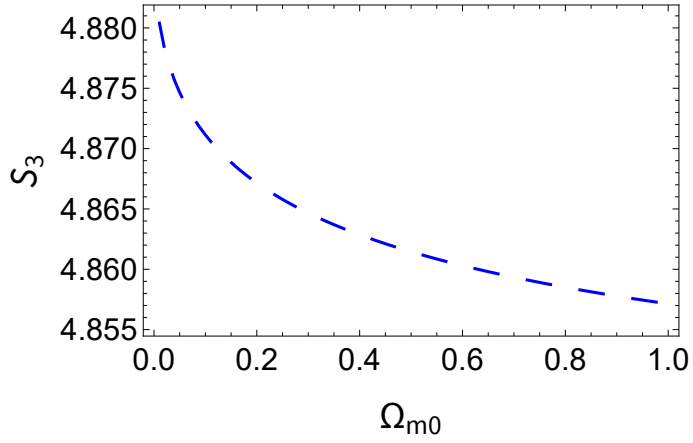

In[98]:=
```
nodeplotw0m11 = ListLinePlot[data2Dw0m11n, PlotStyle → {Magenta, Dashing → {0.05}}, Frame → True,
  FrameLabel → {StyleForm["Ωm0", "Subsection", Black], StyleForm["S3", "Subsection", Black]},
  FrameTicksStyle → Directive[Black, 16], PlotRange → All];
```

In[99]:=
```
nodeplotw0m09 = ListLinePlot[data2Dw0m09n, PlotStyle → {Dashing → {0.05}, Orange}, Frame → True,
  FrameLabel → {StyleForm["Ωm0", "Subsection", Black], StyleForm["S3", "Subsection", Black]},
  FrameTicksStyle → Directive[Black, 16], PlotRange → All];
```

In[100]:=
```
Show[plotw0m092, plotw0m112, plotw0m102, c0plotw0m09, c0plotw0m11,
  c0plotw0m10, FrameLabel → {StyleForm["Ωm0", "Subsection", Black, FontSize → 30],
    StyleForm["S3(z=0)", "Subsection", Black, FontSize → 30]},
  FrameTicksStyle → Directive[Black, 24], PlotRange → {{0, 1}, {4.84, 4.92}},
  Axes → False, AspectRatio → 3 / 2, ImageSize → Large];
```

In[101]:=
```
Show[nodeplotw0m09, plotw0m092, PlotRange → All]
```

Out[101]=

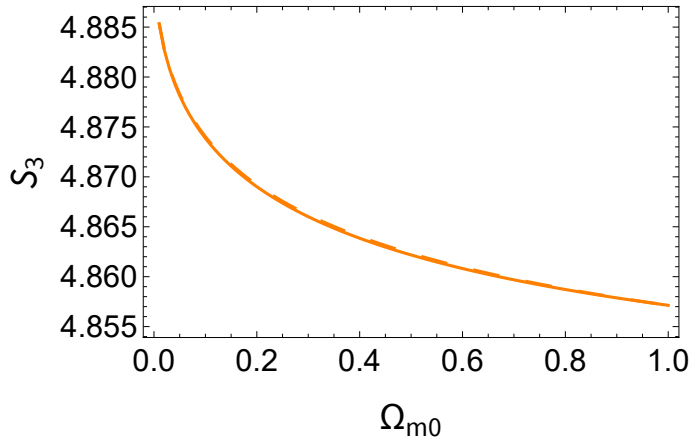

In[102]:=
```
Show[nodeplotw0m10, plotw0m102];
```

In[103]:=
```
Show[plotw0m092, plotw0m112, plotw0m102, c0plotw0m09,
 c0plotw0m11, c0plotw0m10, nodeplotw0m09, nodeplotw0m10, nodeplotw0m11,
 FrameLabel → {StyleForm["Ωm0", "Subsection", Black, FontSize → 30],
   StyleForm["S3(z=0)", "Subsection", Black, FontSize → 30]},
 FrameTicksStyle → Directive[Black, 24], PlotRange → {{0.1, 1}, {4.85, 4.89}}, Axes → False,
 AspectRatio → 3 / 2, ImageSize → Large, Epilog → {Black, PointSize[Large], Point[{0.3, 4.8647}],
   Text[Style["ΛCDM", FontSize → 16, Black], Offset[{20, 10}, {0.3, 4.865}]]}]
```

Out[•]=

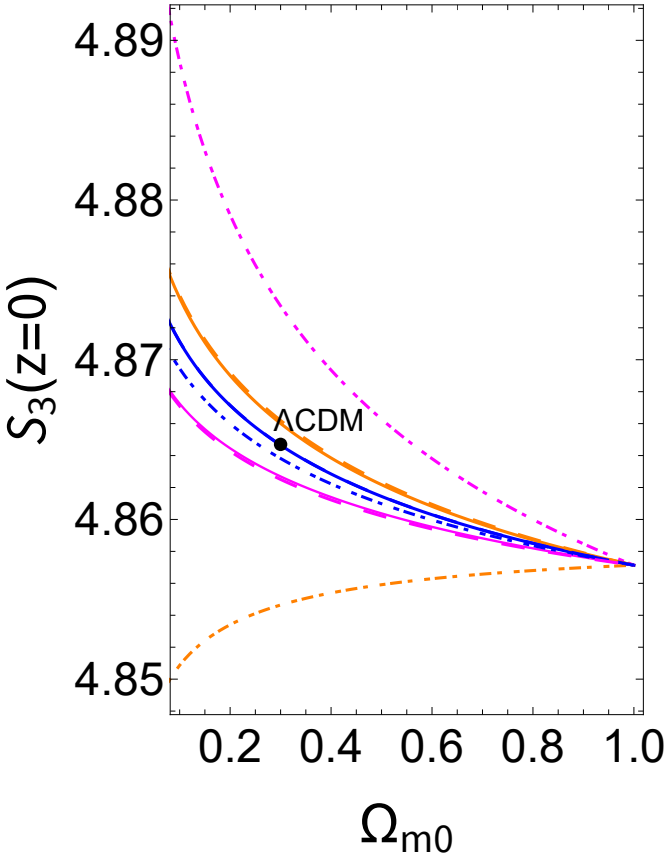

Bibliography

[1] H. Velten, H. A. Borges, S. Carneiro, R. Fazolo, and S. Gomes. *Large-scale structure and integrated Sachs–Wolfe effect in decaying vacuum cosmology.* Mon. Not. Roy. Astron. Soc. **452** 2220 (2015). arXiv:1504.02416. Cited on page vii.

[2] H. Velten and R. Fazolo. *Revealing the nonadiabatic nature of dark energy perturbations from galaxy clustering data.* Phys. Rev. D **96** 083502 (2017). arXiv:1707.03224. Cited on pages vii, 23, and 40.

[3] H. Velten, R. E. Fazolo, R. von Marttens, and S. Gomes. *Degeneracy between nonadiabatic dark energy models and ΛCDM : Integrated Sachs-Wolfe effect and the cross correlation of CMB with galaxy clustering data.* Phys. Rev. D **97** 103514 (2018). arXiv:1803.10181. Cited on pages vii, 23, and 40.

[4] H. Velten and R. E. Fazolo. *Skewness of matter distribution in clustering dark energy cosmologies.* Phys. Rev. D **101** 023518 (2020). arXiv:1912.00094. Cited on pages vii, 2, 30, 39, 41, and 46.

[5] R. E. Fazolo, L. Amendola, and H. Velten. *Skewness as a test of dark energy perturbations.* Phys. Rev. D **105** 103521 (2022). arXiv:2202.08355. Cited on pages vii, 2, 42, 43, 45, 46, 48, 49, 50, 51, 52, 53, and 56.

[6] F. Bernardeau. *Skewness and Kurtosis in large scale cosmic fields.* Astrophys. J. **433** 1 (1994). arXiv:astro-ph/9312026. Cited on pages xi, 37, 46, 47, 49, and 53.

[7] M. Wolk, H. J. McCracken, S. Colombi, J. N. Fry, M. Kilbinger, P. Hudelot, Y. Mellier, and O. Ilbert. *Evolution of hierarchical clustering in the CFHTLS-Wide since z˜1.* Mon. Not. Roy. Astron. Soc. **435** 2 (2013). arXiv:1301.3301. Cited on pages xi, 51, 53, 54, 55, and 56.

[8] S. Perlmutter, G. Aldering, S. Deustua, S. Fabbro, G. Goldhaber, D. E. Groom, A. G. Kim, M. Y. Kim, R. A. Knop, P. Nugent, C. R. Pennypacker, M. della Valle, R. S. Ellis, R. G. McMahon, N. Walton, A. Fruchter, N. Panagia, A. Goobar, I. M. Hook, C. Lidman, R. Pain, P. Ruiz-Lapuente, B. Schaefer, and Supernova Cosmology Project. *Cosmology From Type IA Supernovae: Measurements, Calibration Techniques, and Implications.* In *American Astronomical Society Meeting Abstracts* volume 29 of *Bulletin of the American Astronomical Society* page 1351 1997. arXiv:astro-ph/9812473. Cited on pages 1 and 7.

[9] A. G. Riess, A. V. Filippenko, P. Challis, A. Clocchiatti, A. Diercks, P. M. Garnavich, R. L. Gilliland, C. J. Hogan, S. Jha, R. P. Kirshner, B. Leibundgut, M. M. Phillips, D. Reiss, B. P. Schmidt, R. A. Schommer, R. C. Smith, J. Spyromilio, C. Stubbs, N. B. Suntzeff, and J. Tonry. *Observational Evidence from Supernovae for an Accelerating Universe and*

a Cosmological Constant. The Astronomical Journal **116** 1009 (1998). arXiv:astro-ph/9805201. Cited on pages 1 and 7.

[10] T. M. C. Abbott, F. B. Abdalla, S. Allam, A. Amara, J. Annis, J. Asorey, S. Avila, O. Ballester, M. Banerji, W. Barkhouse, L. Baruah, M. Baumer, K. Bechtol, M. R. Becker, A. Benoit-Lévy, G. M. Bernstein, E. Bertin, J. Blazek, S. Bocquet, D. Brooks, D. Brout, E. Buckley-Geer, D. L. Burke, V. Busti, R. Campisano, L. Cardiel-Sas, A. C. arnero Rosell, M. Carrasco Kind, J. Carretero, F. J. Castander, R. Cawthon, C. Chang, C. Conselice, G. Costa, M. Crocce, C. E. Cunha, C. B. D'Andrea, L. N. da Costa, R. Das, G. Daues, T. M. Davis, C. Davis, J. De Vicente, D. L. DePoy, J. DeRose, S. Desai, H. T. Diehl, J. P. Dietrich, S. Dodelson, P. Doel, A. Drlica-Wagner, T. F. Eifler, A. E. Elliott, A. E. Evrard, A. Farahi, A. Fausti Neto, E. Fernandez, D. A. Finley, M. Fitzpatrick, B. Flaugher, R. J. Foley, P. Fosalba, D. N. Friedel, J. Frieman, J. García-Bellido, E. Gaz tanaga, D. W. Gerdes, T. Giannantonio, M. S. S. Gill, K. Glazebrook, D. A. Goldstein, M. Gower, D. Gruen, R. A. Gruendl, J. Gschwend, R. R. Gupta, G. Gutierrez, S. Hamilton, W. G. Hartley, S. R. Hinton, J. M. Hislop, D. Hollowood, K. Honscheid, B. Hoyle, D. Huterer, B. Jain, D. J. James, T. Jeltema, M. W. G. Johnson, M. D. Johnson, S. Juneau, T. Kacpr zak, S. Kent, G. Khullar, M. Klein, A. Kovacs, A. M. G. Koziol, E. Krause, A. Kremin, R. Kron, K. Kuehn, S. Kuhlmann, N. Kuropatkin, O. Lahav, J. Lasker, T. S. Li, R. T. Li, A. R. Liddle, M. Lima, H. Lin, P. López-Reyes, N. MacCrann, M. A. G. Maia, J. D. Maloney, M. Manera, M. March, J. Marriner, J. L. Marshall, P. Martini, T. McClintock, T. McKay, R. G. McMahon, P. Melchior, F. Menanteau, C. J. Miller, R. Miquel, J. J. Mohr, E. Morganson, J. Mould, E. Neilsen, R. C. Nichol, D. Nidever, R. Nikutta, F. Nogueira, B. Nord, P. Nugent, L. Nunes, R. L. C. Ogando, L. Old, K. Olsen, A. B. Pace, A. Palmese, F. Paz-Chinchón, H. V. Peiris, W. J. Percival, D. Petravick, A. A. Plazas, J. Poh, C. Pond, A. Por redon, A. Pujol, A. Refregier, K. Reil, P. M. Ricker, R. P. Rollins, A. K. Romer, A. Roodman, P. Rooney, A. J. Ross, E. S. Rykoff, M. Sako, E. Sanchez, M. L. Sanchez, B. Santiago, A. Saro, V. Scarpine, D. Scolnic, A. Scott, S. Serrano, I. Sevilla-Noarbe, E. Sheldon, N. Shipp, M. L. Silveira, R. C. Smith, J. A. Smith, M. Smith, M. Soares-Santos, F. Sobre ira, J. Song, A. Stebbins, E. Suchyta, M. Sullivan, M. E. C. Swanson, G. Tarle, J. Thaler, D. Thomas, R. C. Thomas, M. A. Troxel, D. L. Tucker, V. Vikram, A. K. Vivas, A. R. Wal ker, R. H. Wechsler, J. Weller, W. Wester, R. C. Wolf, H. Wu, B. Yanny, A. Zenteno, Y. Zhang, and J. Zuntz. *The Dark Energy Survey Data Release 1*. ArXiv e-prints (2018). URL: https://doi.org/10.3847/1538-4365/aae9f0 arXiv:1801.03181. Cited on page 1.

[11] A. Padilla. *Lectures on the Cosmological Constant Problem*. ArXiv e-prints (2015). arXiv:1502.05296. Cited on pages 1, 8, and 22.

[12] H. E. S. Velten, R. F. vom Marttens, and W. Zimdahl. *Aspects of the cosmological "coincidence problem"*. European Physical Journal C **74** 3160 (2014). arXiv:1410.2509. Cited on pages 1, 8, and 22.

[13] Planck Collaboration, N. Aghanim, M. Arnaud, M. Ashdown, J. Aumont, C. Baccigalupi, A. J. Banday, R. B. Barreiro, J. G. Bartlett, N. Bartolo, E. Battaner, R. Battye, K. Benabed, A. Benoît, A. Benoit-Lévy, J. P. Bernard, M. Bersanelli, P. Bielewicz, J. J. Bock, A. Bonaldi, L. Bonavera, J. R. Bond, J. Borrill, F. R. Bouchet, C. Burigana, R. C. Butler, E. Calabrese, J. F. Cardoso, A. Catalano, A. Challinor, H. C. Chiang, P. R. Christensen, E. Churazov, D. L. Clements, L. P. L. Colombo, C. Combet, B. Comis, A. Coulais, B. P. Crill, A. Curto, F. Cuttaia, L. Danese, R. D. Davies, R. J. Davis, P. de Bernardis, A. de Rosa, G. de Zotti,

J. Delabrouille, F. X. Désert, C. Dickinson, J. M. Diego, K. Dolag, H. Dole, S. Donzelli, O. Doré, M. Douspis, A. Ducout, X. Dupac, G. Efstathiou, F. Elsner, T. A. Enßlin, H. K. Eriksen, J. Fergusson, F. Finelli, O. Forni, M. Frailis, A. A. Fraisse, E. Franceschi, A. Frejsel, S. Galeotta, S. Galli, K. Ganga, R. T. Génova-Santos, M. Giard, J. González-Nuevo, K. M. Górski, A. Gregorio, A. Gruppuso, J. E. Gudmundsson, F. K. Hansen, D. L. Harrison, S. Henrot-Versillé, C. Hernández-Monteagudo, D. Herranz, S. R. Hildebrandt, E. Hivon, W. A. Holmes, A. Hornstrup, K. M. Huffenberger, G. Hurier, A. H. Jaffe, W. C. Jones, M. Juvela, E. Keihänen, R. Keskitalo, R. Kneissl, J. Knoche, M. Kunz, H. Kurki-Suonio, F. Lacasa, G. Lagache, A. Lähteenmäki, J. M. Lamarre, A. Lasenby, M. Lattanzi, R. Leonardi, J. Lesgourgues, F. Levrier, M. Liguori, P. B. Lilje, M. Linden-Vørnle, M. López-Caniego, J. F. Macías-Pérez, B. Maffei, G. Maggio, D. Maino, N. Mandolesi, A. Mangilli, M. Maris, P. G. Martin, E. Martínez-González, S. Masi, S. Matarrese, A. Melchiorri, J. B. Melin, M. Migliaccio, M. A. Miville-Deschênes, A. Moneti, L. Montier, G. Morgante, D. Mortlock, D. Munshi, J. A. Murphy, P. Naselsky, F. Nati, P. Natoli, F. Noviello, D. Novikov, I. Novikov, F. Paci, L. Pagano, F. Pajot, D. Paoletti, F. Pasian, G. Patanchon, O. Perdereau, L. Perotto, V. Pettorino, F. Piacentini, M. Piat, E. Pierpaoli, D. Pietrobon, S. Plaszczynski, E. Pointecouteau, G. Polenta, N. Ponthieu, G. W. Pratt, S. Prunet, J. L. Puget, J. P. Rachen, M. Reinecke, M. Remazeilles, C. Renault, A. Renzi, I. Ristorcelli, G. Rocha, M. Rossetti, G. Roudier, J. A. Rubiño-Martín, B. Rusholme, M. Sandri, D. Santos, A. Sauvé, M. Savelainen, G. Savini, D. Scott, L. D. Spencer, V. Stolyarov, R. Stompor, R. Sunyaev, D. Sutton, A. S. Suur-Uski, J. F. Sygnet, J. A. Tauber, L. Terenzi, L. Toffolatti, M. Tomasi, D. Tramonte, M. Tristram, M. Tucci, J. Tuovinen, L. Valenziano, J. Valiviita, B. Van Tent, P. Vielva, F. Villa, L. A. Wade, B. D. Wandelt, I. K. Wehus, D. Yvon, A. Zacchei, and A. Zonca. *Planck 2015 results. XXII. A map of the thermal Sunyaev-Zeldovich effect.* AAP **594** A22 (2016). arXiv:1502.01596. Cited on pages 1, 4, 22, and 57.

[14] E. Hubble. *A Relation between Distance and Radial Velocity among Extra-Galactic Nebulae.* Proceedings of the National Academy of Science **15** 168 (1929). Cited on page 3.

[15] D. Wands, O. F. Piattella, and L. Casarini. *Physics of the Cosmic Microwave Background Radiation.* Astrophysics and Space Science Proceedings **45** 3 (2016). arXiv:1504.06335. Cited on pages 4 and 9.

[16] S. Weinberg. *The cosmological constant problem.* Rev. Mod. Phys. **61** 1 (1989). URL: https://link.aps.org/doi/10.1103/RevModPhys.61.1. Cited on page 8.

[17] M. Shimon. *Elucidation of 'Cosmic Coincidence'.* arXiv e-prints page arXiv:2204.02211 (2022). arXiv:2204.02211. Cited on page 8.

[18] L. Senatore. *Lectures on Inflation.* In *Proceedings, Theoretical Advanced Study Institute in Elementary Particle Physics: New Frontiers in Fields and Strings (TASI 2015): Boulder, CO, USA, June 1-26, 2015* pages 447–543 2017. arXiv:1609.00716. Cited on page 10.

[19] A. Lewis and S. Bridle. *Cosmological parameters from CMB and other data: A Monte Carlo approach.* Phys. Rev. D **66** 103511 (2002). arXiv:astro-ph/0205436. Cited on pages 11 and 20.

[20] S. Dodelson. *Modern cosmology.* Academic Press San Diego, CA 2003. URL: https://cds.cern.ch/record/1282338. Cited on pages 12, 18, and 19.

[21] V. Mukhanov. *Physical Foundations of Cosmology.* 2005. Cited on page 12.

[22] S. Weinberg. *Cosmology*. Oxford University Press 2008. Cited on page 12.

[23] H. Kodama and M. Sasaki. *Cosmological Perturbation Theory*. Progress of Theoretical Physics Supplement **78** 1 (1984). Cited on page 12.

[24] L. Amendola and S. Tsujikawa. *Dark Energy: Theory and Observations*. Cambridge University Press 2015. Cited on pages 12, 19, 20, 23, 31, 34, 35, 36, and 37.

[25] R. H. Brandenberger. *Lectures on the theory of cosmological perturbations*. Lect. Notes Phys. **646** 127 (2004). arXiv:hep-th/0306071. Cited on page 12.

[26] K. A. Malik and D. Wands. *Cosmological perturbations*. Phys. Rept. **475** 1 (2009). arXiv:0809.4944. Cited on page 12.

[27] J. M. Bardeen. *Gauge-invariant cosmological perturbations*. Phys. Rev. D **22** 1882 (1980). URL: https://link.aps.org/doi/10.1103/PhysRevD.22.1882. Cited on page 14.

[28] J. M. Bardeen, J. R. Bond, N. Kaiser, and A. S. Szalay. *The statistics of peaks of Gaussian random fields*. Astrophysical Journal **304** 15 (1986). Cited on page 18.

[29] O. F. Piattella. *Lecture Notes in Cosmology*. UNITEXT for Physics. Springer Cham 2018. arXiv:1803.00070. Cited on page 19.

[30] J. C. Fabris and H. Velten. *Neo-newtonian theories*. 2014. arXiv:1501.01614. Cited on page 20.

[31] E. A. MILNE. *A NEWTONIAN EXPANDING UNIVERSE*. The Quarterly Journal of Mathematics **os-5** 64 (1934). URL: https://doi.org/10.1093/qmath/os-5.1.64 arXiv:https://academic.oup.com/qjmath/article-pdf/os-5/1/64/4481651/os-5-1-64.pdf. Cited on page 20.

[32] W. H. McCREA and E. A. MILNE. *NEWTONIAN UNIVERSES AND THE CURVATURE OF SPACE*. The Quarterly Journal of Mathematics **os-5** 73 (1934). URL: https://doi.org/10.1093/qmath/os-5.1.73 arXiv:https://academic.oup.com/qjmath/article-pdf/os-5/1/73/4481663/os-5-1-73.pdf. Cited on page 20.

[33] W. H. McCrea. *Relativity Theory and the Creation of Matter*. Proceedings of the Royal Society of London Series A **206** 562 (1951). Cited on page 20.

[34] J. A. S. Lima, V. Zanchin, and R. Brandenberger. *On the Newtonian cosmology equations with pressure*. Monthly Notices of the Royal Astronomical Society **291** L1 (1997). URL: https://doi.org/10.1093/mnras/291.1.L1 arXiv:https://academic.oup.com/mnras/article-pdf/291/1/L1/4082454/291-1-L1.pdf. Cited on pages 20 and 21.

[35] E. Harrison. *Cosmology without general relativity*. Annals of Physics **35** 437 (1965). URL: https://www.sciencedirect.com/science/article/pii/0003491665902496. Cited on pages 20 and 21.

[36] I. G. McCarthy, A. M. C. L. Brun, J. Schaye, and G. P. Holder. *The thermal Sunyaev–Zel'dovich effect power spectrum in light of Planck*. Mon. Not. Roy. Astron. Soc. **440** 3645 (2014). arXiv:1312.5341. Cited on page 22.

[37] R. C. Batista. *A Short Review on Clustering Dark Energy*. Universe **8** 22 (2021). arXiv:2204.12341. Cited on page 23.

[38] L. R. Abramo, R. C. Batista, L. Liberato, and R. Rosenfeld. *Physical approximations for the nonlinear evolution of perturbations in inhomogeneous dark energy scenarios.* Phys. Rev. D **79** 023516 (2009). URL: https://link.aps.org/doi/10.1103/PhysRevD.79.023516. Cited on page 23.

[39] D. Sapone and M. Kunz. *Fingerprinting dark energy.* Phys. Rev. D **80** 083519 (2009). URL: https://link.aps.org/doi/10.1103/PhysRevD.80.083519. Cited on page 23.

[40] P. Creminelli, G. D'Amico, J. Norena, and F. Vernizzi. *The Effective Theory of Quintessence: the w<-1 Side Unveiled.* JCAP **02** 018 (2009). arXiv:0811.0827. Cited on page 23.

[41] E. J. Copeland, M. Sami, and S. Tsujikawa. *Dynamics of dark energy.* Int. J. Mod. Phys. D **15** 1753 (2006). arXiv:hep-th/0603057. Cited on page 23.

[42] J. Yoo and Y. Watanabe. *Theoretical Models of Dark Energy.* International Journal of Modern Physics D **21** 1230002 (2012). arXiv:1212.4726. Cited on page 23.

[43] S. Tsujikawa. *Quintessence: a review.* Classical and Quantum Gravity **30** 214003 (2013). URL: https://doi.org/10.1088/0264-9381/30/21/214003. Cited on page 23.

[44] P. A. R. Ade et al. *Planck 2015 results. XIV. Dark energy and modified gravity.* Astron. Astrophys. **594** A14 (2016). arXiv:1502.01590. Cited on page 23.

[45] C. Armendariz-Picon, V. Mukhanov, and P. J. Steinhardt. *Essentials of k-essence.* Phys. Rev. D **63** 103510 (2001). URL: https://link.aps.org/doi/10.1103/PhysRevD.63.103510. Cited on page 23.

[46] J. K. Erickson, R. R. Caldwell, P. J. Steinhardt, C. Armendariz-Picon, and V. Mukhanov. *Measuring the Speed of Sound of Quintessence.* Phys. Rev. Lett. **88** 121301 (2002). URL: https://link.aps.org/doi/10.1103/PhysRevLett.88.121301. Cited on page 23.

[47] T. Padmanabhan. *Accelerated expansion of the universe driven by tachyonic matter.* Phys. Rev. D **66** 021301 (2002). URL: https://link.aps.org/doi/10.1103/PhysRevD.66.021301. Cited on page 23.

[48] J. S. Bagla, H. K. Jassal, and T. Padmanabhan. *Cosmology with tachyon field as dark energy.* Phys. Rev. D **67** 063504 (2003). arXiv:astro-ph/0212198. Cited on page 23.

[49] T. Padmanabhan and T. R. Choudhury. *Can the clustered dark matter and the smooth dark energy arise from the same scalar field?* Phys. Rev. D **66** 081301 (2002). URL: https://link.aps.org/doi/10.1103/PhysRevD.66.081301. Cited on page 23.

[50] L. R. W. Abramo and F. Finelli. *Cosmological dynamics of the tachyon with an inverse power-law potential.* Phys. Lett. B **575** 165 (2003). arXiv:astro-ph/0307208. Cited on page 23.

[51] J. E. Gunn and I. Gott,J. Richard. *On the Infall of Matter Into Clusters of Galaxies and Some Effects on Their Evolution.* APJ **176** 1 (1972). Cited on page 23.

[52] T. Padmanabhan. *Structure Formation in the Universe.* 1993. Cited on page 23.

[53] V. Sahni and P. Coles. *Approximation methods for nonlinear gravitational clustering.* Phys. Rept. **262** 1 (1995). arXiv:astro-ph/9505005. Cited on page 23.

[54] R. C. Batista and V. Marra. *Clustering dark energy and halo abundances.* JCAP **11** 048 (2017). arXiv:1709.03420. Cited on pages 23, 40, and 57.

[55] A. Mehrabi, S. Basilakos, and F. Pace. *How clustering dark energy affects matter perturbations.* Mon. Not. Roy. Astron. Soc. **452** 2930 (2015). arXiv:1504.01262. Cited on page 23.

[56] F. Bernardeau, R. Juszkiewicz, A. Dekel, and F. R. Bouchet. *Omega from the skewness of the cosmic velocity divergence.* Mon. Not. Roy. Astron. Soc. **274** 20 (1995). arXiv:astro-ph/9404052. Cited on pages 24, 25, 31, 33, 34, 36, 37, 38, 39, 40, 51, and 57.

[57] F. Bernardeau, S. Colombi, E. Gaztanaga, and R. Scoccimarro. *Large scale structure of the universe and cosmological perturbation theory.* Phys. Rept. **367** 1 (2002). arXiv:astro-ph/0112551. Cited on pages 25, 31, 33, 37, 38, 39, 40, 45, 51, and 57.

[58] P. J. E. Peebles. *The large-scale structure of the universe.* 1980. Cited on pages 25, 31, 32, 36, and 37.

[59] J. Einasto, A. Klypin, G. Hütsi, L.-J. Liivamägi, and M. Einasto. *Evolution of skewness and kurtosis of cosmic density fields.* Astron. Astrophys. **652** A94 (2021). arXiv:2011.13292. Cited on pages 25, 31, and 37.

[60] R. R. R. Reis, M. Makler, and I. Waga. *Skewness as a test for quartessence.* Phys. Rev. D **69** 101301 (2004). arXiv:astro-ph/0403378. Cited on pages 31 and 39.

[61] A. Yahil. *Nonlinear comparison of large-scale densities and velocities.* In B. Rocca-Volmerange, J. M. Deharveng, and J. Tran Thanh Van, editors, *The Early Observable Universe from Diffuse Backgrounds* volume 11 page 359 1991. Cited on page 32.

[62] M. White and M. Srednicki. *Window Functions for Cosmic Microwave Background Experiments.* APJ **443** 6 (1995). arXiv:astro-ph/9402037. Cited on page 33.

[63] W. Cui, L. Liu, X. Yang, Y. Wang, L. Feng, and V. Springel. *An ideal mass assignment scheme for measuring the Power Spectrum with FFTs.* Astrophys. J. **687** 738 (2008). arXiv:0804.0070. Cited on page 33.

[64] E. Gaztanaga and P. Fosalba. *Cosmological perturbation theory and the spherical collapse model: Part 2. NonGaussian initial conditions.* Mon. Not. Roy. Astron. Soc. **301** 524 (1998). arXiv:astro-ph/9712263. Cited on page 34.

[65] P. Fosalba and E. Gaztanaga. *Cosmological perturbation theory and the spherical collapse model. Part 3. The Velocity divergence field and the Omega dependence.* Mon. Not. Roy. Astron. Soc. **301** 535 (1998). arXiv:astro-ph/9802165. Cited on pages 37 and 46.

[66] K. Benabed and F. Bernardeau. *Testing quintessence models with large scale structure growth.* Phys. Rev. D **64** 083501 (2001). arXiv:astro-ph/0104371. Cited on pages 40 and 47.

[67] E. Sefusatti and F. Vernizzi. *Cosmological structure formation with clustering quintessence.* Journal of Cosmology and Astroparticle Physics **2011** 047 (2011). URL: https://doi.org/10.1088/1475-7516/2011/03/047. Cited on page 40.

[68] J. B. Dent, S. Dutta, and T. J. Weiler. *New perspective on the relation between dark energy perturbations and the late-time integrated Sachs-Wolfe effect.* Phys. Rev. D **79** 023502 (2009). URL: https://link.aps.org/doi/10.1103/PhysRevD.79.023502. Cited on page 40.

[69] P. Creminelli, G. D'Amico, J. Noreña, L. Senatore, and F. Vernizzi. *Spherical collapse in quintessence models with zero speed of sound.* Journal of Cosmology and Astroparticle Physics **2010** 027 (2010). URL: https://doi.org/10.1088/1475-7516/2010/03/027. Cited on page 40.

[70] F. R. Bouchet, R. Juszkiewicz, S. Colombi, and R. Pellat. *Weakly Nonlinear Gravitational Instability for Arbitrary Omega.* APJL **394** L5 (1992). Cited on page 46.

[71] H. A. Feldman et al. *An estimate of omega_m without priors.* Astrophys. J. Lett. **596** L131 (2003). arXiv:astro-ph/0305078. Cited on page 46.

[72] E. Hivon, F. R. Bouchet, S. Colombi, and R. Juszkiewicz. *Redshift distortions of clustering: A Lagrangian approach.* Astron. Astrophys. **298** 643 (1995). arXiv:astro-ph/9407049. Cited on page 46.

[73] O. Sergijenko and B. Novosyadlyj. *Sound speed of scalar field dark energy: weak effects and large uncertainties.* Phys. Rev. D **91** 083007 (2015). arXiv:1407.2230. Cited on page 46.

[74] G. F. R. Ellis. *The Trace-Free Einstein Equations and inflation.* Gen. Rel. Grav. **46** 1619 (2014). arXiv:1306.3021. Cited on page 46.

[75] H. A. Rizwan ul and S. Unnikrishnan. *Effect of dark energy sound speed and equation of state on CDM power spectrum.* J. Phys. Conf. Ser. **484** 012048 (2014). arXiv:1407.4079. Cited on page 46.

[76] C. Armendariz-Picon, T. Damour, and V. F. Mukhanov. *k - inflation.* Phys. Lett. B **458** 209 (1999). arXiv:hep-th/9904075. Cited on page 46.

[77] J. Garriga and V. F. Mukhanov. *Perturbations in k-inflation.* Phys. Lett. B **458** 219 (1999). arXiv:hep-th/9904176. Cited on page 46.

[78] P. Creminelli, G. D'Amico, J. Norena, L. Senatore, and F. Vernizzi. *Spherical collapse in quintessence models with zero speed of sound.* JCAP **03** 027 (2010). arXiv:0911.2701. Cited on page 47.

[79] A. Moss, E. Copeland, S. Bamford, and T. Clarke. *A model-independent reconstruction of dark energy to very high redshift.* arXiv e-prints page arXiv:2109.14848 (2021). arXiv:2109.14848. Cited on page 47.

[80] R. R. Caldwell. *A Phantom menace?* Phys. Lett. B **545** 23 (2002). arXiv:astro-ph/9908168. Cited on page 47.

[81] P. Hudelot, J. C. Cuillandre, K. Withington, Y. Goranova, H. McCracken, F. Magnard, Y. Mellier, N. Regnault, M. Betoule, H. Aussel, J. J. Kavelaars, P. Fernique, F. Bonnarel, F. Ochsenbein, and O. Ilbert. *VizieR Online Data Catalog: The CFHTLS Survey (T0007 release) (Hudelot+ 2012).* 2012. Cited on page 51.

[82] R. Juszkiewicz, F. R. Bouchet, and S. Colombi. *Skewness induced by gravity.* Astrophys. J. Lett. **412** L9 (1993). arXiv:astro-ph/9306003. Cited on page 51.

[83] A. Lewis. *CAMB Notes.* https://cosmologist.info/notes/CAMB.pdf. Cited on page 53.

[84] A. Challinor and A. Lewis. *The linear power spectrum of observed source number counts.* PRD **84** 043516 (2011). arXiv:1105.5292. Cited on page 53.

[85] J. C. Hill. *The Sunyaev-Zel'dovich Effect and Large-Scale Structure*. 2015. arXiv:1510.06237. Cited on page 57.

[86] J. E. Carlstrom, G. P. Holder, and E. D. Reese. *Cosmology with the Sunyaev-Zel'dovich effect*. Ann. Rev. Astron. Astrophys. **40** 643 (2002). arXiv:astro-ph/0208192. Cited on page 57.

[87] T. Tatekawa and S. Tsujikawa. *Second-order matter density perturbations and skewness in scalar-tensor modified gravity models*. JCAP **09** 009 (2008). arXiv:0807.2017. Cited on page 58.

[88] L. Amendola and C. Quercellini. *Skewness as a test of the equivalence principle*. Phys. Rev. Lett. **92** 181102 (2004). arXiv:astro-ph/0403019. Cited on page 58.